1-1-2013

Ion Current Signal Detection During Cold Starting And Idling Operation In A Diesel Engine

Sanket Anil Gujarathi
Wayne State University,

ION CURRENT SIGNAL DETECTION DURING COLD STARTING AND IDLING OPERATION IN A DIESEL ENGINE

by

Sanket Anil Gujarathi

THESIS

Submitted to the Graduate School of

Wayne State University,

Detroit, Michigan

in partial fulfillment of the requirements

for the degree of

MASTER OF SCIENCE

2013

MAJOR: Mechanical Engineering

Approved by

_____

Advisor Date

DEDICATION

This work is dedicated to my parents, for they have been the ultimate teacher since the very first day of my life and made all the sacrifices for me to follow my dreams. They are the wind beneath my wings and it is to them that all my achievements are dedicated to.

This work is also dedicated to all my Teachers since childhood.

ACKNOWLEDGEMENT

I express my deepest and sincere gratitude to my adviser Prof. Dr. Naeim A. Henein, in whom I have witnessed the unmatched passionate attitude for teaching and the substance of a humble genius. I thank him for giving me the chance to be a part of his research team at Wayne State University. His continuous motivation, influence and guidance have been the key aspects of my extraordinary research journey. I would regard him as one of the best ever teacher in my life and to whom I will be indebted forever.

I would like to thank Dr. Marcis Jansons and Dr. Dinu Taraza for their constant support and valuable feedback during the course of my research. I acknowledge the help from Eugene and Marvin for the machine shop support in machining the sensors. I would also like to thank Dr. Fadi Estefanous for his help and support.

This work would have not been possible without the invaluable training, co-operation and support from Tamer Badawy who also kept me testing when others would have surely failed. Thank you for sharing the knowledge and skills from time to time. To Amit Shrestha, Ziliang Zheng, Rojan George and Sridhar Koushik, thank you for providing me a fantastic work environment filled with support, advices and assistance. I would also like to thank all my other fellow members of Center for Automotive Research for their co-operation and support. The final thanks must go to my parents for providing me the encouragement and every opportunity of good education. I cannot and would never wish for more.

TABLE OF CONTENTS

DEDICATION ..... **ii**

ACKNOWLEDGEMENT ..... **iii**

TABLE OF CONTENTS ..... **iv**

LIST OF FIGURES ..... **viii**

LIST OF TABLES ..... **xiv**

CHAPTER 1 SCOPE OF WORK **1**

1.1 Introduction 1

1.2 Thesis Outline 2

CHAPTER 2 LITERATURE REVIEW **4**

2.1 Introduction 4

2.2 Diesel Engine Cold Starting 5

2.3 Diesel Engine Idling Operation 5

2.4 Fundamentals of Ionization in Gasoline and Diesel Engines 6

2.5 Conclusions 10

CHAPTER 3 ENGINE SET-UP AND INSTRUMENTATIONS **11**

3.1 Engine Set-Up 11

3.2 Engine Instrumentation 12

3.3 Dynamometer Set-Up 14

3.4 Engine Electronic Control Unit (ECU) 15

3.5 Data Acquisition System and Combustion Analyzer 16

3.6 Ion Current Sensor 18

3.7 Ion Current Measuring Circuit 18

CHAPTER 4 ION CURRENT SIGNAL DETECTION: PROBLEMS AND CAUSES 20

4.1 Introduction 20

4.2 Problem of Ion Current Signal Misdetection 21

4.3 Causes of Ion Current Signal Misdetection 23

4.4 Ion Current Signal Misdetection and Actual Misdetection 27

4.5 Combustion and Ion Current Misdetection during Cold Starting in Diesel Engines ... 29

4.6 Chapter Summary 31

CHAPTER 5 EXPERIMENTAL PROCEDURE 32

5.1 Introduction 32

5.2 Test Procedure 32

5.3 Probe Geometry and Applied Voltage used for Experimental Investigation 33

5.4 SIC Detection using Dynamic Threshold 34

5.5 Misfire Detection from RHR Trace 35

5.6 Chapter Summary 35

CHAPTER 6 EXPERIMENTAL RESULTS: COLD STARTING 36

6.1 Introduction 36

6.2 Effect of Probe Length on Ion Current Signal Characteristics and Detection 37

6.3 Effect of Applied Voltage on Ion Current Characteristics and Detection..... 38

6.4 Combined Effects of Probe Length and Applied Voltage on Ion Current Characteristics and Detection..... 39

6.5 Ion Current in a Cold Start Transient 42

6.6 Effect of Varying Probe Length, Varying Probe Diameter and Varying Applied Voltage on Actual Misdetection..... 52

6.7 Chapter Summary..... 55

CHAPTER 7 EXPERIMENTAL RESULTS: NO LOAD OPERATION..... 56

7.1 Introduction 56

7.2 Effect of Probe Length on Ion Current Signal Detection..... 57

7.3 Effect of Probe Diameter on the Ion Current Signal Detection..... 61

7.4 Effect of Probe Length, Probe Diameter and Applied Voltage on Actual Misdetection 65

7.5 Effect of Probe Length, Probe Diameter and Applied Voltage on the Maximum Amplitude of Ion Current Signal..... 68

7.6 Chapter Summary..... 73

CHAPTER 8 SUMMARY AND CONCLUSIONS..... 74

8.1 Thesis Summary..... 74

8.2 Conclusions 75

REFERENCES **78**

ABSTRACT **82**

AUTOBIOGRAPHICAL STATEMENT **83**

LIST OF FIGURES

Figure 2.4-1 Typical ion current signal in SI engine (Speed= 1300 RPM, torque= 22 Nm, λ = 0.89) [15]..... 8

Figure 2.4-2 Typical ion current signal in CI engine (Speed= 1800 RPM, IMEP= 11 bar, SOI 13.25° bTDC, Injection Pressure 550 bar) [19]..... 9

Figure 3.1-1 Engine Test Cell..... 11

Figure 3.2-1. Engine Instrumentation Layout..... 13

Figure 3.3-1. Dynamometer Set-up and Control Unit..... 14

Figure 3.3-2. Dynamometer Control Unit System, Interface and Display..... 15

Figure 3.4-1. Engine Control Unit Hardware and Control Interface..... 16

Figure 3.5-1. Data Acquisition System Hardware, Controller Interface and Display..... 17

Figure 3.7-1. Ion Current Measuring Circuit..... 19

Figure 3.7-2. Power Supply and Signal Conditioning Unit..... 19

Figure 4.2-1. Percentage of the Ion Current Signal Detection in 100 cycles at Different Engine Loads and Engine Speed= 1800 RPM [22]..... 21

Figure 4.2-2. Cylinder gas pressure, rate of heat release and ion current signal at light load for two arbitrary cycles [Inj. Press= 550bar; Const. Speed= 1800 RPM]..... 22

Figure 4.3-1. High speed images of the visible light produced from the combustion process (Light load: Detection of the ion current) (OPT, IMEP= 1 bar, Const. Speed=1000RPM, SOI= 8° bTDC, Inj. Press= 800 bar) [23]..... 25

Figure 4.3-2. High speed images of the visible light produced from the combustion process (Light load: Misdetection of the ion current) (OPT, IMEP= 1 bar, Const. Speed=1000RPM, SOI= 8° bTDC, Inj. Press= 800 bar) [23] 26

Figure 4.4-1. Cylinder gas pressure, rate of heat release and ion current signal at light load for two arbitrary cycles and a misfired cycle [Inj. Press= 550bar; Const. Speed= 1800 RPM]..... 28

Figure 4.5-1 In-cylinder gas pressure and RHR traces for arbitrary cycles exhibiting different combustion zones during cold starting 30

Figure 5.3-1. Cross sectional view of combustion chamber showing penetration of different probe lengths 34

Figure 6.2-1. Cylinder gas pressure, RHR and ion current signal for five random cycles using the short probe (20.85 mm) at applied voltage of 100V 37

Figure 6.3-1. Cylinder gas pressure, RHR and ion current signal for five random cycles using the short probe (20.85 mm) at applied voltage of 350V 38

Figure 6.4-1. Cylinder gas pressure, RHR and ion current signal for five random cycles using the long probe (28.40 mm) at applied voltage of 100V 39

Figure 6.4-2. Cylinder gas pressure, RHR and ion current signal for five random cycles using the long probe (28.40 mm) at applied voltage of 350V 40

Figure 6.4-3. Cylinder gas pressure, RHR and ion current traces for two cycles with late combustion: one with the short probe length and the other with long probe length and at same applied voltage of 350V 41

Figure 6.5-1 Sample figure representing the Ion Current Signal Detection and Misdetection Data Analysis..... 42

Figure 6.5-2 Representation of (a) Fired and Detected Cycle (b) Fired and Undetected, probes failure cycle and (c) Misfired Cycle 43
Figure 6.5-3. Detailed processed data showing RPM, SIC, LPPC, misfire and ion current misdetection for short probe at applied voltage of 100V..... 44
Figure 6.5-4. Detailed processed data showing RPM, SIC, LPPC, misfire and ion current misdetection for medium probe at applied voltage of 100V..... 44
Figure 6.5-5. Detailed processed data showing RPM, SIC, LPPC, misfire and ion current misdetection for long probe at applied voltage of 100V..... 45
Figure 6.5-6. Detailed processed data showing RPM, SIC, LPPC, misfire and ion current misdetection for short probe at applied voltage of 350V..... 46
Figure 6.5-7. Detailed processed data showing RPM, SIC, LPPC, misfire and ion current misdetection for medium probe at applied voltage of 350V..... 47
Figure 6.5-8. Detailed processed data showing RPM, SIC, LPPC, misfire and ion current misdetection for long probe at applied voltage of 350V..... 47
Figure 6.5-9. Detailed processed data showing RPM, SIC, LPPC, misfire and ion current misdetection for short probe length and large probe diameter at applied voltage of 100V..... 48
Figure 6.5-10. Detailed processed data showing RPM, SIC, LPPC, misfire and ion current misdetection for medium probe length and large probe diameter at applied voltage of 100V..... 49
Figure 6.5-11. Detailed processed data showing RPM, SIC, LPPC, misfire and ion current misdetection for long probe length and large probe diameter at applied voltage of 100V..... 49
Figure 6.5-12. Detailed processed data showing RPM, SIC, LPPC, misfire and ion current misdetection for short probe length and large probe diameter at applied voltage of 350V..... 51

Figure 6.5-13. Detailed processed data showing RPM, SIC, LPPC, misfire and ion current misdetection for medium probe length and large probe diameter at applied voltage of 350V..... 51
Figure 6.5-14. Detailed processed data showing RPM, SIC, LPPC, misfire and ion current misdetection for long probe length and large probe diameter at applied voltage of 350V..... 52
Figure 6.6-1. % Actual Misdetection of ion current for varying probe length with small probe diameter against the applied voltage..... 53
Figure 6.6-2. % Actual Misdetection of ion current for varying probe length with large probe diameter against the applied voltage..... 54
Figure 7.2-1. Detailed processed data showing RPM, SIC, LPPC, misfire and ion current misdetection for short probe at applied voltage of 100V and 1800RPM 58
Figure 7.2-2. Detailed processed data showing RPM, SIC, LPPC, misfire and ion current misdetection for medium probe at applied voltage of 100V and 1800RPM 58
Figure 7.2-3. Detailed processed data showing RPM, SIC, LPPC, misfire and ion current misdetection for long probe at applied voltage of 100V and 1800RPM 59
Figure 7.2-4. Detailed processed data showing RPM, SIC, LPPC, misfire and ion current misdetection for short probe at applied voltage of 350V and 1800RPM 60
Figure 7.2-5. Detailed processed data showing RPM, SIC, LPPC, misfire and ion current misdetection for medium probe at applied voltage of 350V and 1800RPM 60
Figure 7.2-6. Detailed processed data showing RPM, SIC, LPPC, misfire and ion current misdetection for long probe at applied voltage of 350V and 1800RPM 61
Figure 7.3-1. Detailed processed data showing RPM, SIC, LPPC, misfire and ion current misdetection for short probe with increased probe diameter at applied voltage of 100V and 1800RPM..... 62

Figure 7.3-2. Detailed processed data showing RPM, SIC, LPPC, misfire and ion current misdetection for long probe with increased probe diameter at applied voltage of 100V and 1800RPM 63
Figure 7.3-3. Detailed processed data showing RPM, SIC, LPPC, misfire and ion current misdetection for short probe with increased probe diameter at applied voltage of 350V and idling speed 1800RPM 64
Figure 7.3-4. Details processed data showing RPM, SIC, LPPC, misfire and ion current misdetection for long probe with increased probe diameter at applied voltage of 350V and idling speed 1800RPM 64
Figure 7.4-1. Percentage of actual misdetection of the ion current signal for different probe length and engine speeds at 100V (small probe diameter) 65
Figure 7.4-2. Percentage of actual misdetection of the ion current signal for different probe length and engine speeds at 350V (small probe diameter) 66
Figure 7.4-3. Percentage of actual misdetection of the ion current signal for different probe length and idling speeds at 100V (large probe diameter) 67
Figure 7.4-4. Percentage of actual misdetection of the ion current signal for different probe length and idling speeds at 350V (large probe diameter) 67
Figure 7.5-1.(a) and (b): Box plot for ion current amplitude peaks at 1600 rpm at 100V and 350V for the probes with smaller diameter 69
Figure 7.5-2. (a) and (b): Box plot for ion current amplitude peaks at 1600 rpm at 100V and 350V for the probes with larger diameter 69
Figure 7.5-3. (a) and (b): Box plot for ion current amplitude peaks at 1800 rpm at 100V and 350V for the probes with smaller diameter 70

Figure 7.5-4. (a) and (b): Box plot for ion current amplitude peaks at 1800 rpm at 100V and 350V for the probes with larger diameter 70
Figure 7.5-5. (a) and (b): Box plot for ion current amplitude peaks at 2100 rpm at 100V and 350V for the probes with smaller diameter 71
Figure 7.5-6. (a) and (b): Box plot for ion current amplitude peaks at 2100 rpm at 100V and 350V for the probes with larger diameter 71

LIST OF TABLES

Table 3.1-1. Engine Specification and Technical Data..... 12

Table 7.1-1 Injection pulse width at different idling speeds..... 56

CHAPTER 1

SCOPE OF WORK

1.1 *Introduction*

All combustion engines, whether gasoline or diesel, expel noxious emissions as the by-product of combustion and are continuously exposed to the increasing demands on fuel economy while meeting the stringent emission standards. Diesel engines, well-known for their superior fuel economy and high power density, have undergone noticeable improvement since the past decade. This development, particularly in passenger vehicles, has been primarily driven by the demand of higher performance and better driveability combined with strict compliance to NOx and soot emissions. The utilization of turbo-charging and electronically controlled common rail direct fuel injection have further enhanced the capability of diesel engines to achieve superior fuel economy, higher specific power output and high thermal efficiency. However, the problem of cycle misfires causing unacceptable level of unburned hydrocarbon emissions during cold starting in diesel engines is still very obstinate. Combustion instability and misfire are amongst the serious problems that deteriorate the diesel engine performance during starting and idling operation. Consequently, there is a need for a feedback signal indicative of the in-cylinder combustion process which could thereby augment the level of sophistication of combustion control for the ECU (Electronic Control Unit).

Sensing techniques such as in-cylinder combustion gas pressure transducers and ion current probes can be used to produce signals indicative of in cylinder combustion process in

both gasoline and diesel engines. But, compared to pressure transducers, the ion current probes are less expensive and highly sensitive of the cycle-to-cycle in-cylinder combustion process variation. Based on the understanding of ion current technology in the gasoline engines, the ion current signal has been successfully implemented for misfire and knock detection in gasoline engines. However, the application of the ion current signal in diesel engines is yet to be thoroughly developed, particularly for the cold starting and idling operation of diesel engines.

This thesis investigates the ion current signal during the cold starting and idling operation of a diesel engine. The problem of ion current signal detection experienced during cold starting and idling operation is dealt and addressed. Different approaches have been applied to improve the ion current signal detection capability. Furthermore, the study is extended to detect misfires and late combustion during cold starting and idling operation of the diesel engine.

1.2 *Thesis Outline*

This thesis consists of 8 chapters. Chapter 2 is the literature review of the cold starting of diesel engines and the ion formation during the combustion of hydrocarbon fuel. It also covers a review of the characteristics of ion current signal in gasoline and diesel engines. The effect of different probe design on the ion current signal is also described. Chapter 3 gives a detailed discussion of the engine set-up and instrumentation, data acquisition system and the test procedure. This chapter also gives a detailed description of the ion current circuit. The ion current signal detection problem at light loads is thoroughly described in chapter 4. Illustrations from optical measurements and experimental data are used to better understand and describe the causes of ion current signal misdetection. At cold starting, the combustion instability has been

observed throughout the experimental investigations. In addition, the combustion phasing and the different combustion zones are also described in chapter 4. Furthermore, the difference between apparent ion current misdetection and actual misdetection during cold starting and idling operation is demonstrated through experimental data and these two terms are clearly defined for the use in the rest of this work.

Chapter 5 describes the test method and procedure used for the investigation of ion current signal misdetection. Detailed dimensions of the several different ion current sensor probes tested in the study are given in this chapter. The logic behind the algorithms developed for transient and steady state data analysis done throughout the study is also explained. Chapter 6 includes the data analysis and results of cold starting using different probes. Transient data from random cycles recorded during cold starting is used to demonstrate combustion instability and explain the effect of different probe designs on ion current signal detection during cold starting. The detailed processed data for the effect of different probes on the ion current signal at different idling speeds is presented in chapter 7. Chapter 8 gives further explanation of the observed results. Ion current signal characteristics and the effect of the engine operating parameters on the ion current signal are discussed in details to explain the phenomenon of ion current signal misdetection. Final conclusions of the experimental investigation based on the observed results and discussions are then listed at the end of chapter 8.

CHAPTER 2

LITERATURE REVIEW

2.1 *Introduction*

Modern diesel engines are equipped with highly advanced electronically controlled fuel injection systems which allow fuel delivery under very high pressures along with multiple injections per cycle and different injection rate shapings. Furthermore, it also gives more flexibility to the ECU to control different engine parameters in order to meet several emission targets. While, the starting of spark ignition (SI) engines is easy because combustion is initiated by a high energy electric spark, the cold starting of compression ignition (CI) engines is difficult, particularly at low ambient temperatures. Accordingly, a combustion sensor is needed in order to detect misfire or diagnose early or late combustion during cold starting of CI engines. ECU's currently used in diesel engines do not have feedback signals indicative of the combustion process.

Ion current signal has been successfully implemented in SI engines for combustion diagnostics, in-cylinder combustion control, air-fuel ratio estimation, and to detect misfire and knock [1-4]. This chapter covers a review of the cold starting phenomenon in diesel engines, a comparison between the characteristics of ion current signal in gasoline and diesel engines and the effect of probe design parameters on the ion current signal in diesel engines.

2.2 *Diesel Engine Cold Starting*

Misfires and incomplete combustion are major contributors to the white smoke in the diesel engine exhaust during cold starting. The engine misfires when the fuel-vapor mixture formed near the periphery of the sprays fails to autoignite. Auto-ignition of the fuel- air mixture in CI engines primarily depends on parameters such as the air pressure and temperature at the end of compression stroke [5], injection parameters [6, 7], cranking speed [5] and fuel properties particularly the cetane number and volatility [8]. Moreover, low ambient air temperatures directly affect the compression pressure and temperatures, ignition delay and blow-by mass fraction [9]. This kind of engine operation during starting, wherein engine encounters a number of misfires after it fires and reaches a steady idling operation, is referred to as combustion instability [10]. Combustion instability and misfires, during cold starting, thereby leads to increased fuel consumption and high concentration of unburned hydrocarbon emissions which appear as white smoke out of the tail-pipe. Consequently, the desirable characteristics for diesel engine cold starting would be to have proper combustion phasing and avoid misfires till the engine reach the steady idle speed. This can be achieved by detecting misfire and/or diagnosing early or late combustion with the help of technology capable of sensing the combustion process.

2.3 *Diesel Engine Idling Operation*

In diesel engines, idling and light-load operation produce significantly higher hydrocarbon emissions [11]. This is mainly because of the cool wall temperatures, and low gas temperatures. Low wall temperatures reduce the rate of evaporation of the liquid film formed on the wall and the formation of a combustible mixture. During idling, both the air temperature and

pressure near the end of the compression stroke are low because of the relatively high heat losses to the cool walls and the high blow-by losses at the slow idling speed. This results in the reduced fuel evaporation before it impinges on the walls. In addition to the slow physical processes and the formation of an auto-ignitable mixture, the low charge temperatures also slow down the rates of the autoignition reactions and delays the start of the exothermic reactions which lead to combustion. Furthermore, the high fraction of the fuel vapor left without combustion near TDC, has a small chance to be oxidized later in the expansion stroke, because of the low gas mass average temperature. The combination of high concentration of hydrocarbons left unburned near TDC and the poor oxidation during the expansion stroke result in the high hydrocarbon emissions during idling of diesel engines [11].

2.4 *Fundamentals of Ionization in Gasoline and Diesel Engines*

Chemi-ionization and thermal-ionization are the main sources of ionization in hydrocarbon flames [12, 13]. The magnitude of ions produced through both chemi and thermal-ionization is highly dependent on the air-fuel ratio of the charge mixture and the in-cylinder combustion temperature [13-15]. SI (gasoline) engines operate close to the stoichiometric air-fuel ratio with a homogeneous mixture. As a result, the formation of ions through chemi-ionization in the flame front zone is very high. Also, a high ion current is produced in the post flame zone due to the thermal-ionization resulting from the high in-cylinder gas temperatures. On the other hand, combustion of a heterogeneous mixture, typical to CI (diesel) engines, is characterized by auto-ignition of an overall lean mixture, while the local air-fuel ratios vary from very rich to very lean depending on the fuel spray characteristics. Consequently, the in-cylinder

gas temperatures reached are lower compared to that of gasoline engines. Accordingly, the amplitude of the ion current produced in diesel engines is much weaker than that in gasoline engines.

Figure 2.4-1 shows typical traces of cylinder gas pressure and ion current signal in a SI engine. The spark plug is used as ion current sensor and the ion current signal is observed to be characterized by two distinct peaks. Many studies have reported the two peaks in case of SI engines and there is a general agreement which suggests that the first peak is mainly caused by chemi-ionization in the flame front zone around the spark plug gap in the very early stages of flame propagation. The second peak is the result of thermal-ionization of the gases around the spark plug gap caused by the increase of their temperature near the end of the combustion process. [13, 15]. Several investigations have shown that the amplitudes of the peaks significantly vary and depend on the equivalence ratio, in-cylinder combustion temperatures, exhaust gas recirculation (EGR) rate and the type and location of the ion current sensor in the combustion chamber [13-16].

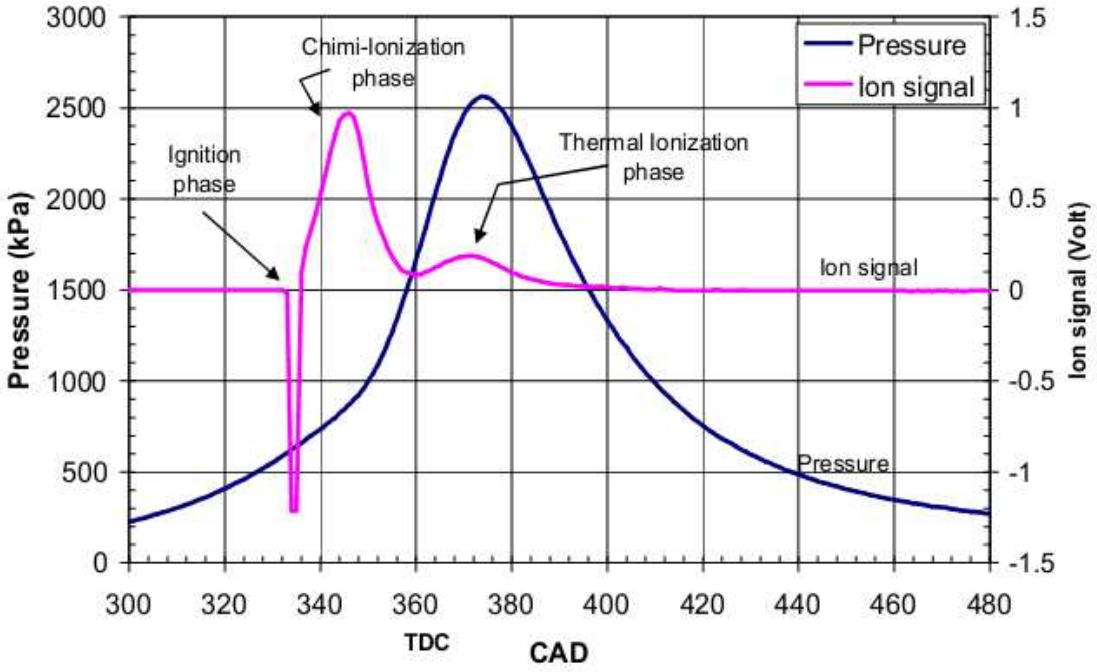

Figure 2.4-1 Typical ion current signal in SI engine (Speed= 1300 RPM, torque= 22 Nm, λ = 0.89) [15]

Unlike gasoline engines, the diesel engines undergo heterogeneous combustion which involves complex processes such as fuel injection, vaporization, fuel-air mixing and auto-ignition. The explanations of ion current signal characteristics in gasoline engines cannot be applied to diesel engines because of the different types of flames resulting from heterogeneous combustion in diesel engine. Accordingly, very limited investigations have been conducted to study ion current signal in diesel engines. Glavmo *et al*. were the first to study ion current signal in diesel combustion wherein, a modified glow plug was used to measure ion current signal from the combustion chamber [17]. Investigations of the ionization in diesel engines reported that the ion current signal can have one, two or more peaks depending on the engine operating conditions such as load, speed, injection pressure and injection timing [13, 18, 19]. Recently, Badawy *et al*. reported that the amplitude and number of peaks in the ion current trace are dependent on the sensor design and its location in combustion chamber [20].

Figure 2.4-2 shows typical traces of the in-cylinder gas pressure, rate of heat release (RHR), mass average gas temperature, needle lift, and ion current signal in a diesel engine. I_1, I_2 and I_3 represent the amplitudes of the first, second and third peaks respectively as observed in the ion current signal trace in Figure 2.4-2. The first peak I_1 occurs just after the peak of the premixed combustion (PPC) in the RHR trace. The second peak I_2 and I_3 appear during the expansion stroke, close to point where mass average gas temperature reaches its peak value. The presence of third peak I_3 is clearly identified only at high loads has been reported to be the result of the flame reflecting back towards the ion sensor probe from the combustion chamber bowl [12, 13].

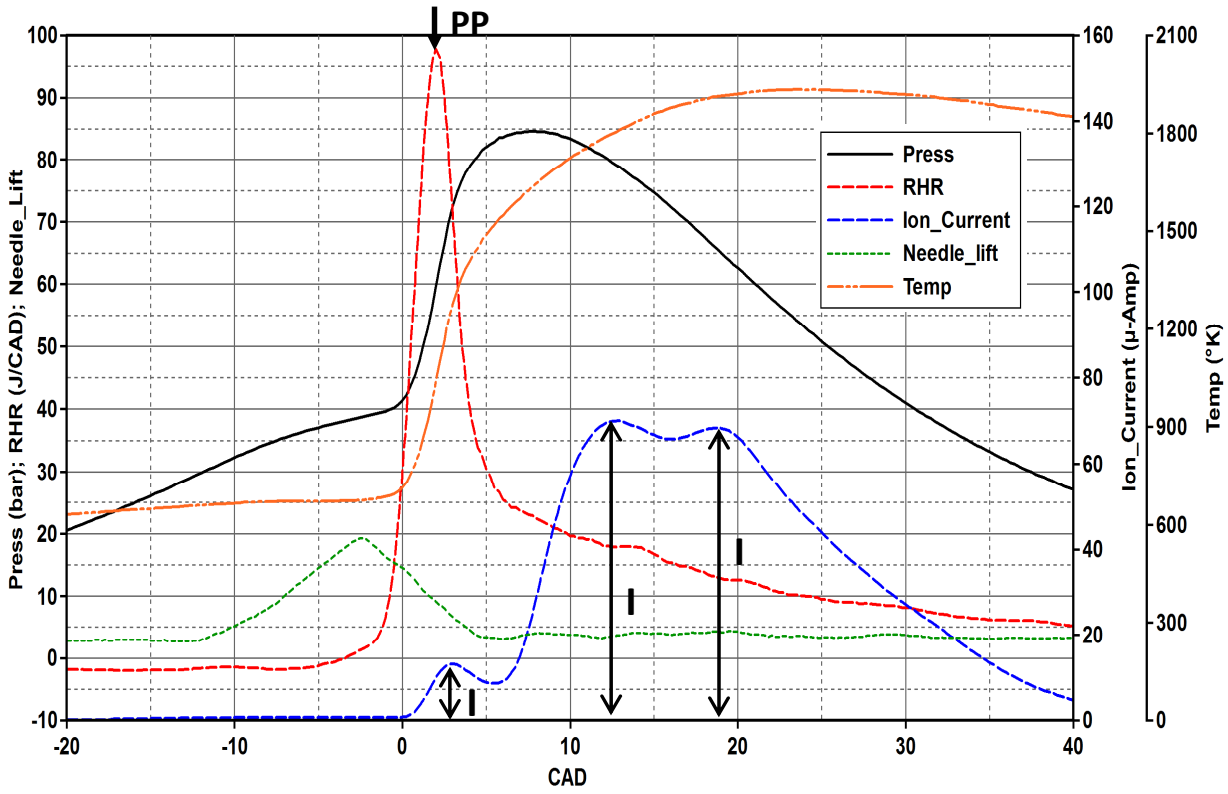

Figure 2.4-2 Typical ion current signal in CI engine (Speed= 1800 RPM, IMEP= 11 bar, SOI 13.25° bTDC, Injection Pressure 550 bar) [19]

2.5 *Conclusions*

The literature review on the cold starting and idling operation of diesel engine suggest that combustion instability and misfires are major hurdles to overcome. Combustion instability and misfires severely degrade the engine performance during starting and idling operations. Also, unacceptable levels of unburned hydrocarbons and increased fuel consumption are the other side effects associated with the cold starting and idling operation in diesel engine. In order to solve these problems it is necessary to have a technology capable of monitoring the course of combustion in each cycle. Thus to facilitate detection of cycle misfire or to diagnose early or late combustion, a feedback signal indicative of the in-cylinder combustion process is necessary.

Comparing the capabilities of the available in-cylinder combustion indicators, namely pressure transducer and ion current sensor, the ion current sensing technology is economically feasible in addition to its sensitivity to variations in the combustion process. Review of ion current signal fundamentals for both gasoline and diesel engines reveal the significance of the ion current signal since it holds detailed information about the combustion process. The sources and characteristics of the ion current signal in diesel combustion are significantly different than those in gasoline engines. However, the ion current signal has been successfully implemented in gasoline engines to detect misfires and therefore it can also be developed to detect misfire and diagnose early or late combustion in diesel engines.

CHAPTER 3

ENGINE SET-UP AND INSTRUMENTATIONS

3.1 *Engine Set-Up*

A Volkswagen 1.9L turbo-charged direct injection diesel engine was used for this A hydraulic dynamometer was coupled to the engine flywheel through a flexible coupling apply load on the engine and to control the engine speed. Engine specifications are shown in Table 3.1-1

The engine was equipped with a high pressure common rail injection system with solenoid operated injectors having five hole nozzle on each injector. A custom made open type ECU giving access to parameters such as injection timing, injection pressure, injection quantity was used to control the engine. The engine test cell and instrumentation are shown in Figure 3.1-1.

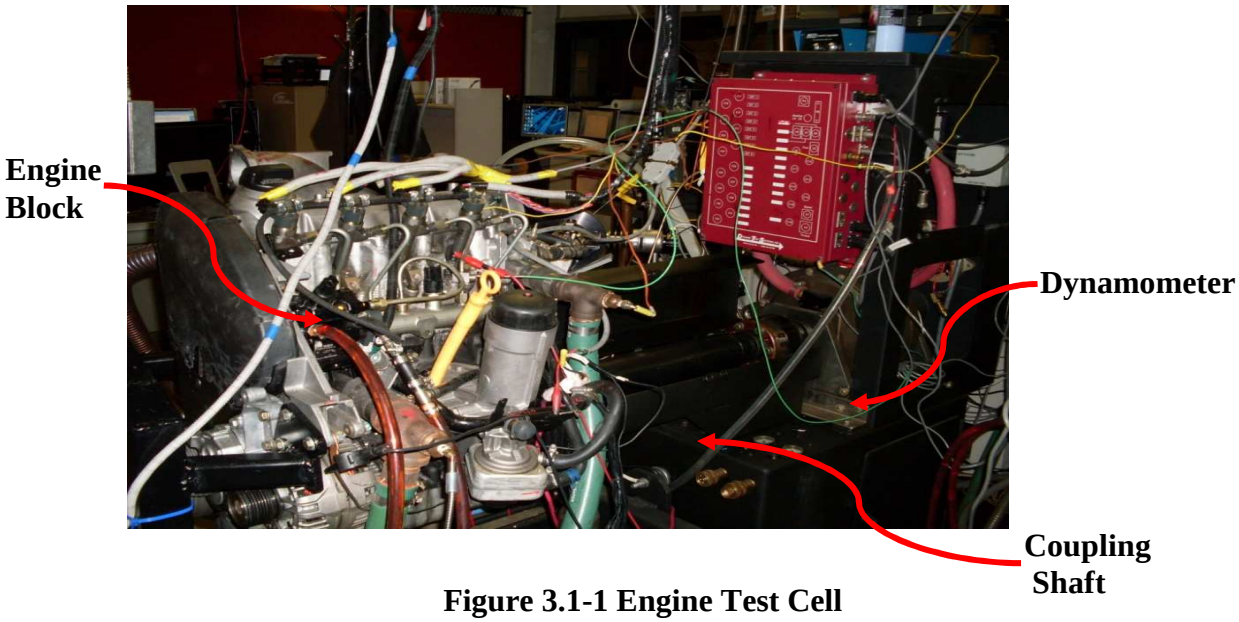

Figure 3.1-1 Engine Test Cell

Table 3.1-1. Engine Specification and Technical Data.

Engine type	Diesel 4-stroke
Number of cylinders	4 - Inline
Bore / stroke (mm)	79.5 / 95.5
Connecting Rod (mm)	144
Displacement (cm^3)	1,896
Compression ratio	19.5 : 1
Max. Torque @ 1900 rpm	220
Max. Power @ 3100 rpm	63
Lubrication oil capacity (lt)	4.5
Lower idling speed (rpm)	900
upper idling speed (rpm)	3,500
Maximum tilting (°)	15 to right

3.2 *Engine Instrumentation*

A brief description of the engine instrumentation is given in this section and a layout of various instruments and measuring equipment is shown in the Figure 3.2-1.

The engine has been instrumented to monitor several engine parameters as seen in Figure 3.2-1. The engine cylinder head is instrumented with a Kistler pressure transducer to measure gas pressure inside each cylinder. The intake manifold is fitted with a pressure transducer and thermocouple to measure intake air pressure and temperature respectively. The high fuel pressure in the common rail injection system is monitored using piezo-resistive type pressure transducer fitted close to common rail so that the change in rail pressure during each engine cycle could be closely observed. The injector in cylinder#4 is instrumented with a needle lift sensor to record the needle lift during the each engine cycle. An optical encoder with 0.25 crank angle degree (CAD) resolution is installed on the crank shaft to measure the instantaneous crank angle position and speed.

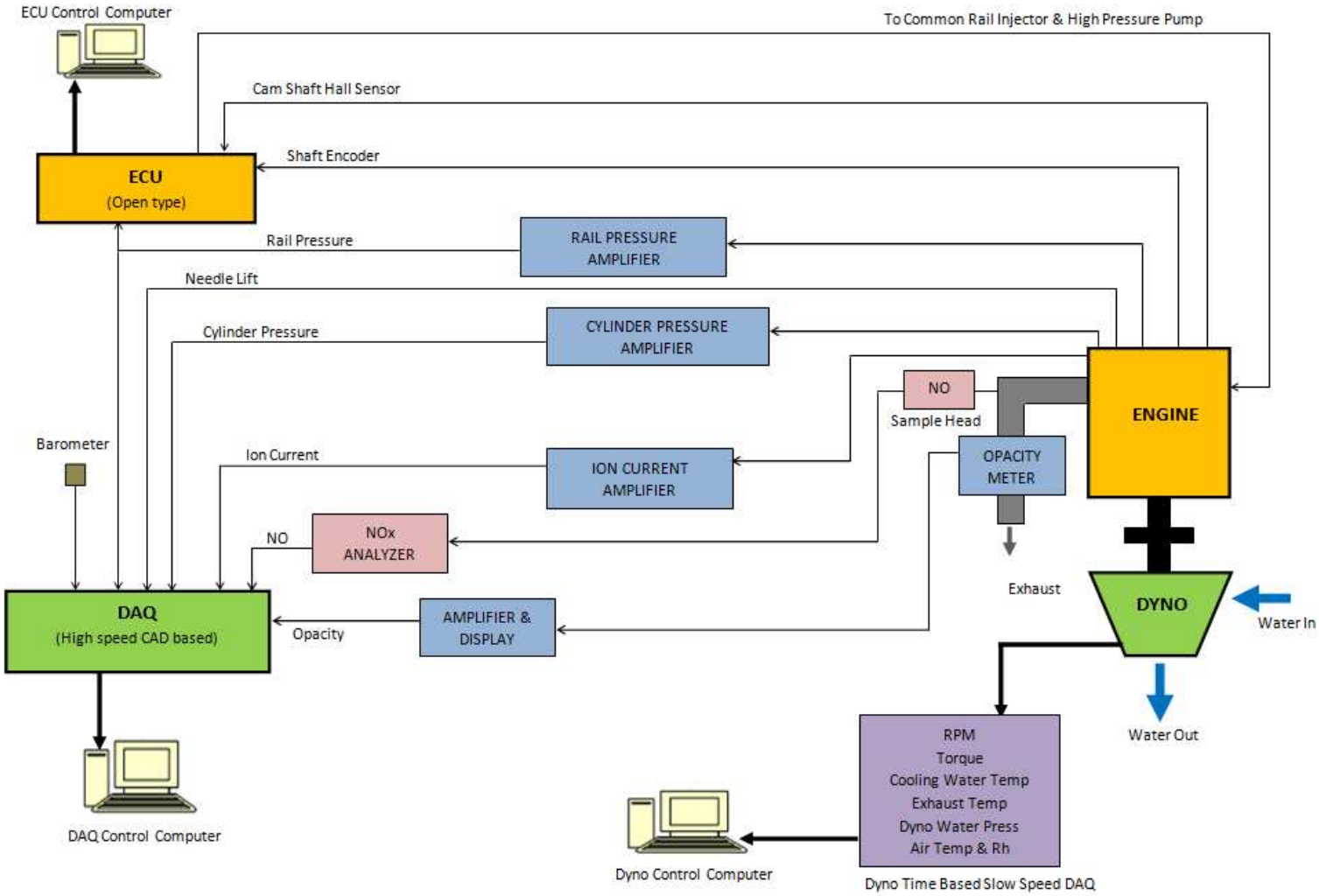

Figure 3.2-1. Engine Instrumentation Layout

3.3 *Dynamometer Set-Up*

The engine is coupled to a hydraulic (water brake) dynamometer from Dynamic Test System (DTS) from Shingle, CA. Figure 3.3-1 shows dynamometer set-up along with its own control unit. The dynamometer is equipped with load cell, speed sensor, several thermocouples and pressure transducers in the cooling water. The dynamometer control unit manages and controls the dynamometer speed once it is set to automatic operation mode by throttling the electric stepper motor operated water outlet valve. The software for dynamometer control unit shown in Figure 3.3-2, along with its time based data acquisition system records, calculates and displays parameters such as brake torque, brake power, speed, jacket cooling in-out temperature, exhaust gas temperature, oil pan temperature, room temperature and relative humidity.

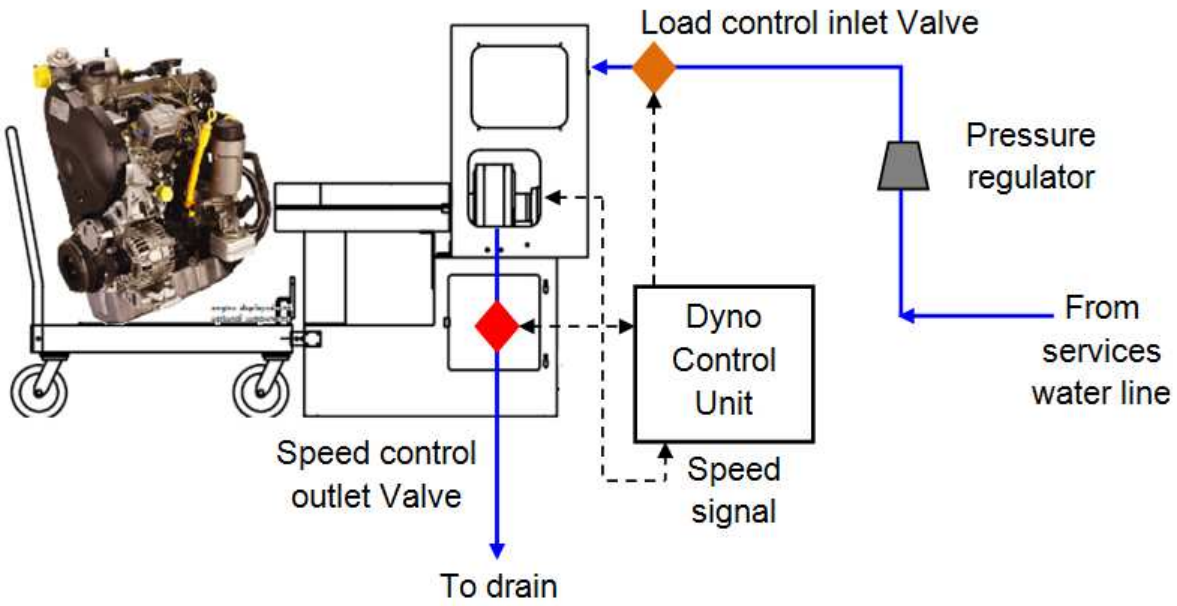

Figure 3.3-1. Dynamometer Set-up and Control Unit

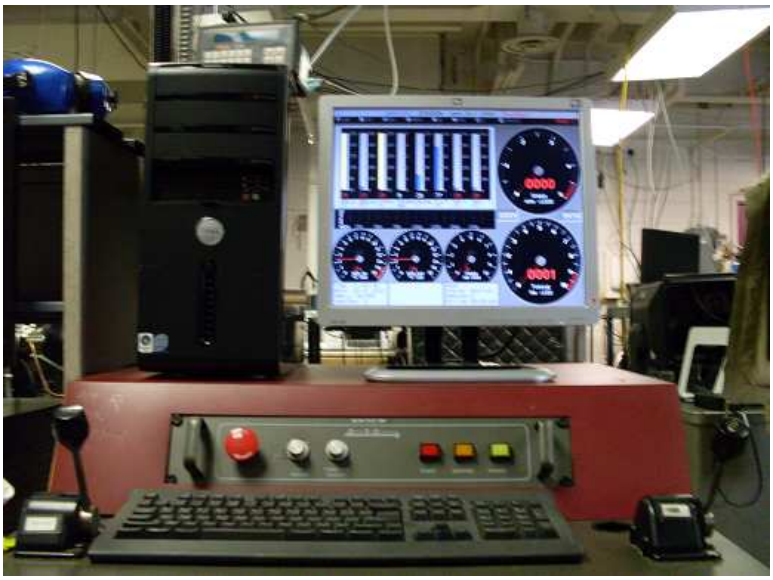

Figure 3.3-2. Dynamometer Control Unit System, Interface and Display

Service line is used to supply water to the dynamometer through a pressure regulator valve to maintain water pressure at 5 bar. The engine load is controlled from the open ECU by adjusting the fuel quantity being delivered to the injectors.

3.4 *Engine Electronic Control Unit (ECU)*

A custom made open type ECU from Electro-Mechanical Associates, Ann Arbor, MI is used to control engine operation. The ECU gave open access to the parameters such as injection timing, injection pressure, injection quantity and multiple injections. The ECU is capable of controlling the injection timing in step of 0.1 CAD and the injection duration in step of 1 µsec. Close loop feedback from the rail pressure sensor is used to control the injection pressure through the open ECU. Figure 3.4-1 shows the ECU hardware and the control interface screen from the control computer.

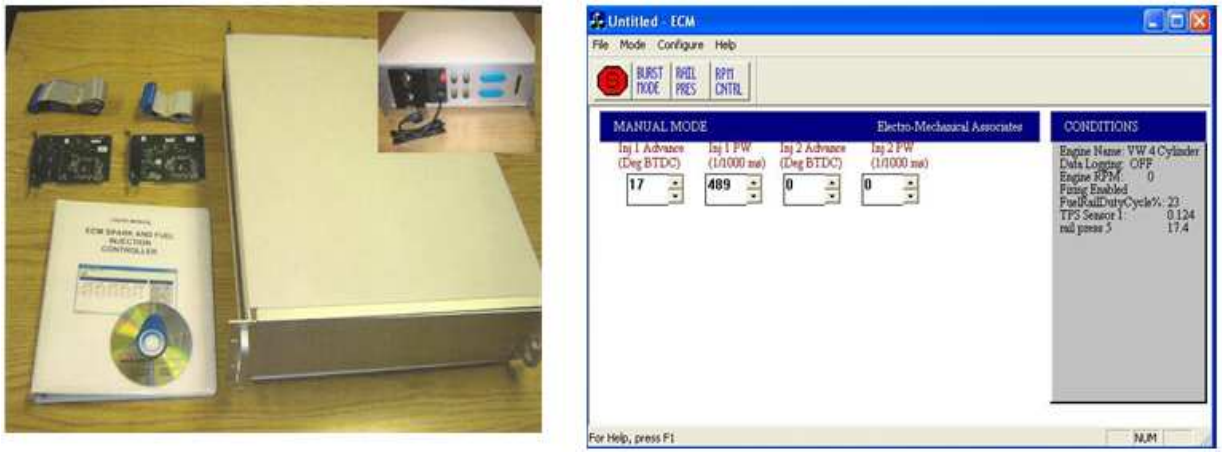

Figure 3.4-1. Engine Control Unit Hardware and Control Interface

The ECU can operate the engine on two modes- manual mode and automatic mode. In the manual mode the injection parameters are required to be entered manually whereas in automatic mode the ECU controls engine through pre defined user values from the look-up tables. In this research work, the manual mode of the ECU is used for the engine to operate at defined parameters throughout the tests.

3.5 *Data Acquisition System and Combustion Analyzer*

A high speed 16 channel data acquisition system from Electro-Mechanical Associates, Ann Arbor, MI is used to record the combustion data from the engine. The data acquisition system records several parameters such as in-cylinder gas pressure, needle lift, ion current signal etc., on crank angle basis with resolution of 0.25 CAD. Figure 3.5-1 shows the data acquisition system hardware and its controller interface.

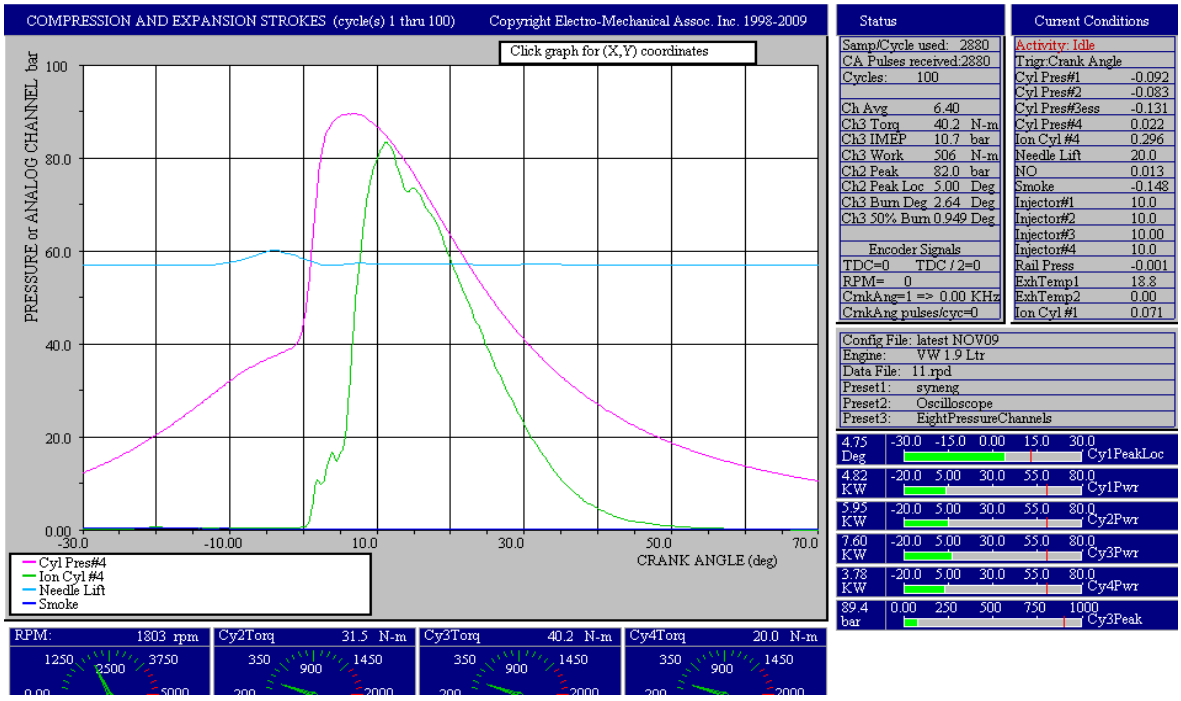

Figure 3.5-1. Data Acquisition System Hardware, Controller Interface and Display

The data acquisition software is used to adjust the gain, offset, smoothening, color, display and other parameters for each channel individually. For the purpose of data smoothening and to avoid excess of noise in the signal, the in-cylinder pressure data is recorded on 5 point average basis whereas ion current signal and needle lift data is recorded on 3 point average basis. The control computer connected to the data acquisition system includes combustion analysis software which calculates and displays various engine operating parameters online from the data

being recorded. Some of the main measured and calculated engine operating parameters are peak cylinder pressure and its location, peak pre-mixed combustion and its location, indicated mean effective pressure, indicated torque, mean engine speed, rpm and ion current peak position.

3.6 *Ion Current Sensor*

The original glow plugs that came with the engine are modified to be used as ion current sensors in this study. The glow plug for each cylinder is replaced by the modified glow plug to measure ion current signal in addition to its original function of heating the air in the combustion chamber. However, the ion current signal is recorded only for the instrumented cylinder #4. The modified glow plug (ion current sensor) needs to be electrically insulated from the engine body and cylinder head to complete the electrical circuit for the flow of ions. The cylinder head acts as one of the electrodes whereas the ion probe (glow plug heater element) which is insulated from the cylinder body acts as another electrode. The ion current signal produced during combustion passes through a 50 ohm resistor; the voltage across the resistor is amplified and recorded by the data acquisition system.

3.7 *Ion Current Measuring Circuit*

Figure 3.7-1 shows the circuit used for measuring ion current signal using the modified glow plug. The ion current measuring circuit consists of a variable DC voltage supply, ion current sensor, a resistance (50 Ω) and a signal conditioning unit. The secondary circuit with 12 volt supply is an energizing circuit, to burn any soot deposits on the glow plug surface.

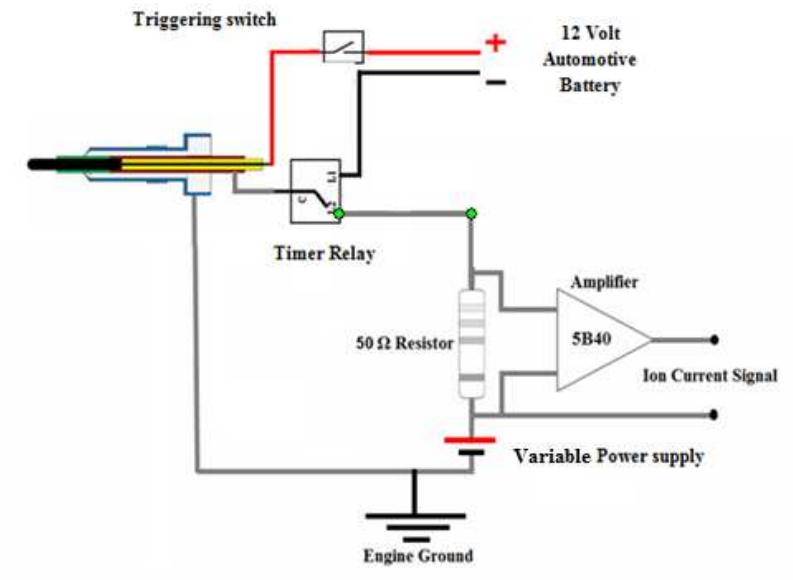

Figure 3.7-1. Ion Current Measuring Circuit

The variable power supply can provide up to 400 DC volts. The acquired ion current is passed through the 50Ω resistance and the voltage drop across the resistance is measured and fed in to the signal condition unit for amplification. Figure 3.7-2 shows the variable power supply unit and the signal conditioning unit. In order to avoid interference of the transformer coils from the power supply, the ion current measuring circuit and signal conditioning circuit are placed in separate cabinets.

Figure 3.7-2. Power Supply and Signal Conditioning Unit

CHAPTER 4

ION CURRENT SIGNAL DETECTION: PROBLEMS AND CAUSES

This chapter covers a detailed analysis of the ion current signal during light loads and idling operation in diesel engines and highlights the problems in signal detection. This is followed by a discussion of causes of such problems. The causes of the cycle-to-cycle variation in ion current signal are further explained by images taken for combustion in an optically accessible engine at light loads.

4.1 *Introduction*

Comparing the capabilities of the available in-cylinder combustion indicators, namely pressure transducer, optical sensors and ion current sensor, the ion current signal carries basic information about diesel combustion which cannot be obtained from other sensors. The combustion in diesel engines can be considered to consist of two modes. The first is the premixed combustion mode and the second is the mixing-diffusion controlled combustion mode. Each of these modes has its mechanisms of ionization. The first peak in the ion current signal corresponds to the premixed combustion and the second peak corresponds to the mixing-diffusion controlled combustion [13, 21]. Moreover, the amplitude and location of the ion current peaks significantly vary with the change in engine load, injection pressure and injection timing [18, 19, 21]. However, in case of heterogeneous mixture combustion, typical to diesel engines, the use of ionization sensing technology has been limited due to the complexity of combustion. Heterogeneous combustion is characterized with auto-ignition of air fuel charge mixture having

an equivalence ratio varying from zero to infinity. Consequently, it is highly impossible to achieve same charge distribution in the combustion chamber for each cycle which therefore results into cycle-to-cycle variations in the ion current signal.

4.2 *Problem of Ion Current Signal Misdetection*

Misdetection of the ion current signal is a problem in its employment as a reliable and robust feedback signal to the ECU.

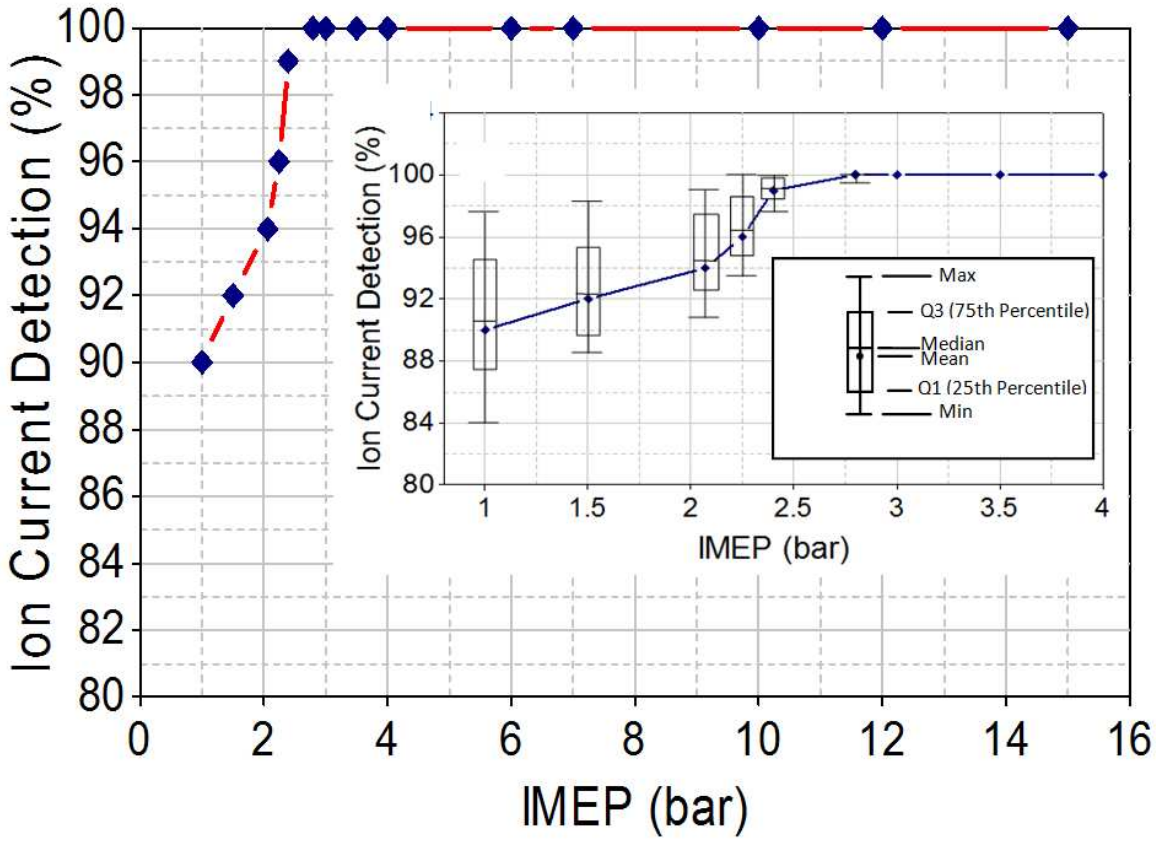

Figure 4.2-1. Percentage of the Ion Current Signal Detection in 100 cycles at Different Engine Loads and Engine Speed= 1800 RPM [22]

Figure 4.2-1 shows the percentage of the ion current signal detected in 100 consecutive cycles at different but steady engine loads starting from IMEP= 1 bar to 15 bar. The lower IMEP represents the idling operation, where as the higher IMEP represents high load operation of the diesel engine. It is observed that the percentage of ion current signal detection is the lowest at idling operation and improves to 100% detection at IMEP values above 3 bar. The zoomed box plot within the Figure 4.2-1 shows a high dispersion in the percentage of ion current signal detected at very low loads and this dispersion exponentially diminishes with the increase in engine load.

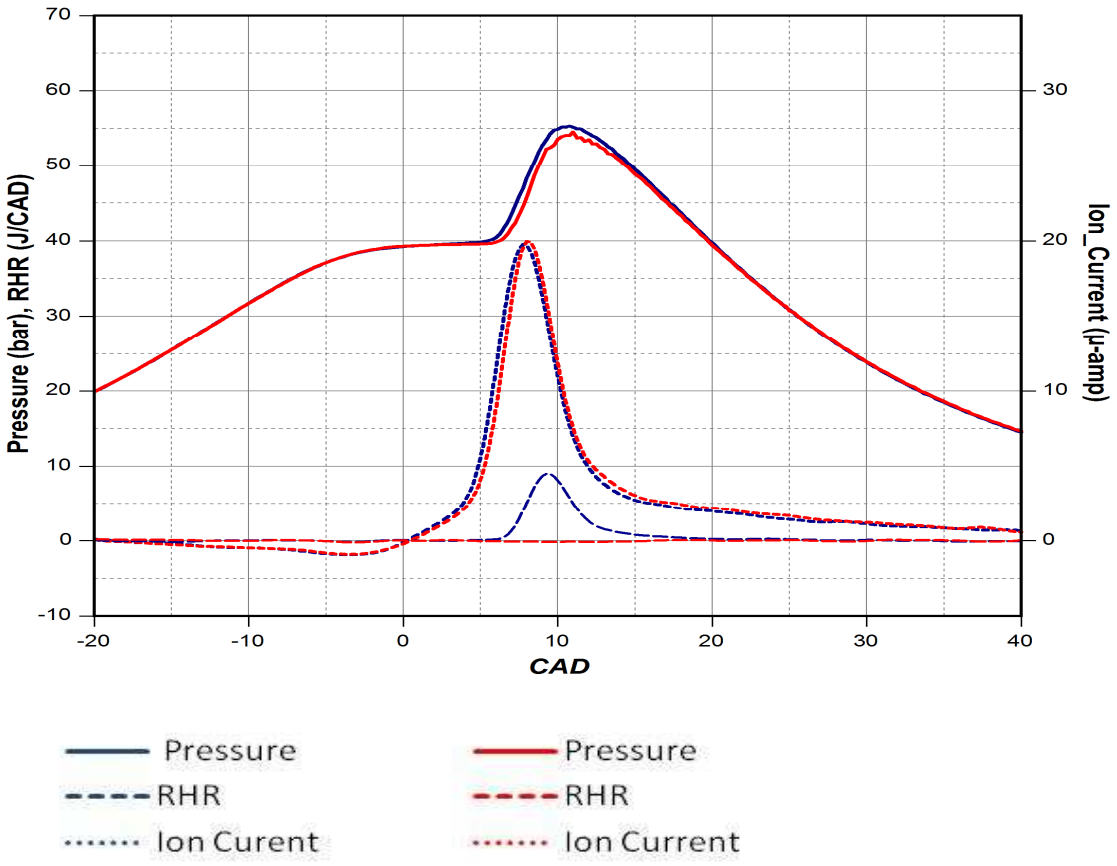

Figure 4.2-2. Cylinder gas pressure, rate of heat release and ion current signal at light load for two arbitrary cycles [Inj. Press= 550bar; Const. Speed= 1800 RPM]

Figure 4.2-2 shows the cylinder gas pressure, RHR and ion current signal traces for two arbitrary cycles at light load and injection pressure of 550 bar, measured during tests on Volkswagen engine. The two combustion events produced comparable pressure and RHR traces. However, although combustion can be detected from the r gas pressure in both cycles, the ion current signal is detected only for one of the cycle. This phenomenon wherein ion current sensor fails to detect the ion current signal in the event of combustion is termed as ion current signal misdetection. The ion current signal misdetection is observed to be prominent during idling and light load operation of diesel engines. This is evident in Figure 4.2-1 and has been reported in other investigations.[22, 23]. Thus, the problem of ion current signal misdetection limits the use of the ion current sensor to detect misfire and therefore reduces its reliability to be used as a feedback signal for combustion diagnostics.

4.3 *Causes of Ion Current Signal Misdetection*

The difference in overall equivalence ratio in gasoline and diesel engines primarily causes a significant differences in the characteristics of the ion current signal produced in these engines [24]. The amount of charge carriers present during the combustion in gasoline engines is fairly high as compared to that in diesel engines. Besides, the ion current signal in diesel combustion lacks reproducibility due to the heterogeneous nature of the charge.

Ion current sensing is a local phenomenon [13, 18]. The magnitude of the ions produced from chemi-ionization and thermal-ionizations depend on the equivalence ratio and the in-cylinder combustion temperatures [13]. Accordingly, the ion current signal misdetection can be

attributed to charge heterogeneity, very lean mixture, and low cylinder combustion gas temperature typical at light loads and idling operation of diesel engines.

The optical investigations on the ionization phenomenon in references [23, 25, 26]; give further insight in ion current signal misdetection at light loads. The details of the engine instrumentation, optical set-up and ion current sensor implementation are described in details in reference [25]. Figure 4.3-1 and Figure 4.3-2 show images of combustion in two random cycles at the same engine operating condition; IMEP= 1 bar and engine speed of 1000 RPM.

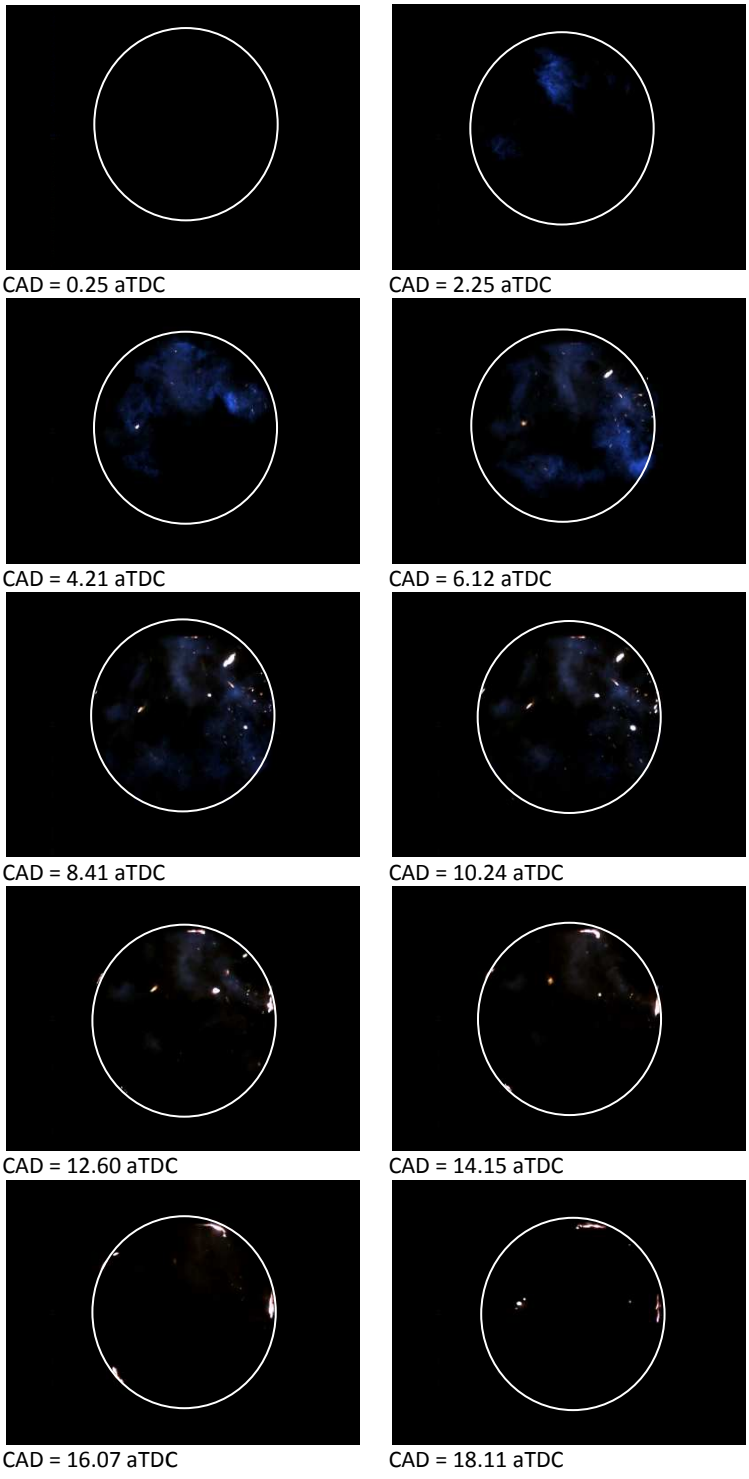

Figure 4.3-1. High speed images of the visible light produced from the combustion process (Light load: Detection of the ion current) (OPT, IMEP= 1 bar, Const. Speed=1000RPM, SOI= 8° bTDC, Inj. Press= 800 bar) [23]

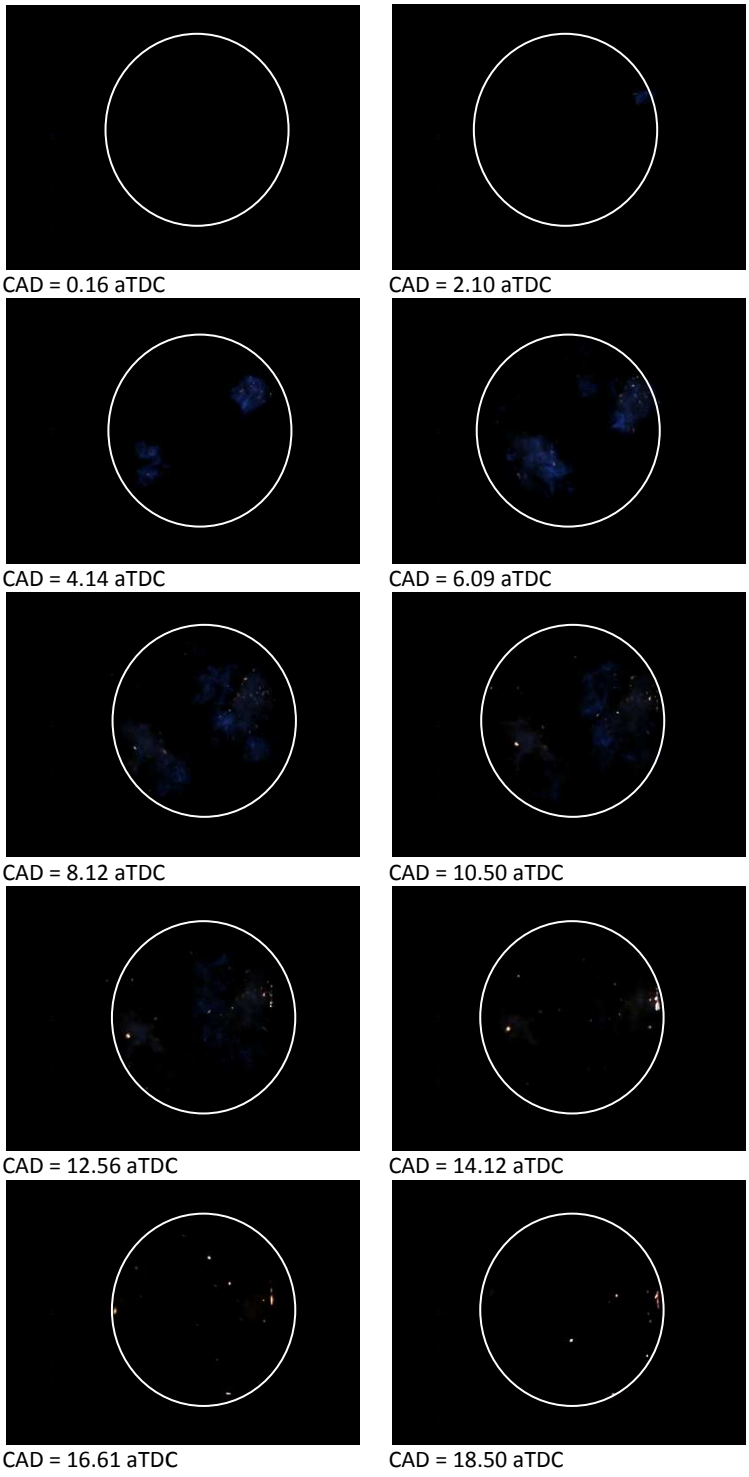

Figure 4.3-2. High speed images of the visible light produced from the combustion process (Light load: Misdetection of the ion current) (OPT, IMEP= 1 bar, Const. Speed=1000RPM, SOI= 8° bTDC, Inj. Press= 800 bar) [23]

Although both the cycles produce same cylinder gas pressure and RHR traces, the ion current signal is not detected in cycle represented in Figure 4.3-2. At light loads, the quantity of fuel injected is very small which results in a fairly overall lean mixture and low combustion gas temperatures. The first appearance of the blue flame in the form visible light, seen in the optical images, marks the start of combustion. The comparison of the blue flame during the combustion event in Figure 4.3-1 and Figure 4.3-2 shows significant cycle-to-cycle combustion variation which thereby results in non-uniform flame distribution across the combustion chamber. As a result, depending on the location of the ion current sensor in the combustion chamber it might not produce a signal if the flame does not occupy the zone around the sensor and the ion current is misdetected as indicated by images in Figure 4.3-2. At medium and higher loads, the quantity of fuel injected is comparatively large and the flame spreads over the whole combustion chamber and the ion current is detected. Hence, the problem of ion current misdetection is usually experienced only at light loads and idling operation of diesel engines.

4.4 *Ion Current Signal Misdetection and Actual Misdetection*

Two definitions will be used to describe the reason behind the absence of an ion current trace in any of the figures. The first is **"Misdetection"** which indicates the absence of the ion current signal that can either be due to failure of the sensor in detecting the ionization or due to absence of ions owing to misfire or low combustion temperatures. The second is "**Actual Misdetection"** which is used to describe only the sensors failure to detect ion current signal in the presence of combustion event. In this case, the absence of the signal is only the fault of the sensor, ignoring the inexistence of signal due to failure of combustion. Figure 4.2-2 shows traces

for two firing cycles, colored red and blue. Firing in the two cycles is evidenced by the red and blue cylinder gas pressure and the RHR traces. The absence of red ion current trace is definitely caused by the failure of the sensor. This is referred to as Misdetection.

Figure 4.4-1 shows cylinder gas pressure, RHR and ion current traces for three random cycles at light loads. The red and blue traces indicate cycles with combustion. However, the absence of a red current signal indicates the failure of the sensor and is referred to as Misdetection. The green traces indicate a very slow rise in RHR and a fairly late combustion in the expansion stroke. This cycle can be considered as misfiring cycle and the absence of the ion current signal is referred to as "Actual Misdetection".

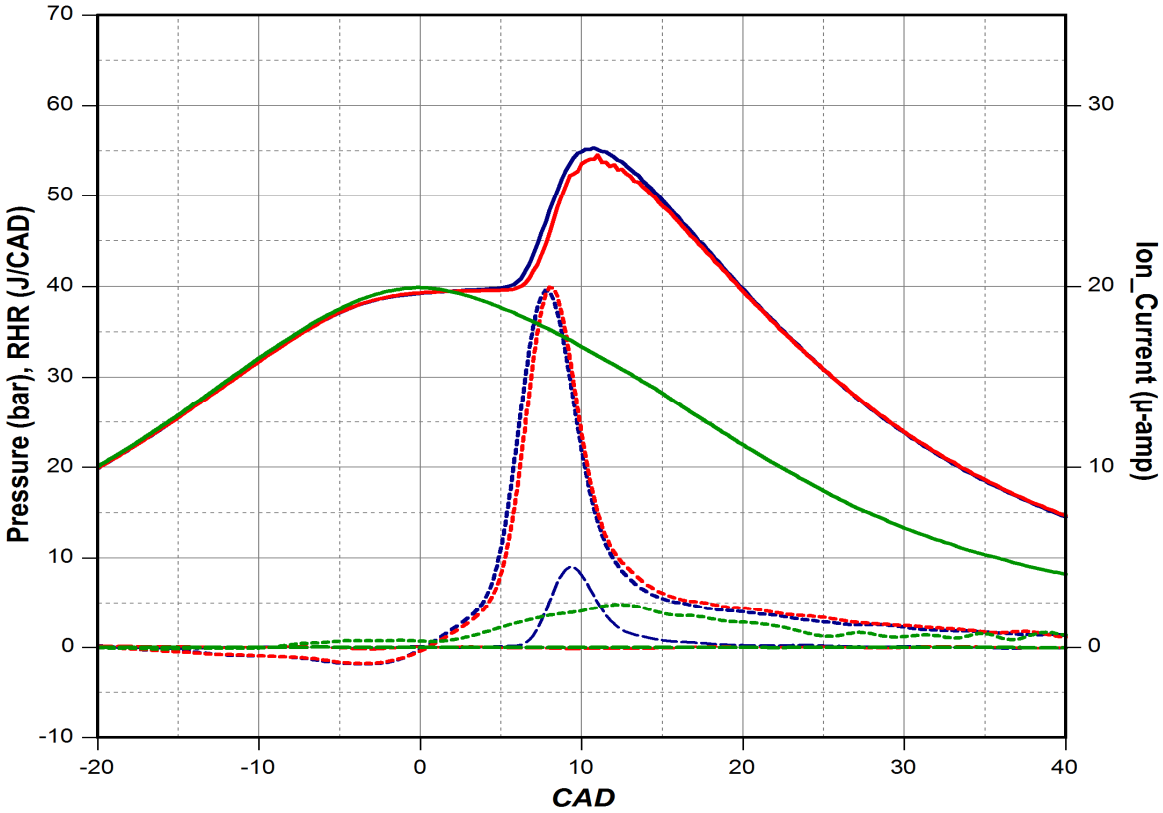

Figure 4.4-1. Cylinder gas pressure, rate of heat release and ion current signal at light load for two arbitrary cycles and a misfired cycle [Inj. Press= 550bar; Const. Speed= 1800 RPM]

4.5 *Combustion and Ion Current Misdetection during Cold Starting in Diesel Engines*

The cold starting in diesel engines is characterized by inherent problems such as misfires and combustion instability leading to significant combustion deterioration during the engine start-up period. Through the period of engine starting, the ignition delay and auto-ignition reactions in diesel combustion exhibit significant discrepancy due to low combustion temperatures reached during engine operation. Consequently, the outcome can be an early combustion, a normal combustion, a very late combustion or even a complete misfire thereby resulting in to combustion instability.

Figure 4.5-1 shows the cylinder gas pressure and RHR traces for seven random cycles recorded during the starting of the engine. The figure shows different combustion phasing during cold starting. Combustion phasing can be determined by many parameters such as the location of the 10%, 90% RHR of the total heat release. In this investigation, LPPC (Location of the peak of RHR due to premixed combustion) is used for combustion phasing.

Figure 4.5-1 shows that combustion phasing was observed as early as -4 CAD and as late as 40 CAD. Therefore, combustion phasing can be considered to be in one of the four zones as shown in the figure. Each cycle can be categorized under one of these zones. It is noticed that the ion current peak in the very late combustion zone is so weak that it cannot be detected by the sensor.

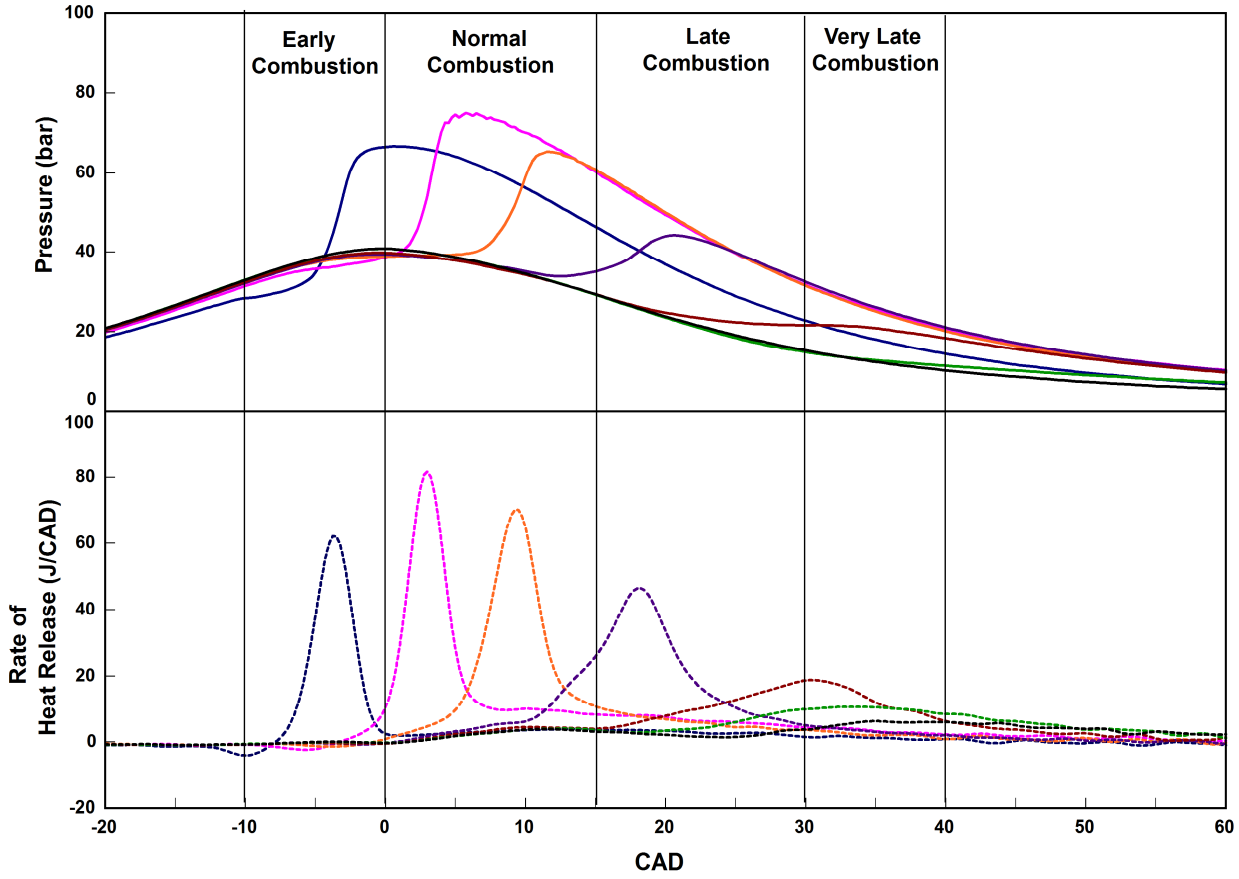

Figure 4.5-1 In-cylinder gas pressure and RHR traces for arbitrary cycles exhibiting different combustion zones during cold starting

Another factor that has an impact on the peak of the ion current signal is the local and average equivalence ratio [12, 13, 18]. Since diesel engines operate on an overall lean fuel-air mixture, the peak of the ion current signal is small compared to that in gasoline engines. During cold starting of diesel engines, although the amount of liquid fuel injected into the combustion chamber is large, the fraction of evaporated fuel is low because of the low mass average air temperatures. This adds to the effect of late combustion on the peak of the ion current signal during the cold start of diesel engines. This poses a challenge in implementing ion current signal as a feedback tool for combustion phasing control during cold starting.

4.6 *Chapter Summary*

The chapter describes the problem of ion current signal misdetection experienced at light loads, typical to idling operation, and cold starting in diesel engines. The causes of the misdetection of the ion current signal are identified after detailed analysis of the combustion process, the ion current signal and images obtained in an optically accessible diesel engine. The lean fuel-air mixture during idling operation and the low in-cylinder combustion temperatures during cold starting result in a weak ion current signal that cannot be detected. This is referred to as Misdetection due to the inability of the sensor of detecting the ion current. The term Actual Misdetection refers to the case when the engine misfires. Misdetection and Actual Misdetection of the ion current signal are problems that need to be addressed before its application as a feedback signal to the engine ECU.

CHAPTER 5

EXPERIMENTAL PROCEDURE

This chapter describes the experiments, test procedure, signals filtering, signal misdetection, and misfiring detection during cold starting and idling.

5.1 *Introduction*

Ion current signal misdetection at idling and light loads is a major problem that needs to be solved before the use of ion current for feedback engine control. The ion current sensor measures the concentration of ionized species in the local area around the probe. [13]. The shape and amplitude of the ion current is influenced by the design of the sensing probe as well as its location in the combustion chamber [18, 20]. To increase the amplitude of the ion current signal, many approaches have considered. These include increasing the probe length, increasing the probe area or changing the applied voltage and polarity of the probe [20, 27, 28].

5.2 *Test Procedure*

The investigation in this thesis is divided into two main sections.

A. Cold Start Tests:

The first consecutive two hundred cycles are recorded at each test point. For each of the cold starting test points the start of injection (SOI) is kept constant at 13° bTDC and the injection pulse width is also maintained constant at 420 µsec.

B. Tests at no-load at three different speeds:

Two hundred consecutive cycles are recorded at each test point under steady state conditions.

A MATLAB code is developed to compute the location of peak of the RHR due to premixed combustion (LPPC) the start of ion current (SIC), and the ratio of cycles where the ion current is not detected to the total number of cycles recorded.

5.3 *Probe Geometry and Applied Voltage used for Experimental Investigation*

The effect of the following three parameters on the ion current signal misdetection is investigated:

1) Probe length: short (20.85 mm), medium (23.7 mm) and long (26.4mm)

2) Probe diameter: small and large: 3.25 mm and 4.75 mm.

3) Applied voltage: 100V to 350V in steps of 50V

Figure 5.3-1 shows the cross sectional view of the combustion chamber along with the penetration of three different probe lengths inside the combustion chamber. Different probe length result into different penetration depth of the probe inside the combustion chamber. The flame type and the volume of ion concentration around the probe can significantly vary with change in the penetration depth of the probe.

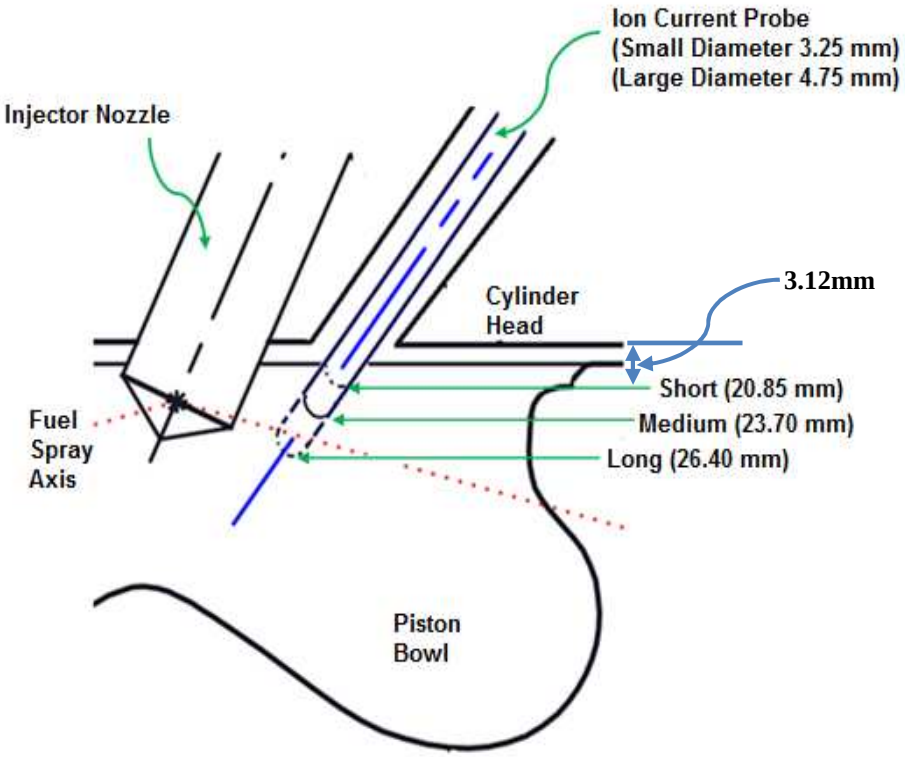

Figure 5.3-1. Cross sectional view of combustion chamber showing penetration of different probe lengths

5.4 *SIC Detection using Dynamic Threshold*

A MATLAB code is used to reduce the noise in the signal and determine the SIC, LPPC and any misdetection on a cycle-by-cycle basis. To reduce the error due to random noise fluctuations, a dynamic threshold for ion current signal is set. A low pass filter is applied to the RHR and ion current signals to get rid of the high frequency noise. A low pass filter with phase correction is used, which has cut-off frequency of 1kHz and a generalized hamming window. The threshold for ion current signal is estimated considering the signal for the 15 CAD (data for

threshold estimation, DTE). The maximum and coefficient of variation (COV) is calculated for this period of signal data for each cycle and the threshold is calculated as stated in Equation 1.

$$\mathbf{Threshold} = [\mathbf{Max(DTE)} + \mathbf{COV(DTE)} \times \mathbf{4} + \mathbf{0.005}] \times \mathbf{2.1} \qquad (\mathbf{Equation\ 1})$$

5.5 *Misfire Detection from RHR Trace*

To assist in identifying misfired cycles, the RHR trace of each cycle is compared with the motored cycle RHR trace. The peak of the RHR trace of the motored cycle is selected as a threshold value to define a cycle misfire. An algorithm is developed in MATLAB to sweep through the RHR trace of each cycle to find the maximum value and its location in CAD. Depending on the comparison of this maximum value with the motoring RHR trace, the cycle is thereby identified as a fired cycle or misfired cycle. The CAD location of the peak of the RHR trace is used to classify combustion as early, normal, late or very late as shown in Figure 4.5-1. A very late combustion cycle is considered be a misfired cycle throughout the investigation.

5.6 *Chapter Summary*

This chapter walks through the experimental approach undertaken towards resolving the ion current signal misdetection. Different probe geometries have been used for the detailed experimental investigation of the ion current signal misdetection with the aim to improve ion current signal detection and its utilization for misfire detection during cold starting and idling operation. The approach used for the detailed analysis of the transient and steady state data is thoroughly described in this chapter.

CHAPTER 6

EXPERIMENTAL RESULTS: COLD STARTING

This chapter presents results of investigations on the effect of the probe geometry and the applied voltage on the amplitude of the ion current signal. Probes of different lengths and diameters are used to determine the ability of the sensor to detect the misfiring cycles.

6.1 *Introduction*

The shape and amplitude of the ion current signal depends on (a) surface area of the probe exposed inside the combustion chamber, (b) the location of the probe in the combustion chamber and (c) the applied voltage across the electrodes [18, 20] . Short, medium and long probe lengths are used to study the effect of increasing the penetration depth of the probe into combustion chamber on the detection of the ion current signal. The effect of change in the probe diameter along with change in the probe length is also investigated using small and large diameter probes. Furthermore, the applied voltage is varied from 100 to 350V for each probe length and probe diameter to study the effect applied voltage on the ion current signal detection. Due to redundant nature of the results and to avoid repetition of figures limited data analysis is reported.

6.2 *Effect of Probe Length on Ion Current Signal Characteristics and Detection*

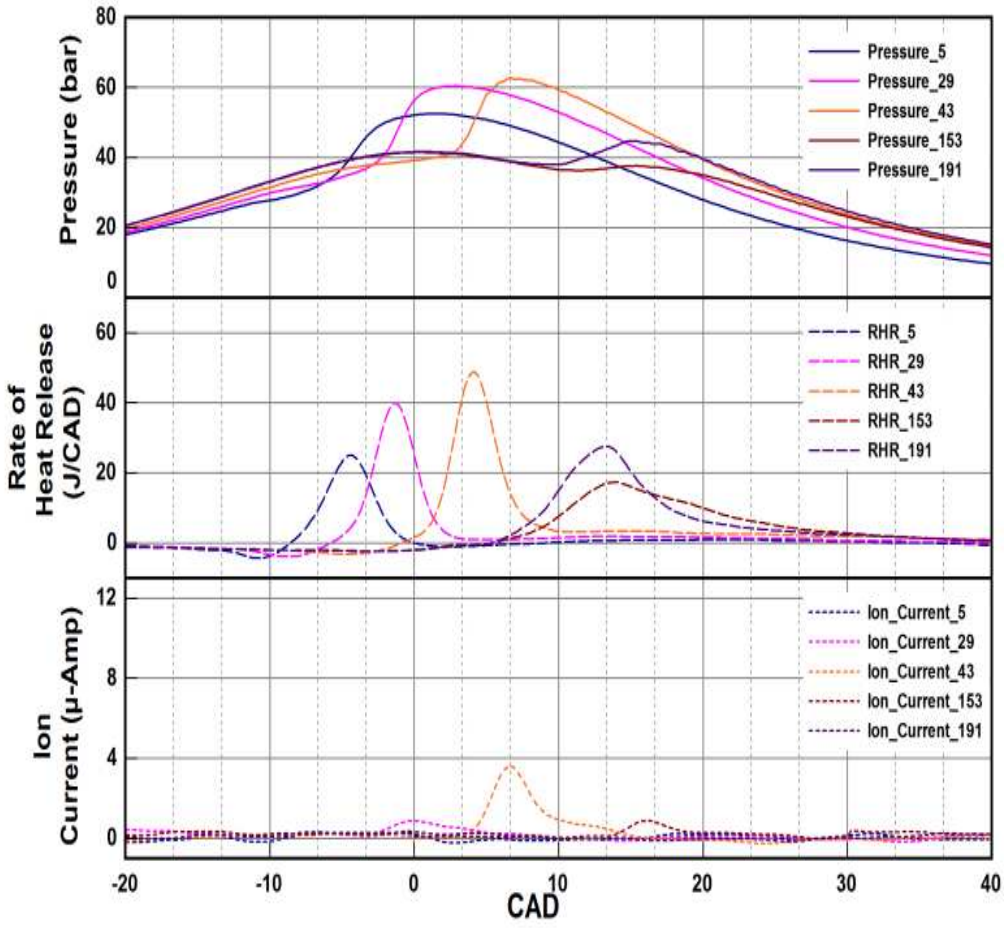

Figure 6.2-1. Cylinder gas pressure, RHR and ion current signal for five random cycles using the short probe (20.85 mm) at applied voltage of 100V

Figure 6.2-1 shows cylinder gas pressure, RHR and ion current signal traces for five randomly selected cycles recorded with a short probe length at an applied voltage of 100V. It is noticed the short probe failed to detect ion current signal for some cycles where combustion occurred as evidenced from their respective pressure and RHR traces.

6.3 *Effect of Applied Voltage on Ion Current Characteristics and Detection*

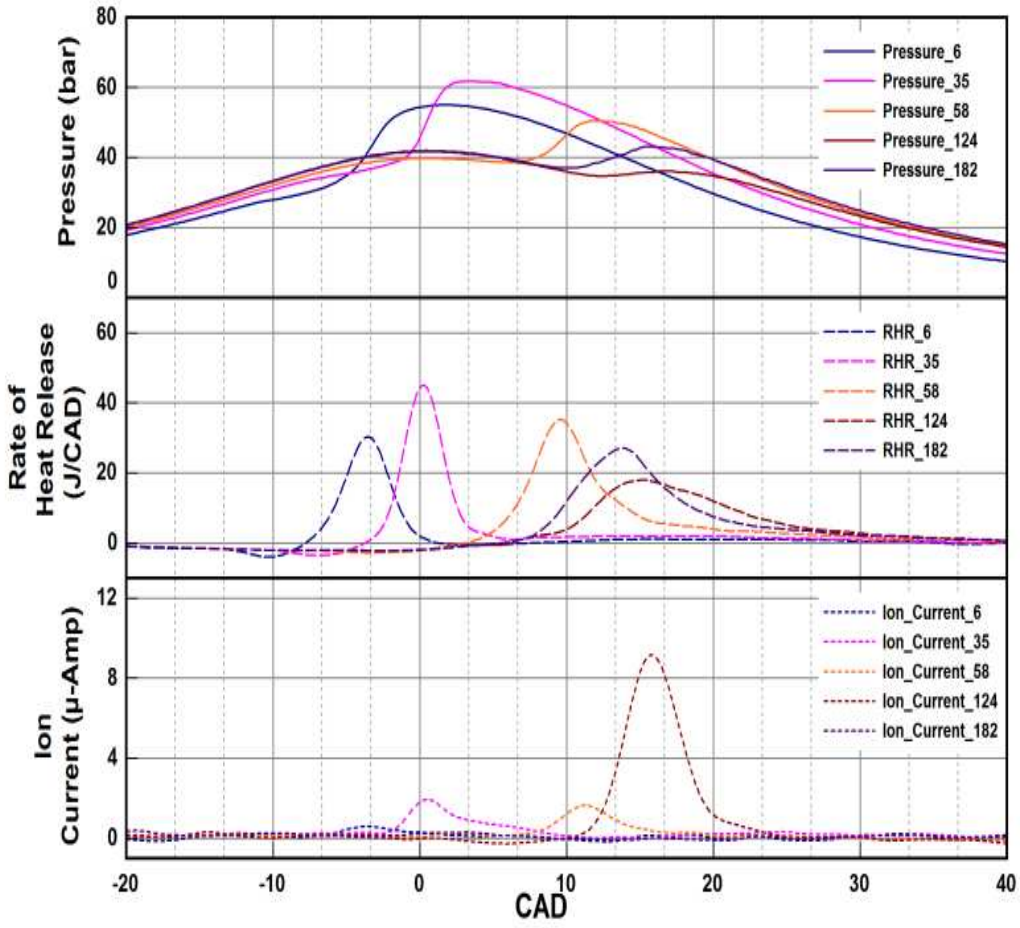

Figure 6.3-1. Cylinder gas pressure, RHR and ion current signal for five random cycles using the short probe (20.85 mm) at applied voltage of 350V

Figure 6.3-1 shows the effect of increasing the applied DC voltage from 100 to 350V. By increasing the voltage the amplitude of the ion current signals increased. However, raising the voltage by a factor of 3.5 did not improve the ion current signal to the point of detecting the combustion in all cycles.

6.4 *Combined Effects of Probe Length and Applied Voltage on Ion Current Characteristics and Detection*

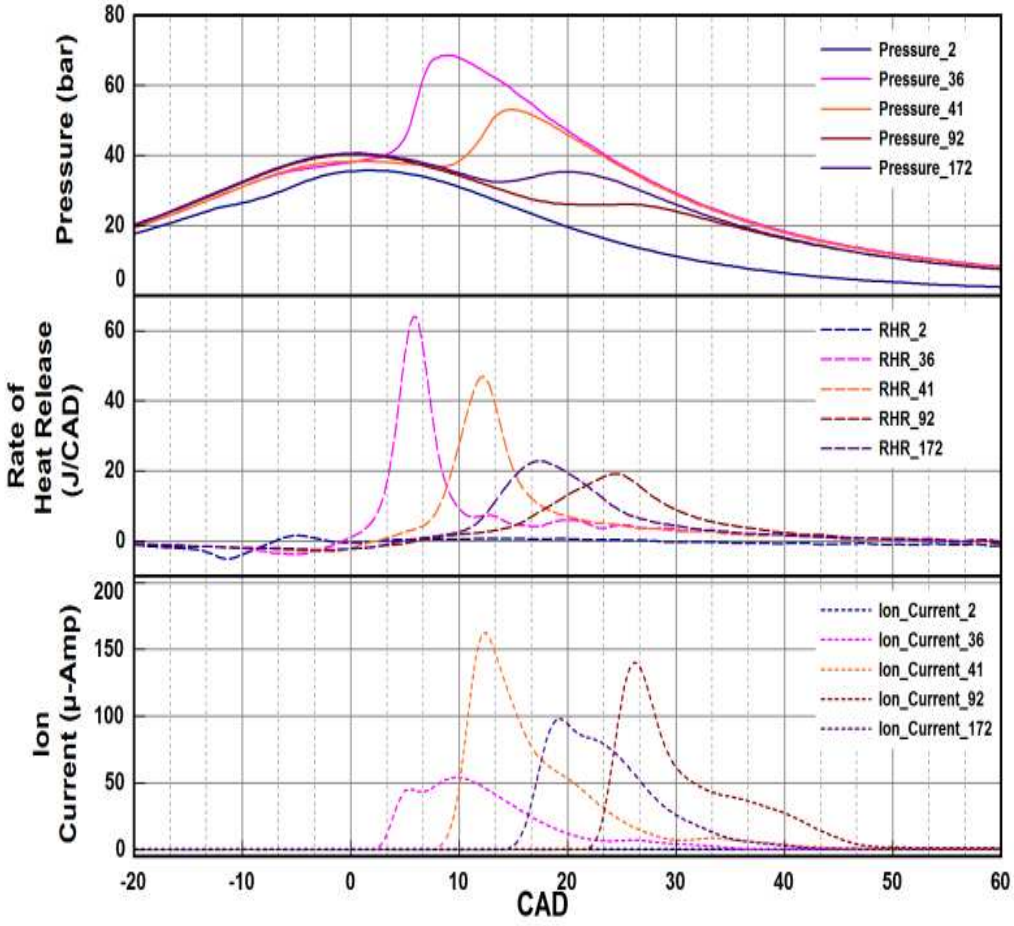

Figure 6.4-1. Cylinder gas pressure, RHR and ion current signal for five random cycles using the long probe (28.40 mm) at applied voltage of 100V

Figure 6.4-1 shows cylinder gas pressure, RHR and ion current signal for random cycles recorded during cold starting with a probe (28.40 mm long) at an applied voltage of 100V. By increasing the probe length a larger area of the probe was exposed to the combustion products and produced signals with higher amplitudes compared to that with short probe length. It is also worth

noting that using a longer probe length undoubtedly detected the ion current signal under all combustion phases encounters during cold starting. Furthermore, it is worth noting that the ion current signal is detected for all the cycles except for the misfired cycle seen in Figure 6.4-2.

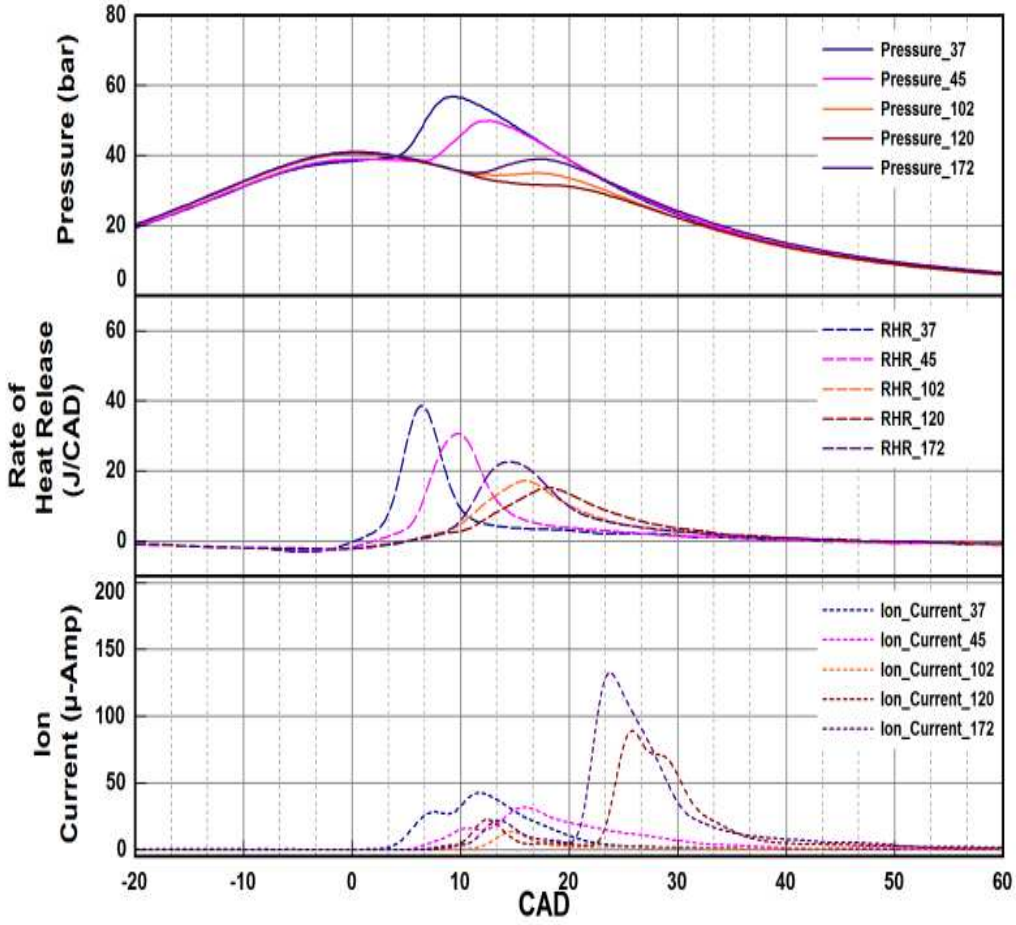

Figure 6.4-2. Cylinder gas pressure, RHR and ion current signal for five random cycles using the long probe (28.40 mm) at applied voltage of 350V

Figure 6.4-3 shows in-cylinder gas pressure, RHR and ion current signal traces for random cycles recorded during cold starting using a long probe (28.40 mm) and higher applied voltage of 350V. Increasing the applied voltage from 100V to 350V further increased the amplitude of the ion current signal recorded.

The pressure traces of arbitrary cycles in Figure 6.2-1, Figure 6.3-1, Figure 6.4-1, and Figure 6.4-2 demonstrate random cycle to cycle variation and combustion deterioration in some cycles during cold starting. Even under such varying operating conditions the effect of the probe length on the ion current signal detection and its amplitude is noteworthy and seen in Figure 6.4-3.

Figure 6.4-3 shows data for two comparable combustion cycles both exhibiting a very late combustion but one with a short probe (20.85 mm)and the second with a long probe (28.40 mm), at applied voltage of 350V. The long probe length successfully detected ion current signal for the very late combustion event, whereas short probe length failed to detect any ion current signal.

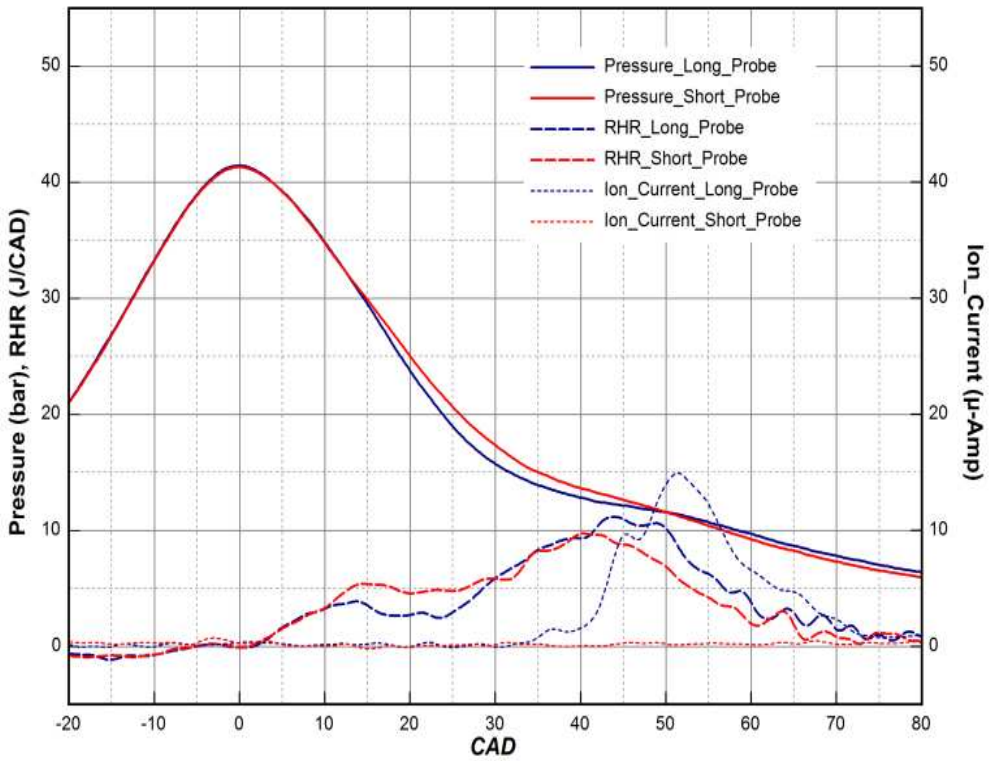

Figure 6.4-3. Cylinder gas pressure, RHR and ion current traces for two cycles with late combustion: one with the short probe length and the other with long probe length and at same applied voltage of 350V

6.5 *Ion Current in a Cold Start Transient*

A detailed cycle-by-cycle analysis was made on two hundred consecutive cycles recorded during a cold starting transient, using probes of different lengths. A sample of the results is given in Figure 6.5-1 for the first 200 cycles. The following parameters are shown for each of the 200 cycle in four sections starting from the top. (1) Instantaneous engine speed, (2) LPPC and SIC, (3) RHR, where "1" is for a fired cycle and "0" is for a misfired cycle; also shown in the same section the ion current where "1" is for detected and "0" is for misdetected. (4) Actual misdetected ion current signal, which indicates very weak combustion, complete combustion failure. The details of the few cycles are shown in Figure 6.5-2.

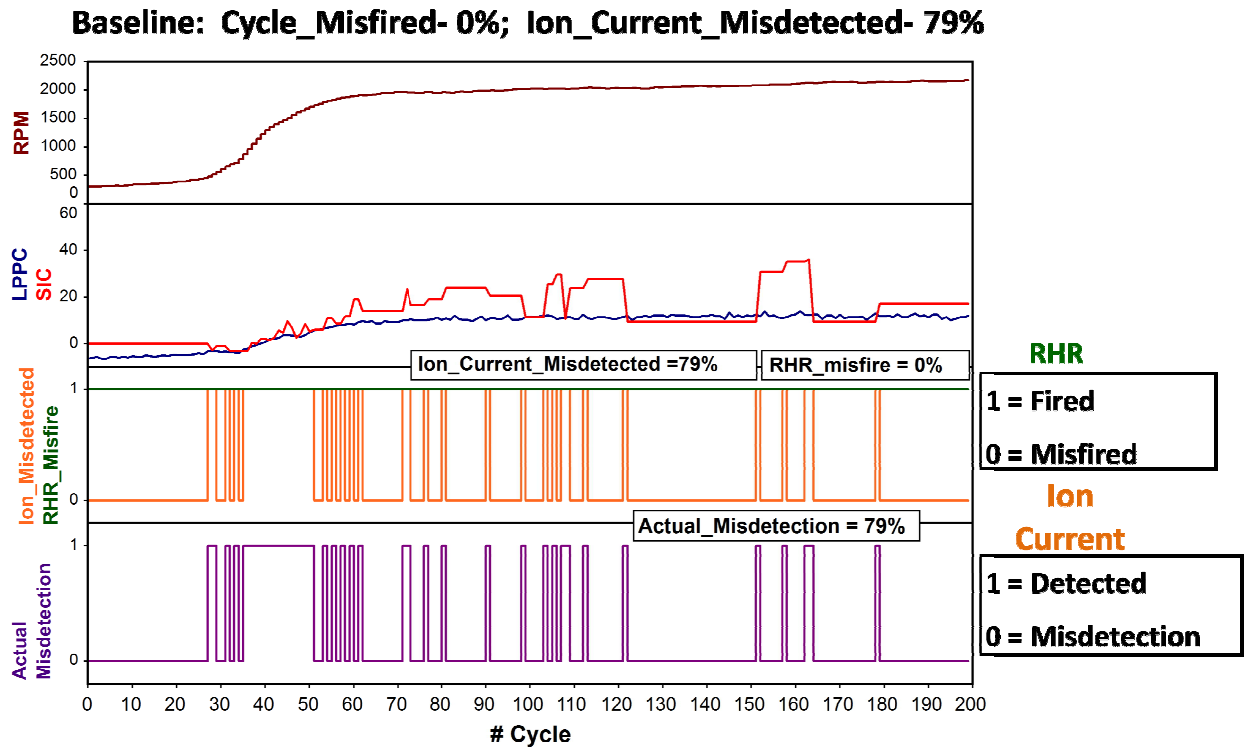

Figure 6.5-1 Sample figure representing the Ion Current Signal Detection and Misdetection Data Analysis

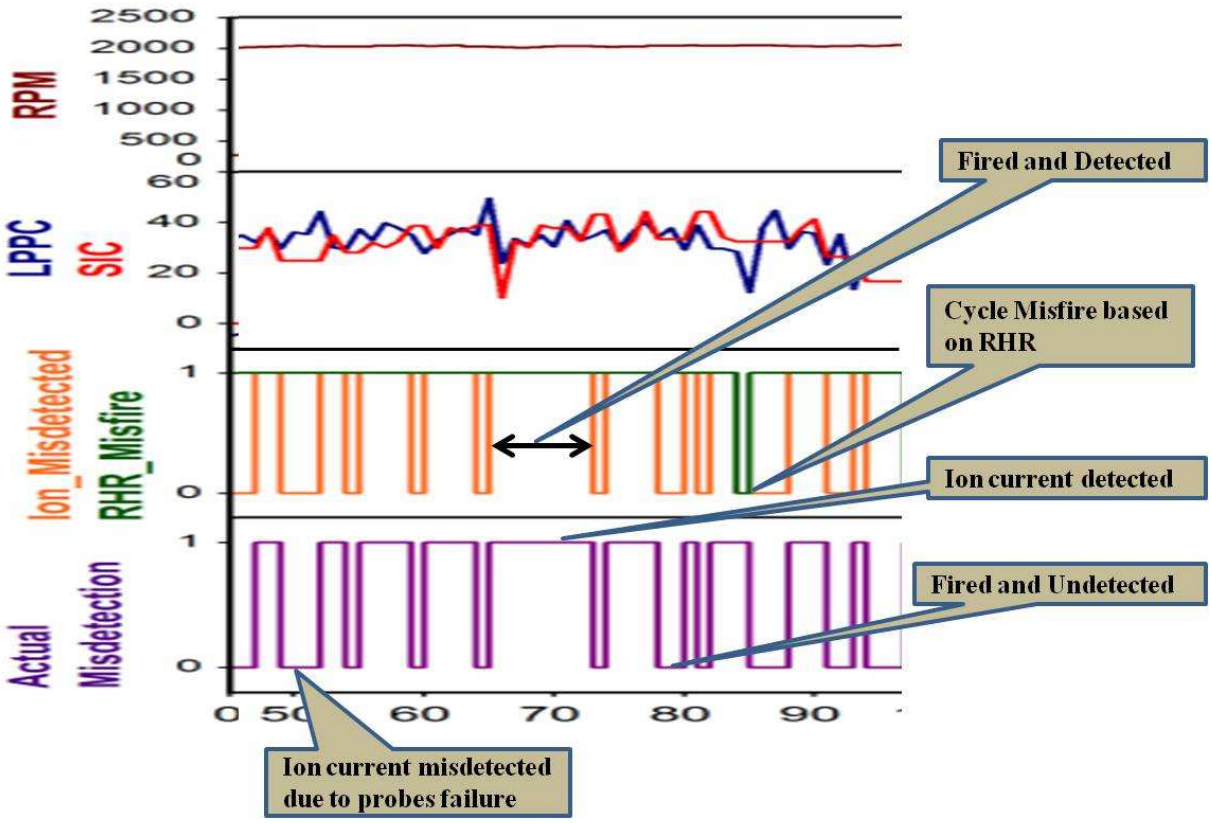

Figure 6.5-2 Representation of (a) Fired and Detected Cycle (b) Fired and Undetected, probes failure cycle and (c) Misfired Cycle

6.5.1 Effect of Probe Length at Applied Voltage of 100V

Figure 6.5-3, Figure 6.5-4 and Figure 6.5-5 show results of the processed data for short, medium and long probes respectively at an applied voltage of 100V. For short probe length (Figure 6.5-3), misfire cannot be detected from the RHR but the fired cycles with ion current misdetection are 79%. This implies that only 21% of the firing cycles are detected with the ion current signal. With medium probe length (Figure 6.5-4), the ion current detection improved significantly by increasing the penetration depth of the probe. No misfire is detected from RHR but the number of cycles with ion current signal misdetection is reduced to 24.5%.

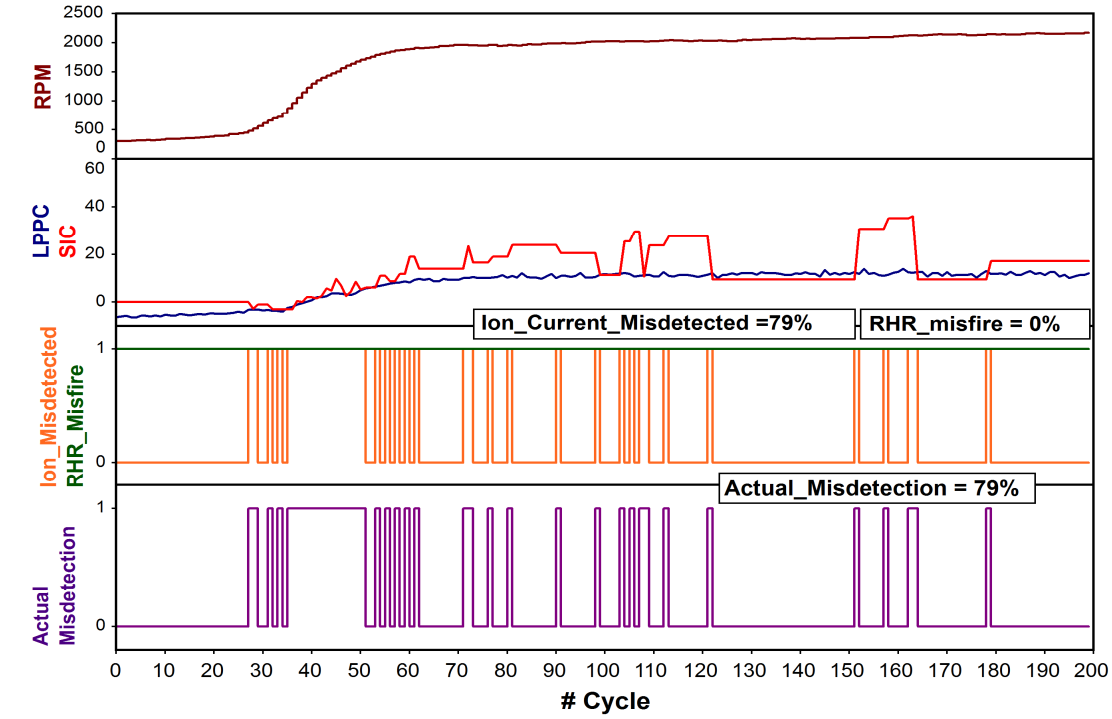

Figure 6.5-3. Detailed processed data showing RPM, SIC, LPPC, misfire and ion current misdetection for short probe at applied voltage of 100V

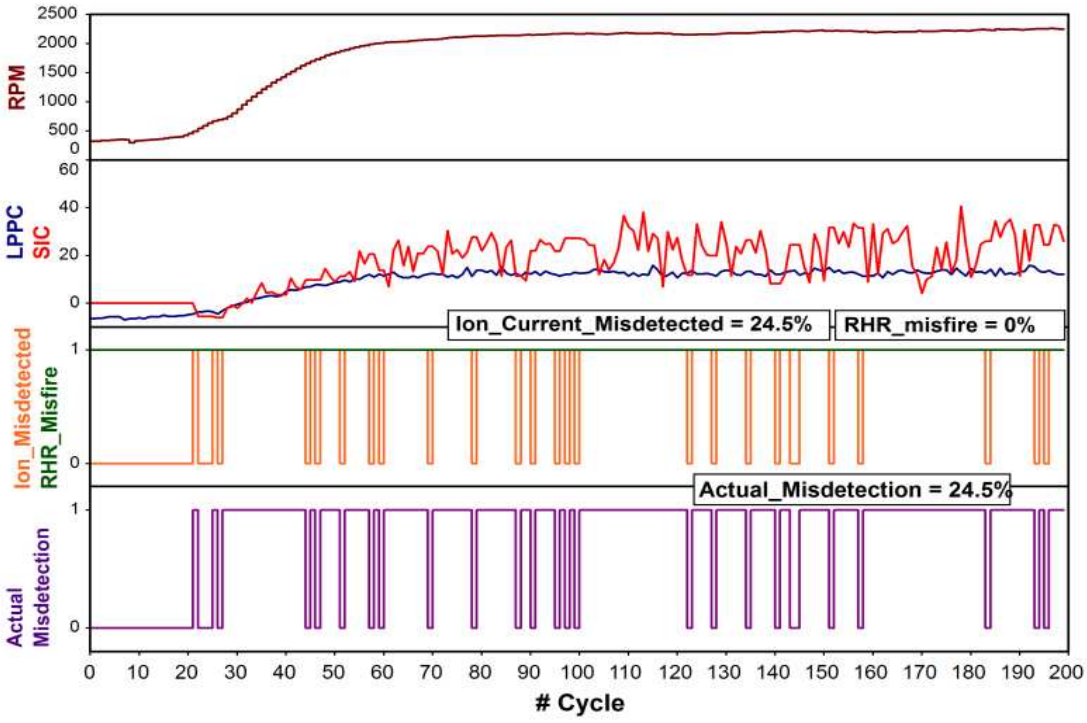

Figure 6.5-4. Detailed processed data showing RPM, SIC, LPPC, misfire and ion current misdetection for medium probe at applied voltage of 100V

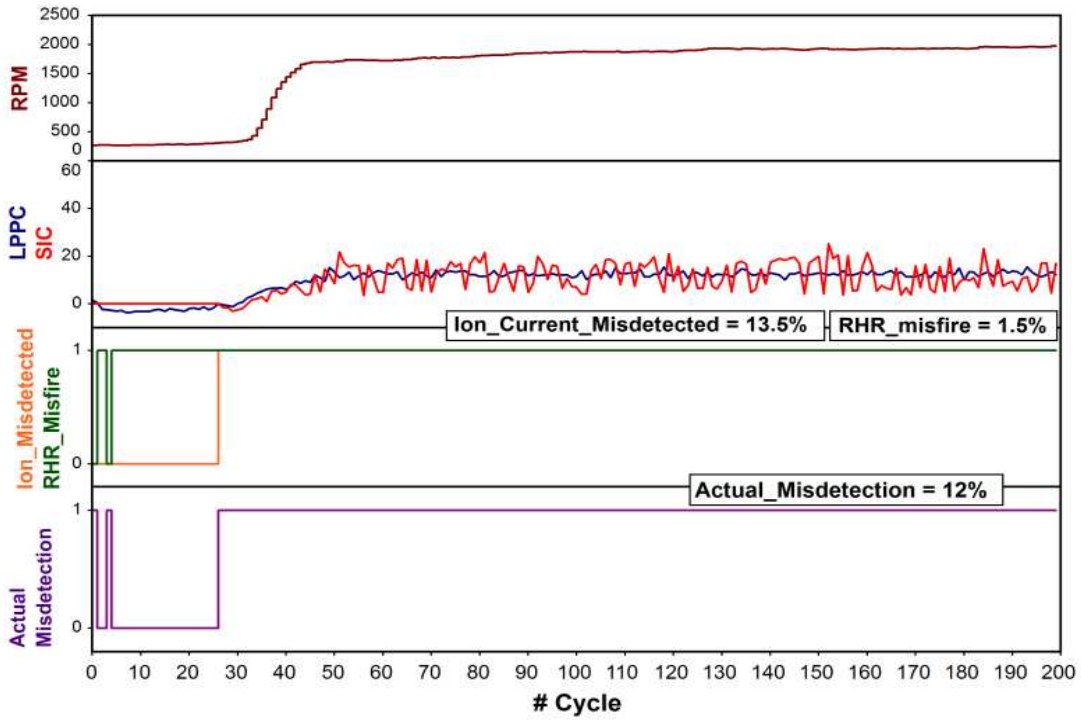

Figure 6.5-5. Detailed processed data showing RPM, SIC, LPPC, misfire and ion current misdetection for long probe at applied voltage of 100V

Further increase in the probe length to the long probe (Figure 6.5-5), caused the percentage of fired cycles with ion current misdetection to significantly decrease to 13.5% along with misfired cycles based on RHR recorded as 1.5%. Therefore, the number of actual cycles with ion current misdetection excluding the misfired cycles is only 11%. Moreover, during engine acceleration, it is also observed that SIC detected by all the three probes is fairly accurate. While approaching idling speed, the accuracy for detecting the SIC is low for the short probe and significantly improved for longer probe. Also, the variation in the SIC is highest for the short probe and is reduced with the increase in the probe length.

6.5.2 Effect of Probe Length at Applied Voltage of 350V

Figure 6.5-6, Figure 6.5-7 and Figure 6.5-8 show results for the short, medium and long probes with applied voltage of 350V. With the increase in the applied voltage, the electromagnetic field around the electrodes increases and therefore the probe attracts more charge carriers. Figure 6.5-6 shows ion current detection for short probe improved by 10% with the increase in applied voltage from 100 to 350V. For medium probe (Figure 6.5-7), the actual misdetection of ion current is found to be 11% and it further reduces to 8% for long probe length (Figure 6.5-8). Also, an increase in the applied voltage improves the accuracy of SIC detection for all the three probes.

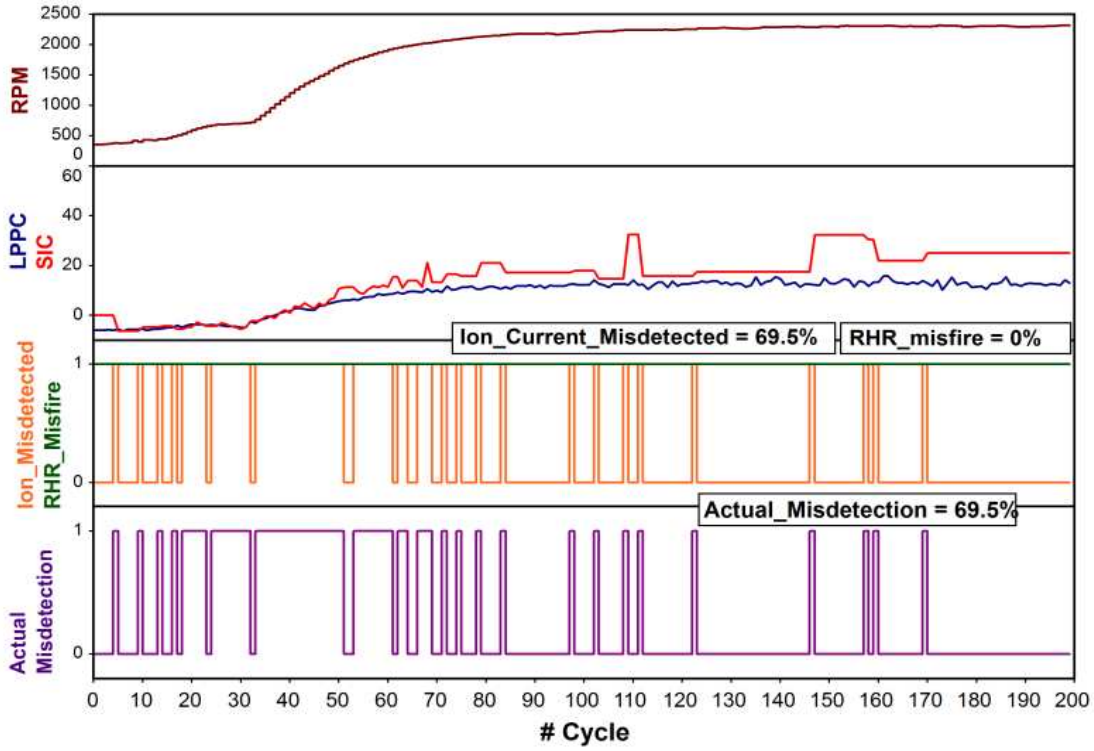

Figure 6.5-6. Detailed processed data showing RPM, SIC, LPPC, misfire and ion current misdetection for short probe at applied voltage of 350V

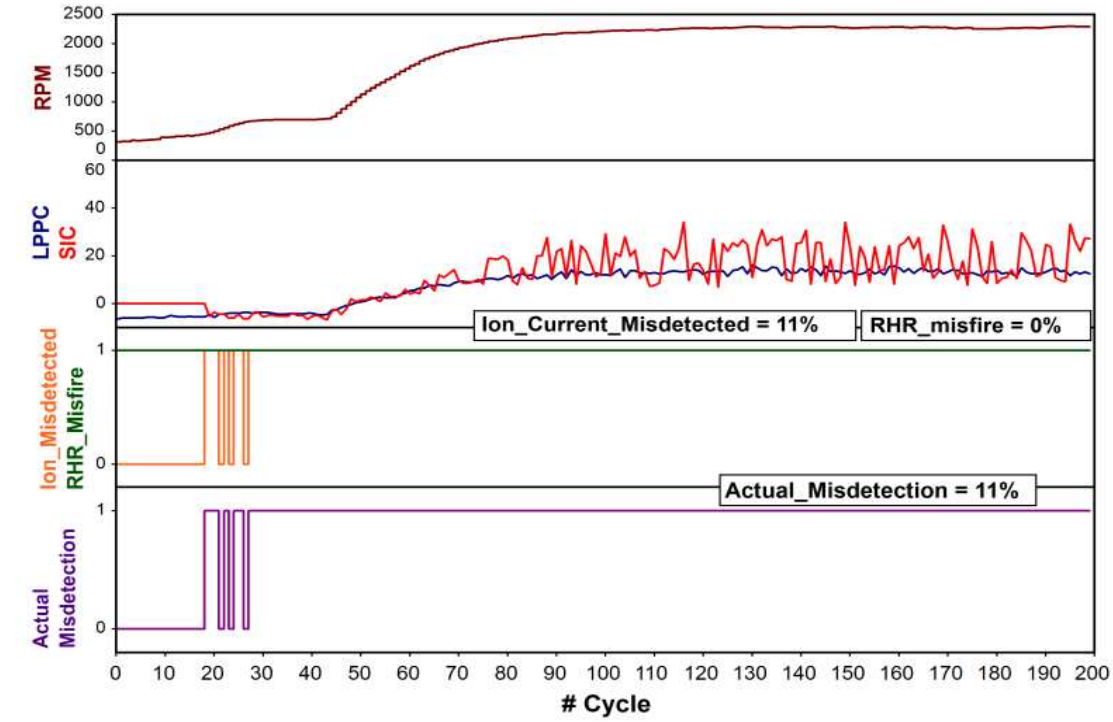

Figure 6.5-7. Detailed processed data showing RPM, SIC, LPPC, misfire and ion current misdetection for medium probe at applied voltage of 350V

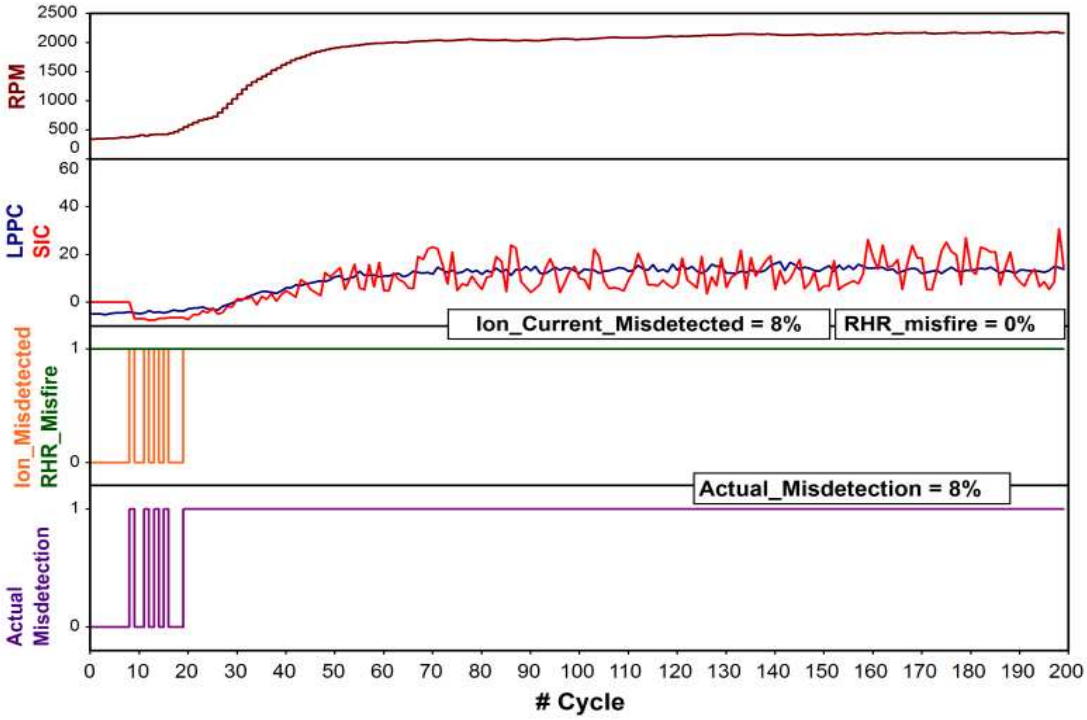

Figure 6.5-8. Detailed processed data showing RPM, SIC, LPPC, misfire and ion current misdetection for long probe at applied voltage of 350V

6.5.3 Effect of Probe Diameter at Applied Voltage of 100V

The surface area of the probe exposed into the combustion chamber for sensing the ion current can be increased by changing the probe length as well as probe diameter. Same tests of varying the probe length from short to long probe with applied voltage from 100 to 350V are conducted for the larger probe diameter. Figure 6.5-9, Figure 6.5-10 and Figure 6.5-11 show the data for a large probe diameter for the short, medium and long probe lengths respectively at applied voltage of 100V.

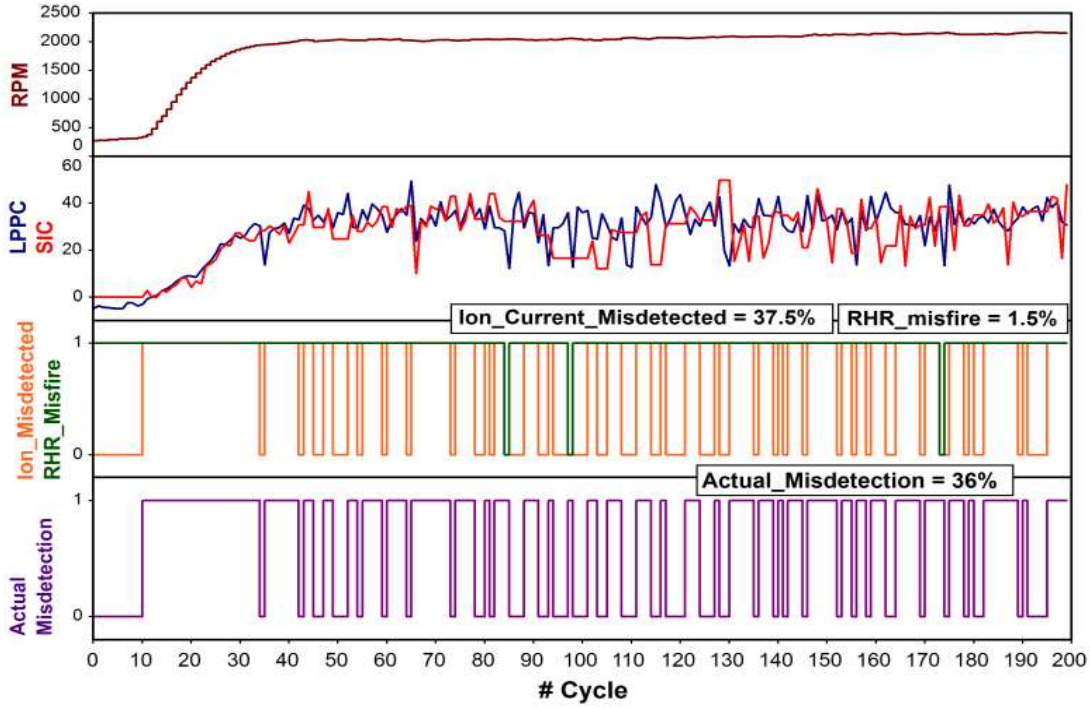

Figure 6.5-9. Detailed processed data showing RPM, SIC, LPPC, misfire and ion current misdetection for short probe length and large probe diameter at applied voltage of 100V

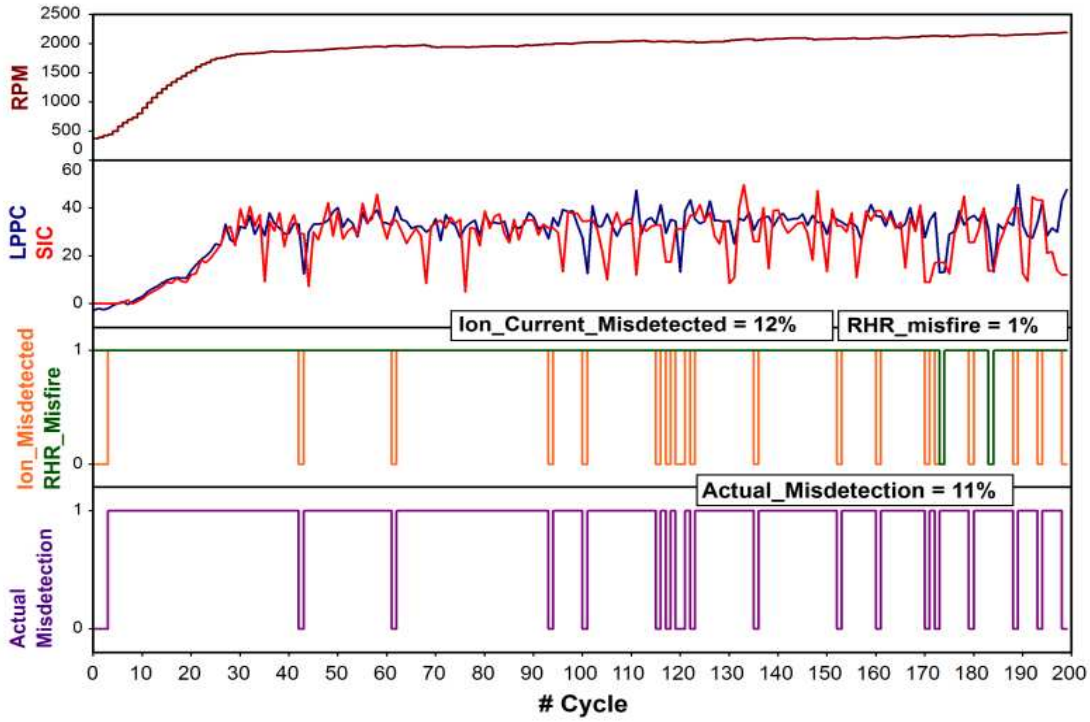

Figure 6.5-10. Detailed processed data showing RPM, SIC, LPPC, misfire and ion current misdetection for medium probe length and large probe diameter at applied voltage of 100V

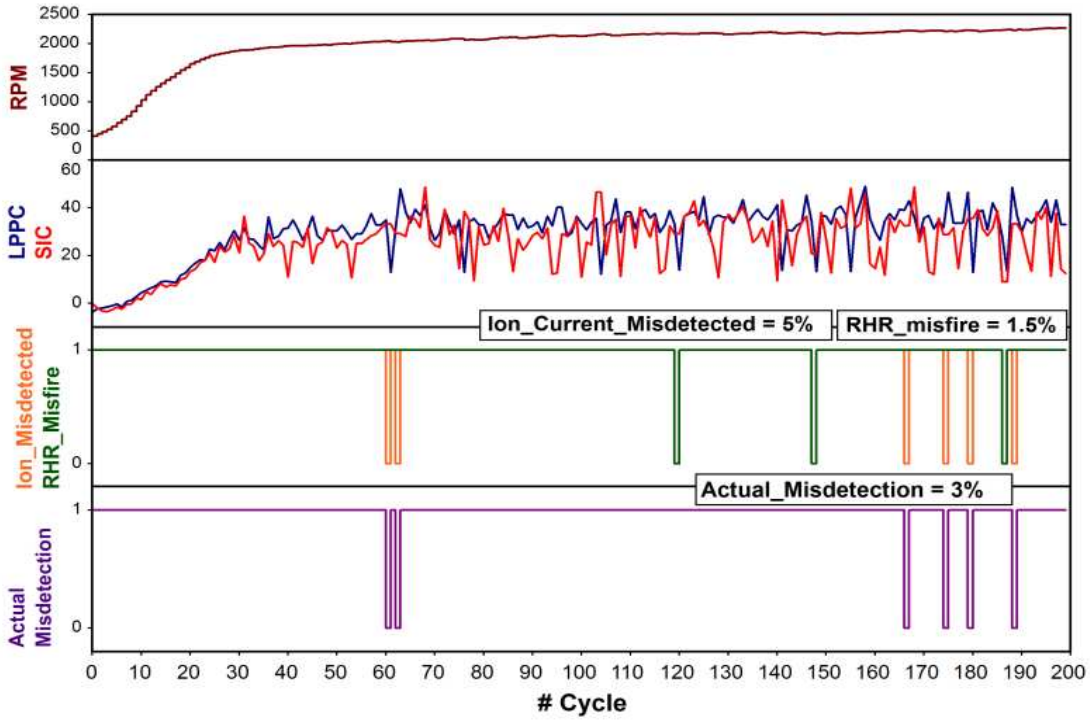

Figure 6.5-11. Detailed processed data showing RPM, SIC, LPPC, misfire and ion current misdetection for long probe length and large probe diameter at applied voltage of 100V

Figure 6.5-9 shows that for a short probe, the number of cycles with ion current misdetection is 37.5% and the number of misfired in the RHR trace is 1.5%. Therefore, the actual misdetection of the ion current signal is 36%. For medium probe shown in Figure 6.5-10, the number of cycles with ion current misdetection is reduced to 12%, whereas 1% misfired. Thus, the number of cycles with the actual ion current misdetection for the medium probe is 11%. Figure 6.5-11 shows the data for the long probe where the cycles with ion current misdetection recorded is 5% out of which 1.5% misfired implying the actual misdetection of the ion current signal of only 3%. The accuracy in detecting the SIC with respect to LPPC improved significantly compared to the respective probes with smaller diameter.

6.5.4 Effect of Probe Diameter at Applied Voltage of 350V

By further increasing the voltage to 350V, for the increased probe diameter, the ion current signal misdetection considerably reduced for all the three probe lengths. For the short probe shown in Figure 6.5-12 the actual misdetection dropped down to 29% from 36% at 100V, which is also significant improvement in ion current detection as compared to 69.5% misdetection with a smaller probe diameter at 350V. For medium probe, the actual misdetection is reduced to 8% as shown in Figure 6.5-13. In the case of long probe shown in Figure 6.5-14, the actual misdetection of the ion current is observed to be only 2%.

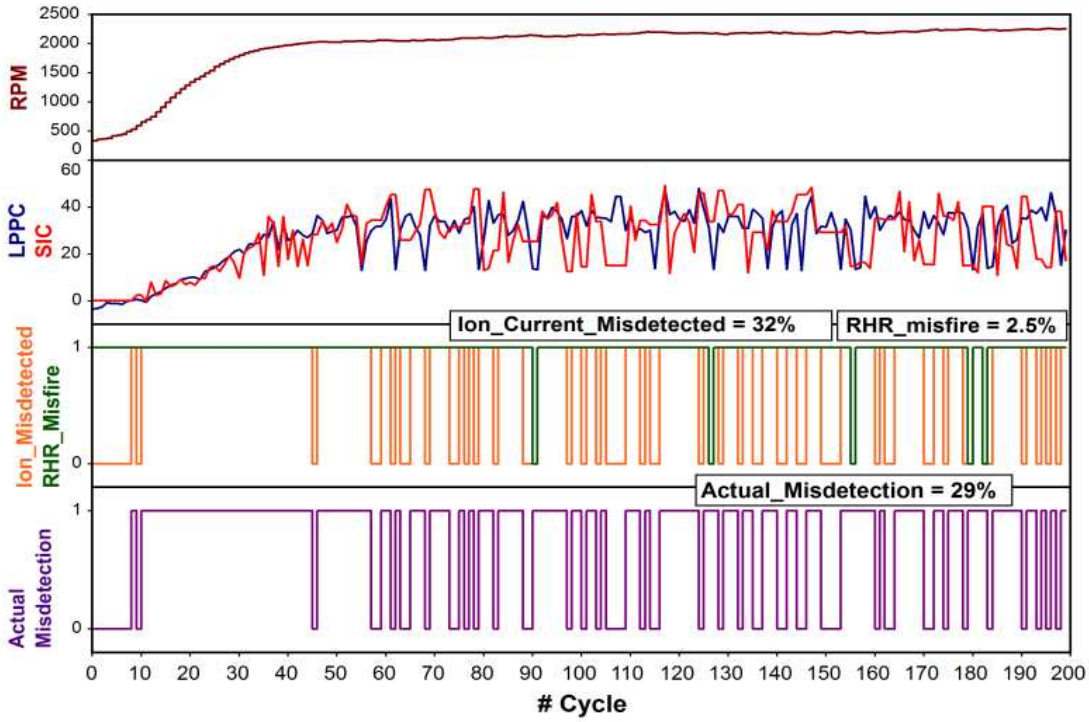

Figure 6.5-12. Detailed processed data showing RPM, SIC, LPPC, misfire and ion current misdetection for short probe length and large probe diameter at applied voltage of 350V

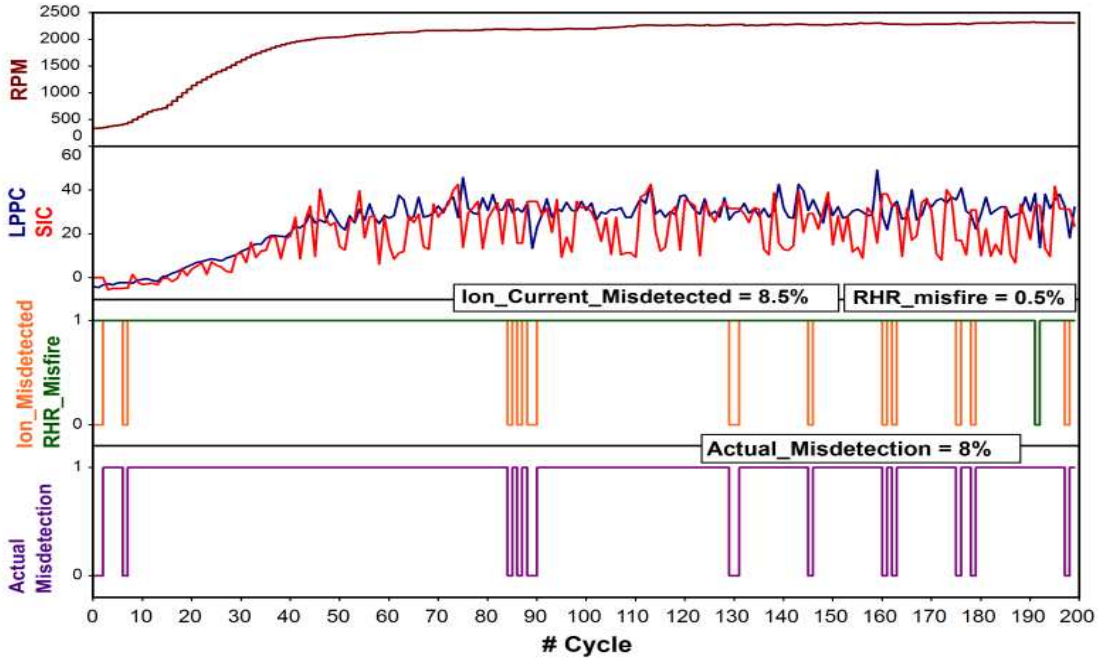

Figure 6.5-13. Detailed processed data showing RPM, SIC, LPPC, misfire and ion current misdetection for medium probe length and large probe diameter at applied voltage of 350V

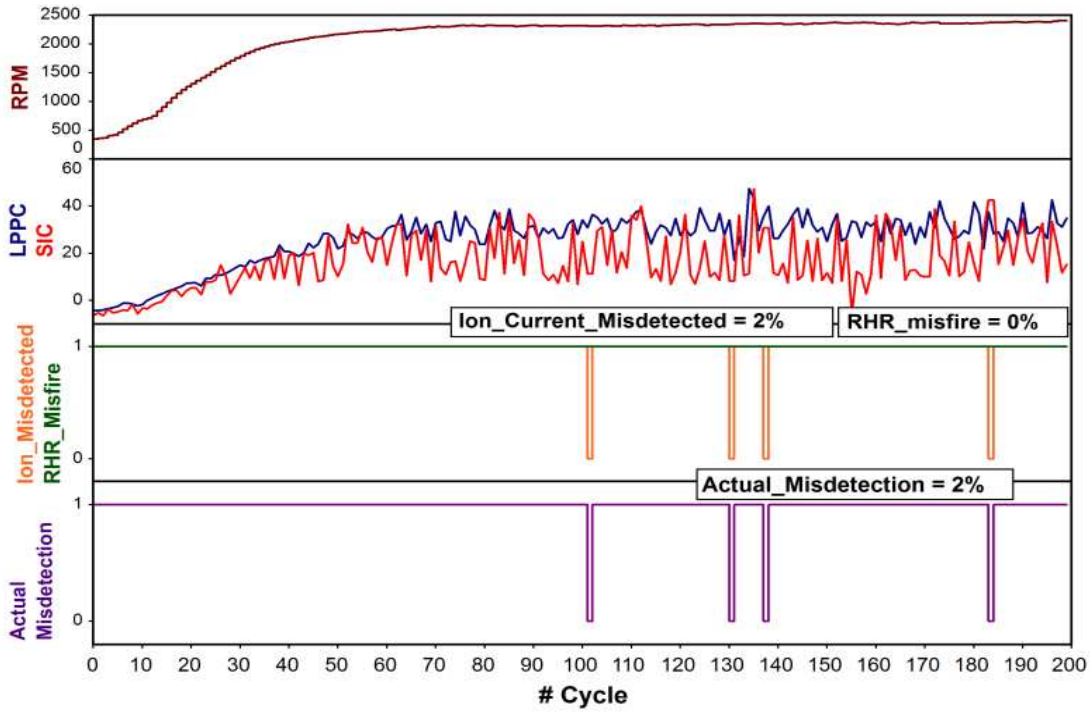

Figure 6.5-14. Detailed processed data showing RPM, SIC, LPPC, misfire and ion current misdetection for long probe length and large probe diameter at applied voltage of 350V

6.6 *Effect of Varying Probe Length, Varying Probe Diameter and Varying Applied Voltage on Actual Misdetection*

Figure 6.6-1 and Figure 6.6-2 shows the percentage of actual misdetection of ion current signal with different probe lengths for small and large probe diameter respectively and plotted against the applied voltage. In Figure 6.6-1, which show the actual misdetection for the small probe diameter, the short probe exhibits the highest misdetection due to the smallest sensing area exposed into the combustion chamber. Although the applied voltage improves the detection of the ion current signal, the maximum improvement achieved is only about 10%. On the other hand, the actual misdetection significantly decreases as the probe length is increased.

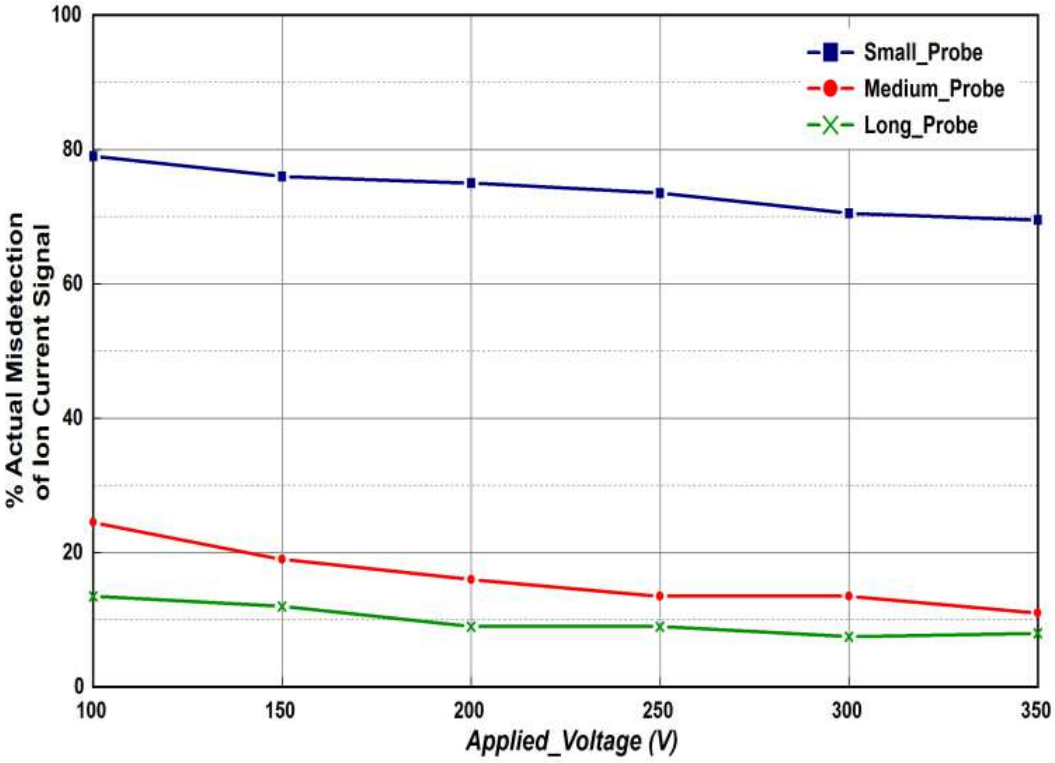

Figure 6.6-1. % Actual Misdetection of ion current for varying probe length with small probe diameter against the applied voltage

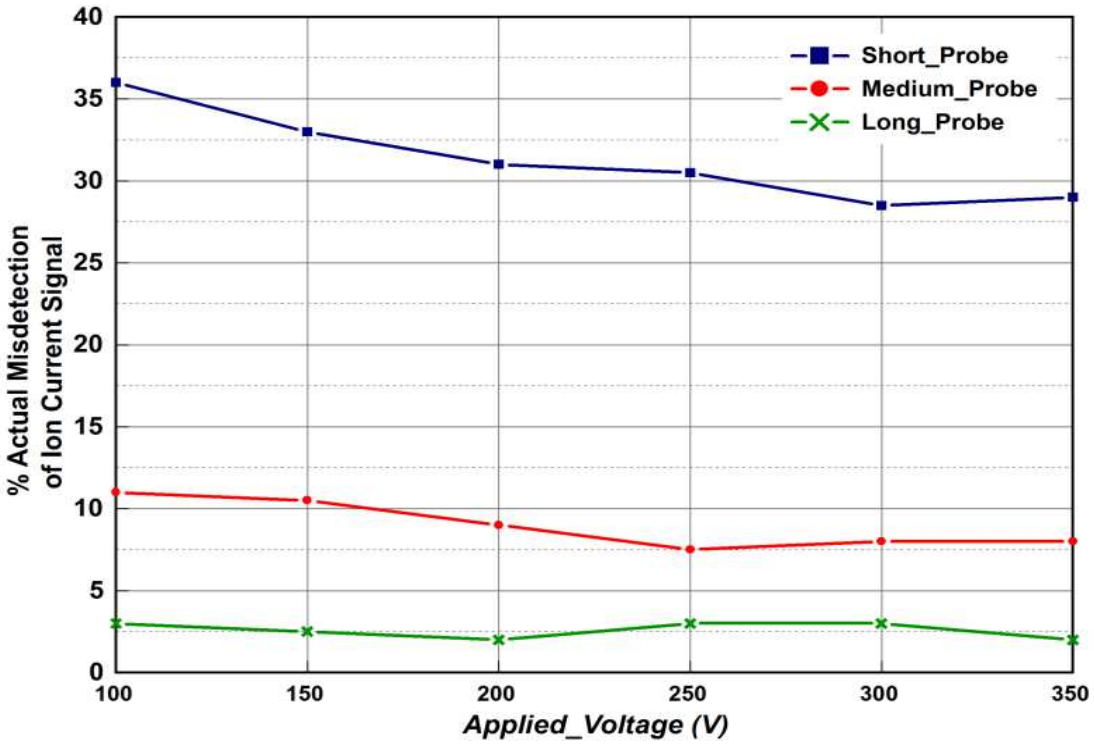

Figure 6.6-2. % Actual Misdetection of ion current for varying probe length with large probe diameter against the applied voltage

Figure 6.6-2 shows an enormous enhancement in the ion current detection for the probes with large diameter. The actual misdetection of the ion current signal for the short probe dropped to 36% compared with 79.5% for the same probe length but with smaller probe diameter at 100V. In addition, increasing the voltage to 350V aided in improving the detection of the ion current by 7%. The medium and long probes showed a major improvement of the ion current signal detection with total actual misdetection lower than 8%.

6.7 *Chapter Summary*

The results from the detailed experimental investigation on the effect of ion current sensor design to improve ion current signal detection during cold starting is described in this chapter. Data from random cycles during the cold starting and cycle-to-cycle data is analyzed to study the effect of change in design parameters and probe intrusion in the combustion chamber, which is related to probe length. Increasing the probe length, diameter and applied DC voltage improve the ion current signal detection during cold starting. However, effect of changing the probe length and changing the probe diameter shows more significant improvement as compared to increase in the applied voltage. Also, increasing probe length, diameter and applied voltage improve the accuracy in determining the SIC during the transient cold starting.

CHAPTER 7

EXPERIMENTAL RESULTS: NO LOAD OPERATION

7.1 *Introduction*

The phenomenon of ion current signal misdetection is reported to occur more often at light loads and idling [22]. It is worth noting that the amount of fuel injected inside the combustion chamber is the least at idling conditions which results in a higher chance of ion current misdetection. Since the overall equivalence ratio is very lean, the concentration of ions formed is low compared to medium and high engine loads. Results for cold starting show that ion current misdetection can be reduced by increasing probe length, diameter and the applied voltage. Therefore, the study is carried out by varying the probe length and diameter at no-load and different speeds in order to examine the ability of the ion current sensor to detect ion current signal during unwarmed up operation. The test conditions are conducted with constant SOI at 13°bTDC. Table 7.1-1 details the injection pulse width duration used for operating the engine at three different speeds.

Table 7.1-1 Injection pulse width at different idling speeds

Speed (RPM)	Injection Pulse width (μsec)
1600	312.5
1800	370.4
2100	396.8

Three idling speeds viz., 1600 RPM, 1800 RPM and 2100 RPM were used for the investigation. However, due to redundant nature of the data, the detailed processed data is shown only for 1800 RPM and at applied voltages of 100V and 350V. The effect of the probe length at all speeds is summarized in the later part of the chapter.

7.2 *Effect of Probe Length on Ion Current Signal Detection*

7.2.1 At Applied Voltage of 100V

At 1800 RPM and applied voltage of 100V, the effect of probe length on the ion current signal detection is shown in Figure 7.2-1, Figure 7.2-2, and Figure 7.2-3 for the short, medium and long probes respectively. For the short probe, the ion current signal misdetection is noted to be 33% as shown in Figure 7.2-1. Also, it is observed that the SIC indicates a small inaccuracy for the short probe as it lags the LPPC due to low signal strength. As the probe length increased from short to medium to long probe the ion current misdetection is reduced from 33% to 8% to 0% respectively. The SIC is advanced with the increase in the probe length suggesting that signal sensing improved with the increase in probe length.

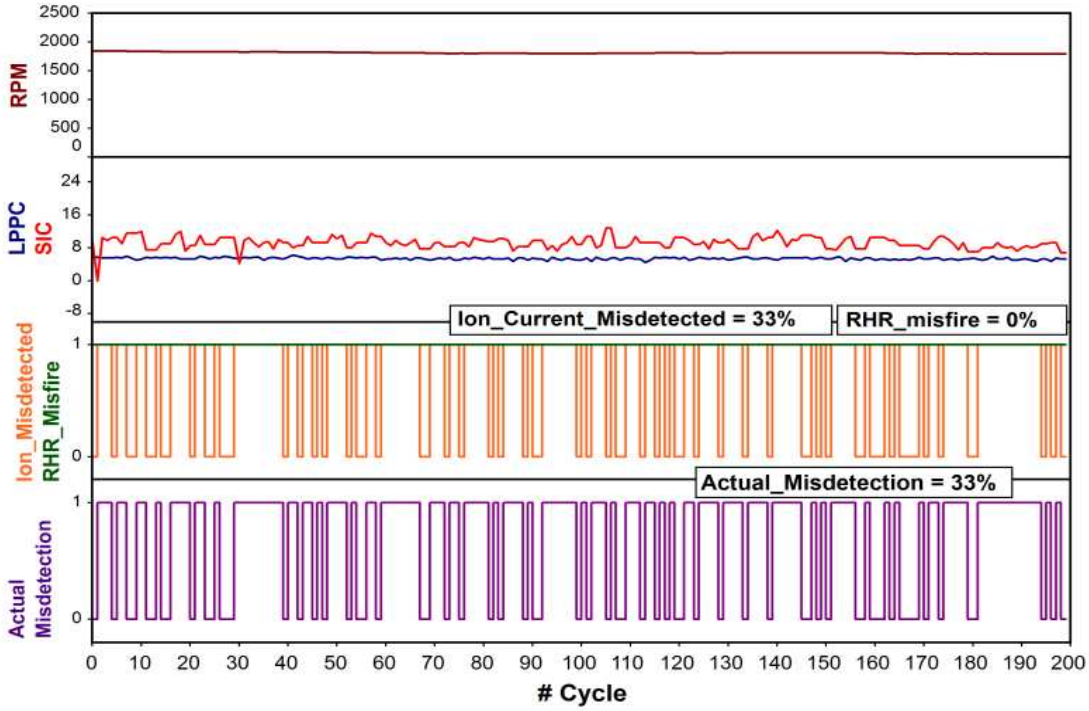

Figure 7.2-1. Detailed processed data showing RPM, SIC, LPPC, misfire and ion current misdetection for short probe at applied voltage of 100V and 1800RPM

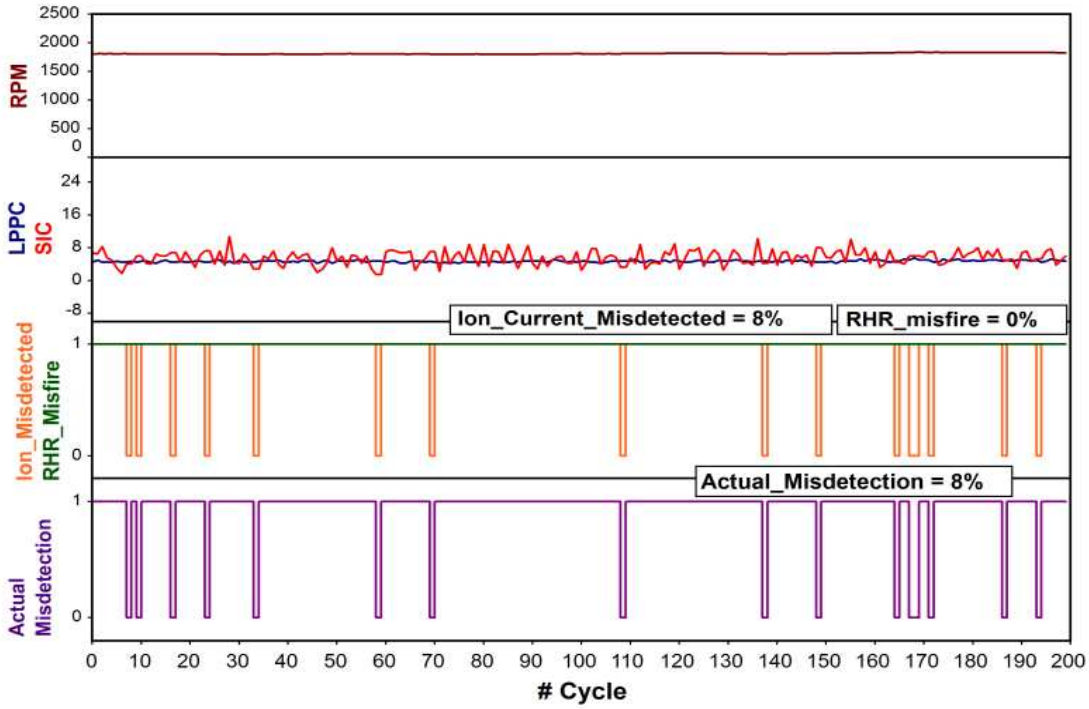

Figure 7.2-2. Detailed processed data showing RPM, SIC, LPPC, misfire and ion current misdetection for medium probe at applied voltage of 100V and 1800RPM

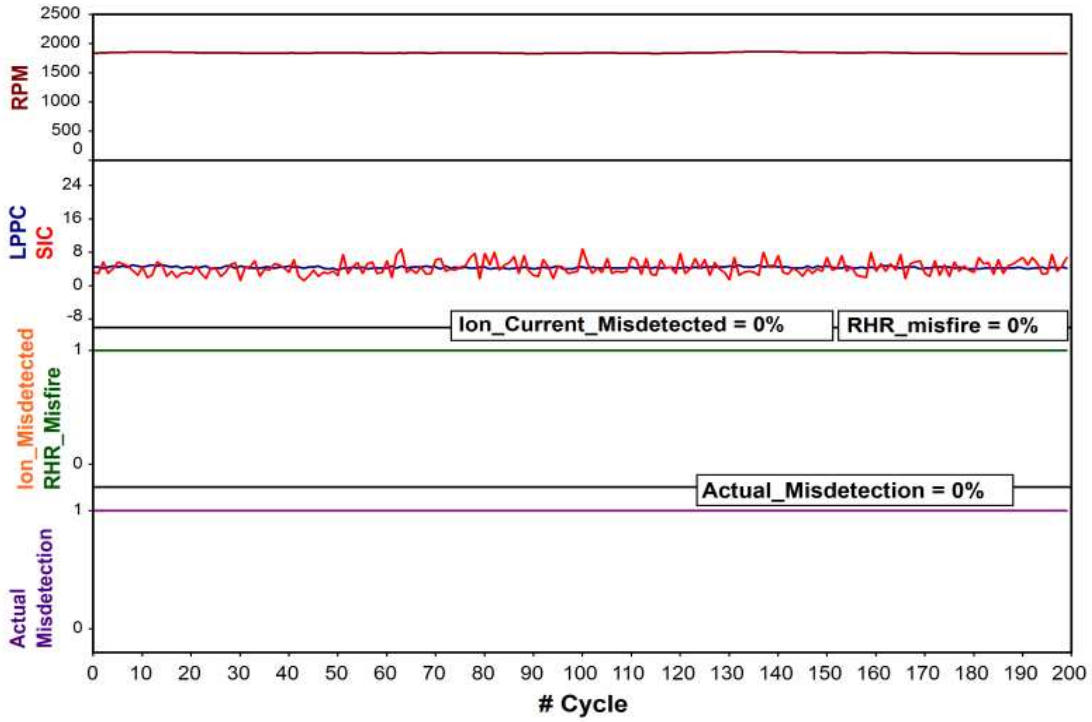

Figure 7.2-3. Detailed processed data showing RPM, SIC, LPPC, misfire and ion current misdetection for long probe at applied voltage of 100V and 1800RPM

7.2.2 At Applied Voltage of 350V

Figure 7.2-4, Figure 7.2-5, and Figure 7.2-6 show results for the effect of increasing applied voltage to 350V on short, medium and long probes respectively. The increase in voltage reduced the signal misdetection for short probe to 3%. Further, the medium probe showed only one cycle with ion current signal misdetection in Figure 7.2-5. Whereas long probe successfully detected ion current signal for all the cycles recorded as seen in Figure 7.2-6. Although the misdetection by increasing the applied voltage show a significant improvement in the ion current detection for the short probe, the SIC detection is however not as accurate as compared to longer probe length.

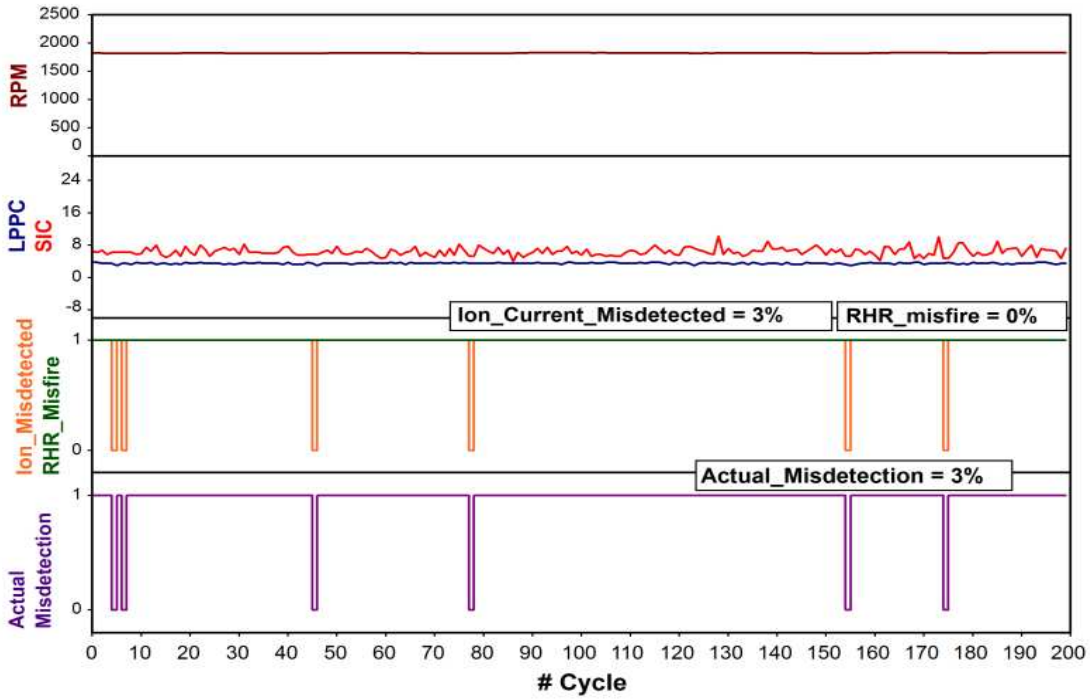

Figure 7.2-4. Detailed processed data showing RPM, SIC, LPPC, misfire and ion current misdetection for short probe at applied voltage of 350V and 1800RPM

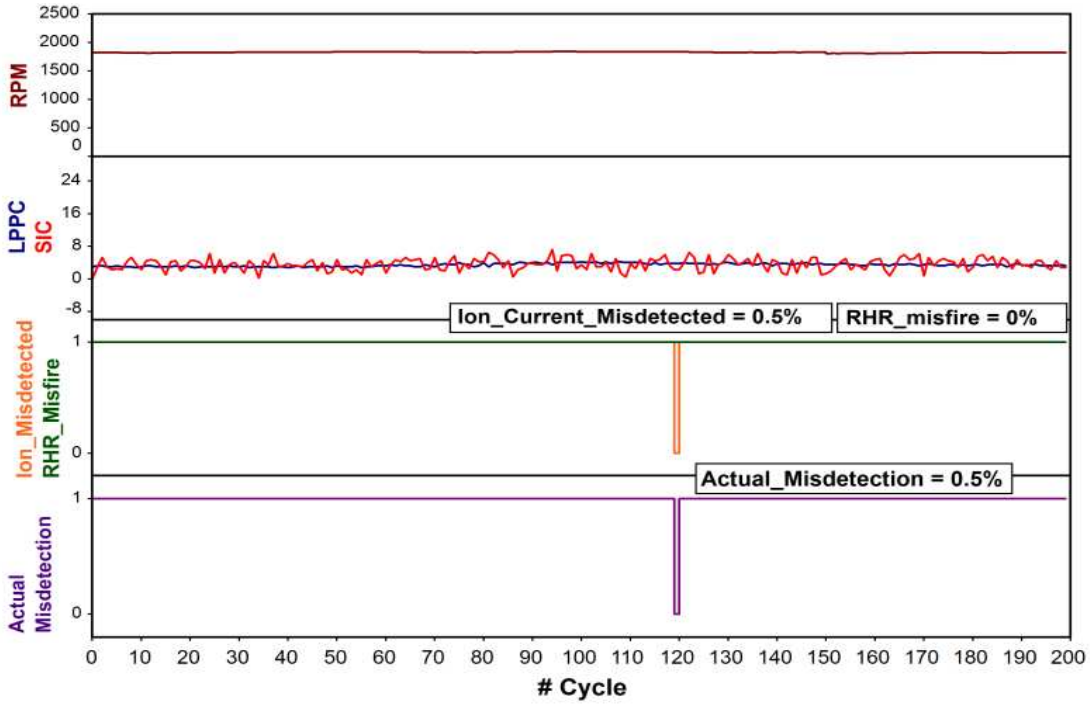

Figure 7.2-5. Detailed processed data showing RPM, SIC, LPPC, misfire and ion current misdetection for medium probe at applied voltage of 350V and 1800RPM

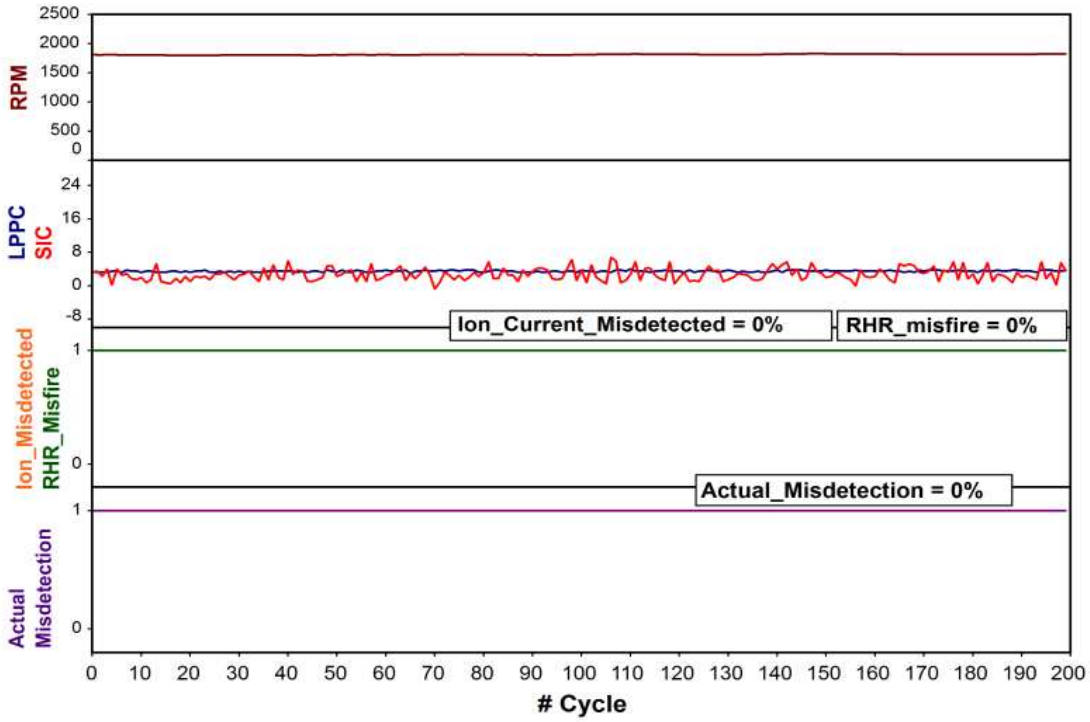

Figure 7.2-6. Detailed processed data showing RPM, SIC, LPPC, misfire and ion current misdetection for long probe at applied voltage of 350V and 1800RPM

7.3 *Effect of Probe Diameter on the Ion Current Signal Detection*

Changing the probe diameter increases the surface area for sensing the ion current inside the combustion chamber. Tests with two different probe diameters at different applied voltages from 100 to 350V are conducted for misdetection analysis at 1600, 1800 and 2100 rpm. Results of the detailed analysis are shown only for the short and long probe length at 100 and 350V at 1800 RPM.

7.3.1 At Applied Voltage of 100V

Figure 7.3-1 and Figure 7.3-2 shows results for short probe and long probe at 1800 rpm and with the applied voltage of 100V. Short probe showed ion current signal misdetection only for 2% of the cycles whereas the long probe has no misdetection of ion current signal for all the cycles recorded.

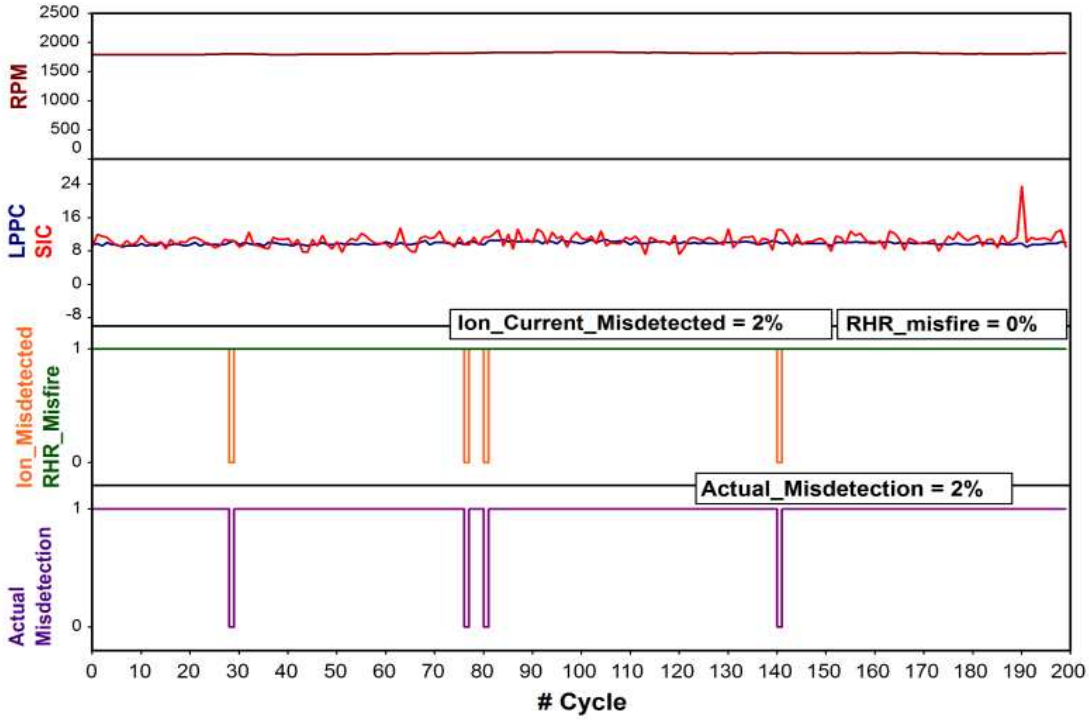

Figure 7.3-1. Detailed processed data showing RPM, SIC, LPPC, misfire and ion current misdetection for short probe with increased probe diameter at applied voltage of 100V and 1800RPM

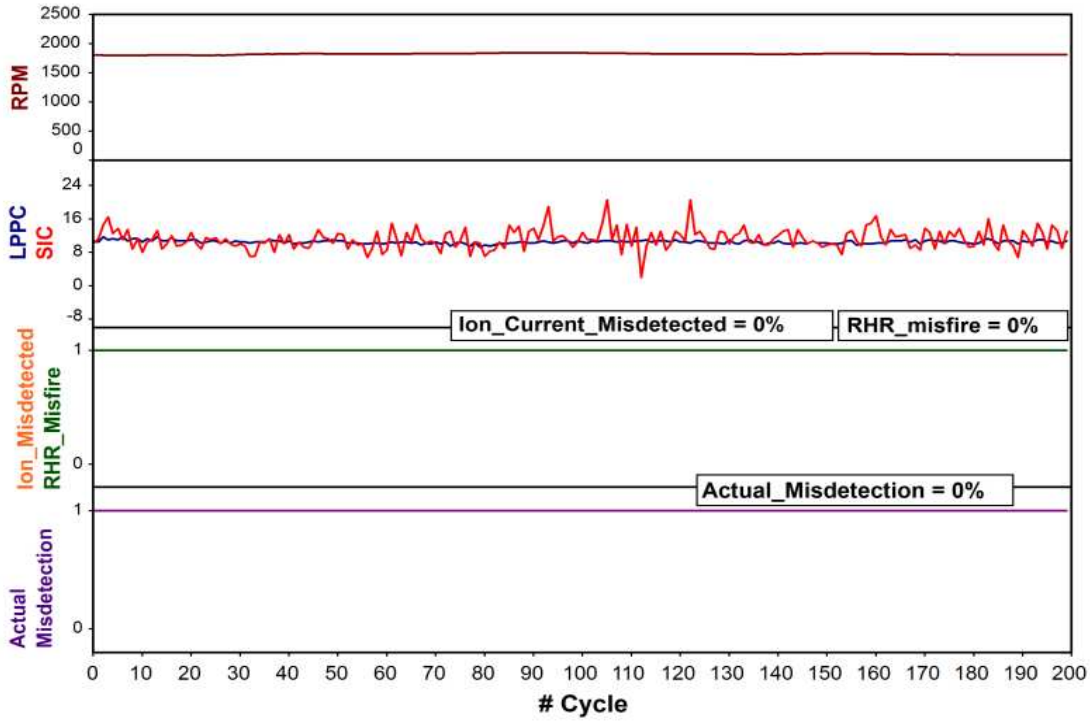

Figure 7.3-2. Detailed processed data showing RPM, SIC, LPPC, misfire and ion current misdetection for long probe with increased probe diameter at applied voltage of 100V and 1800RPM

7.3.2 At Applied Voltage of 350V

Figure 7.3-3 and Figure 7.3-4 shows the ion current misdetection with short and long probe at 1800 rpm and at applied voltage of 350V. For short probe, only one cycle has ion current signal misdetection. In case of the long probe, as seen in Figure 7.3-4, one of the cycles shows ion current misdetection which is also a misfired cycle; therefore, the actual misdetection of the ion current signal is 0%. Moreover, the large diameter probe shows an accurate detection of the SIC compared to small diameter probe irrespective of probe lengths or applied voltages.

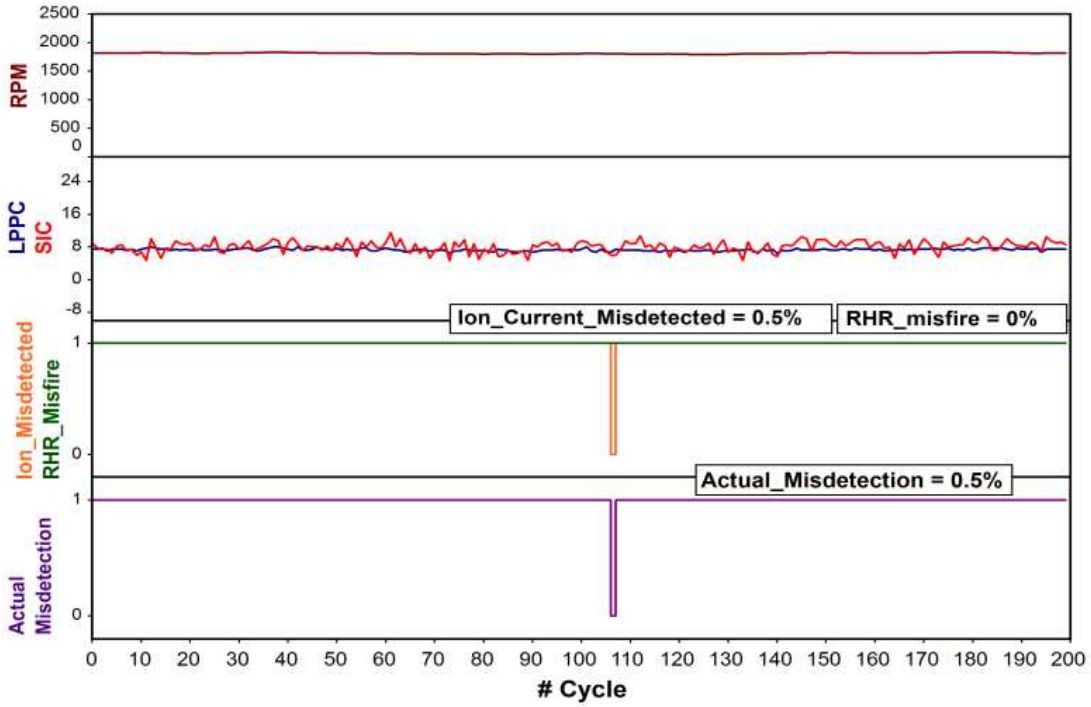

Figure 7.3-3. Detailed processed data showing RPM, SIC, LPPC, misfire and ion current misdetection for short probe with increased probe diameter at applied voltage of 350V and idling speed 1800RPM

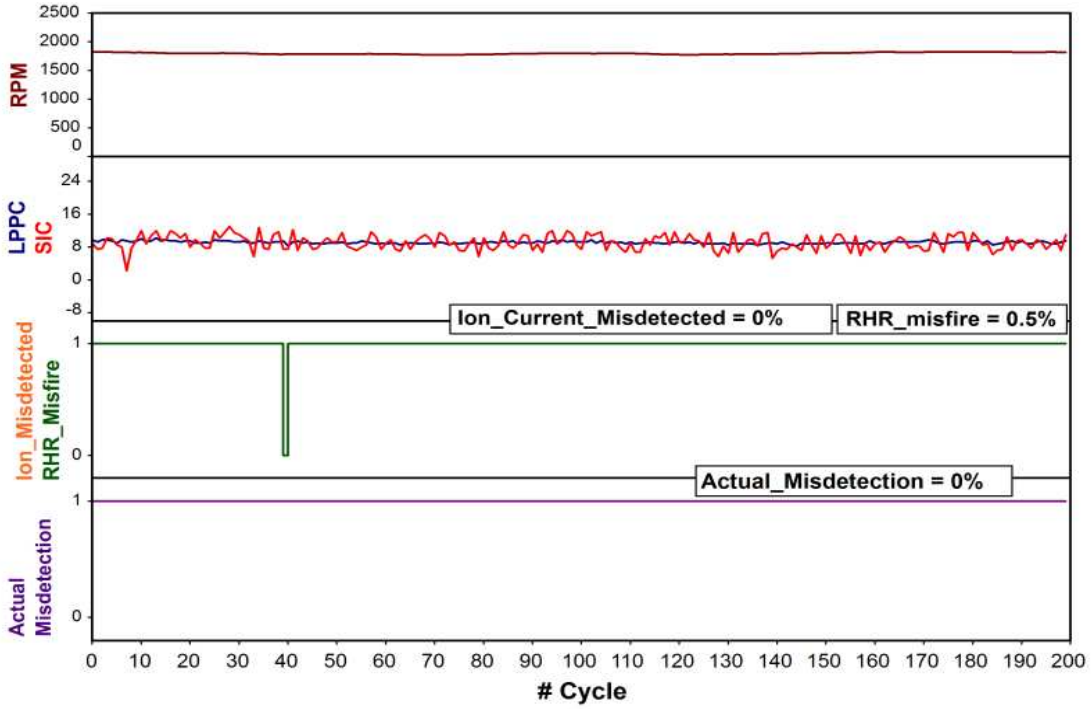

Figure 7.3-4. Details processed data showing RPM, SIC, LPPC, misfire and ion current misdetection for long probe with increased probe diameter at applied voltage of 350V and idling speed 1800RPM

7.4 *Effect of Probe Length, Probe Diameter and Applied Voltage on Actual Misdetection*

Figure 7.4-1 and Figure 7.4-2 show the actual misdetection of the ion current signal at three different speeds for short, medium, and long probe at 100 and 350V using the small probe diameter. The short probe shows the worst ion current signal detection at all speeds and applied voltages. Increasing the probe length indicates a significant reduction in the actual misdetection of the ion current signal. The actual misdetection at 1800 rpm shows least percentage compared to 1600 and 2100 rpm. Increasing the applied voltage from 100 to 350V drops the actual misdetection percentage for the medium and long probe below 10% as shown in Figure 7.4-2.

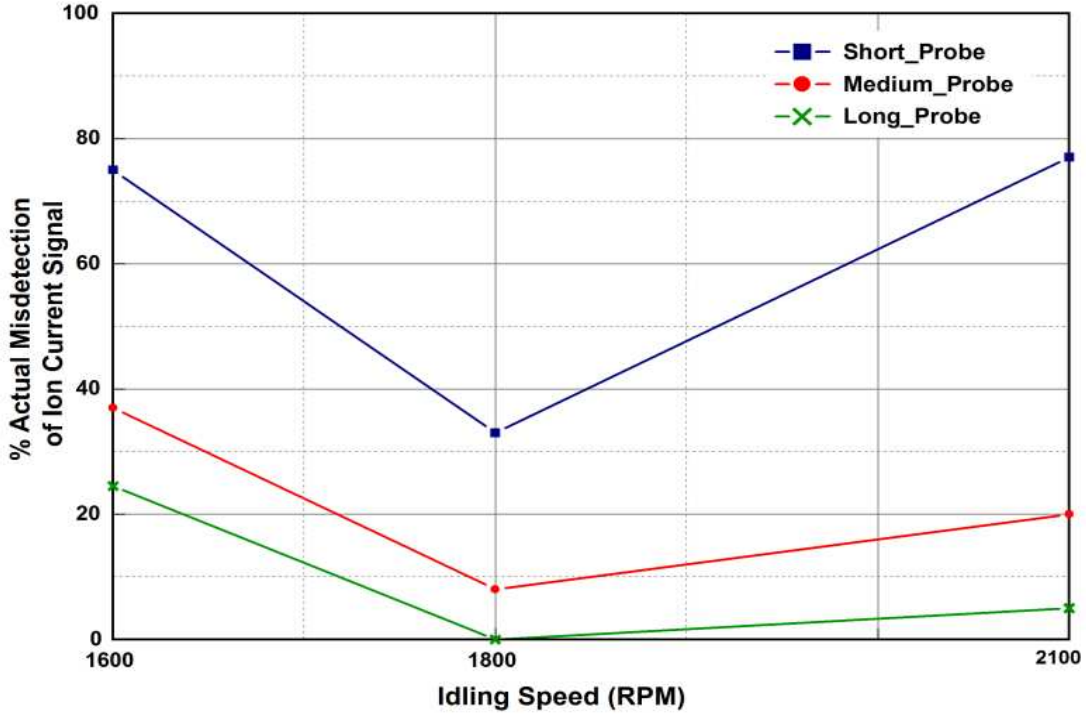

Figure 7.4-1. Percentage of actual misdetection of the ion current signal for different probe length and engine speeds at 100V (small probe diameter)

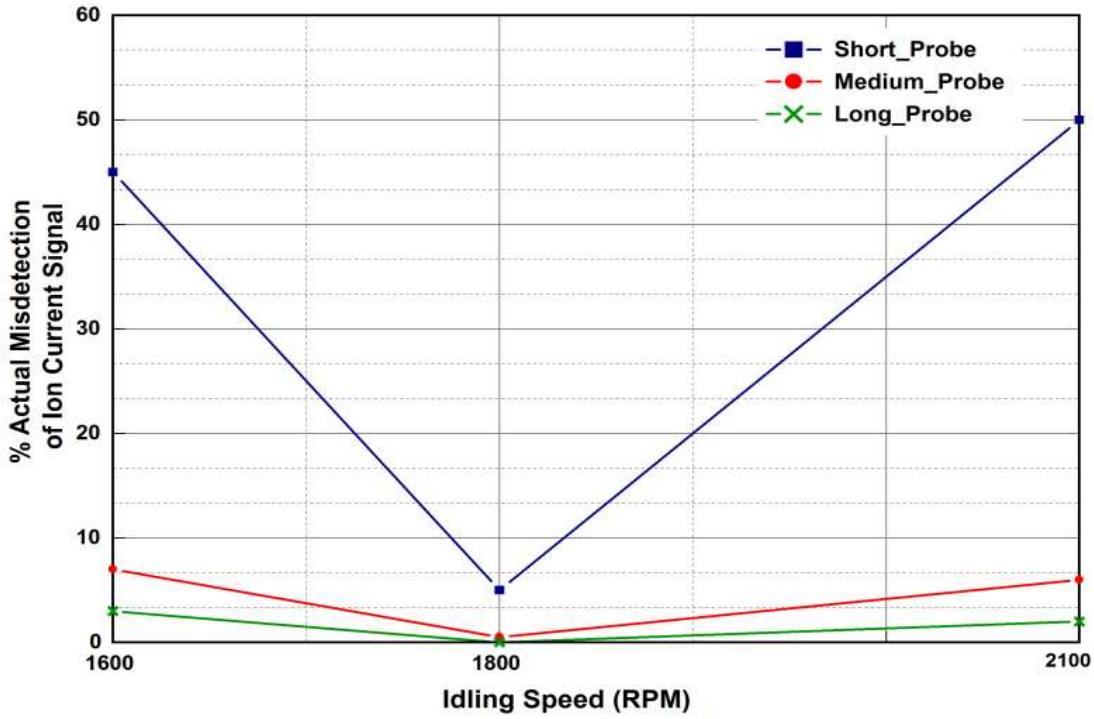

Figure 7.4-2. Percentage of actual misdetection of the ion current signal for different probe length and engine speeds at 350V (small probe diameter)

Further, the actual misdetection of the ion current signal is plotted for the large probe diameter as shown in Figure 7.4-3 and Figure 7.4-4. It is observed that increasing the probe diameter resulted in a huge drop in the actual misdetection percentage of the ion current signal, and it is recorded below 5% for all the cases. Also, there is a trivial change seen in misdetection percentage at different idling speeds. Use of medium and long probes yielded ion current signal misdetections lower than 0.5% at all tested speeds and applied voltages. Figure 7.4-4 shows that the medium and long probe successfully detected the ion current signal for all the cycles recorded.

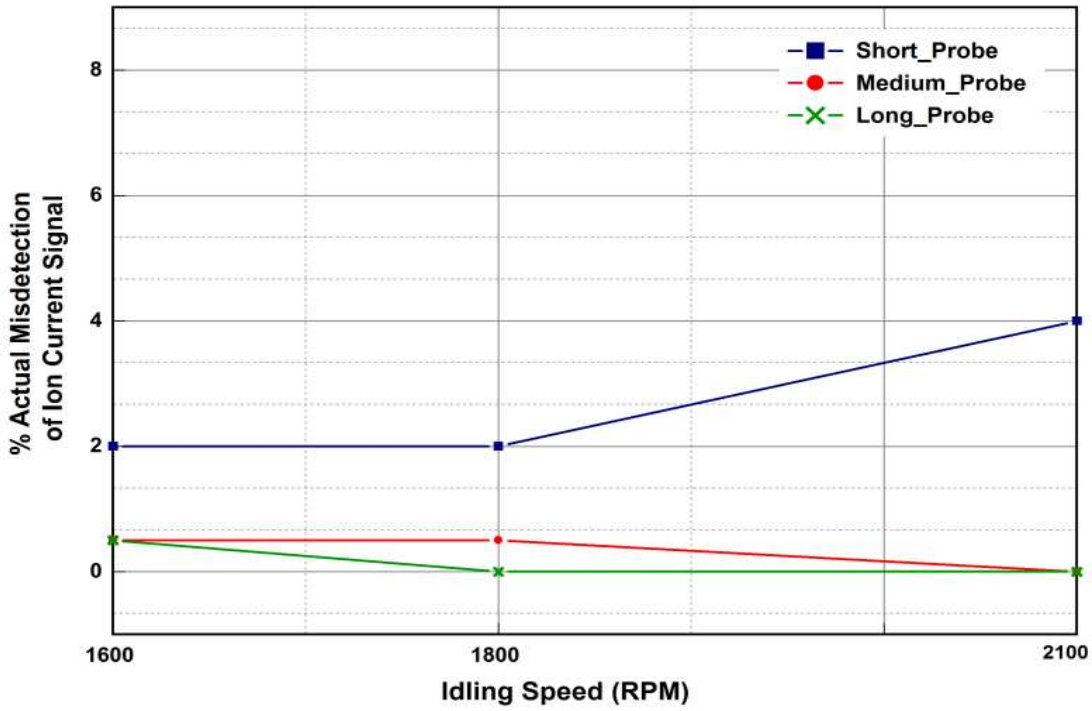

Figure 7.4-3. Percentage of actual misdetection of the ion current signal for different probe length and idling speeds at 100V (large probe diameter)

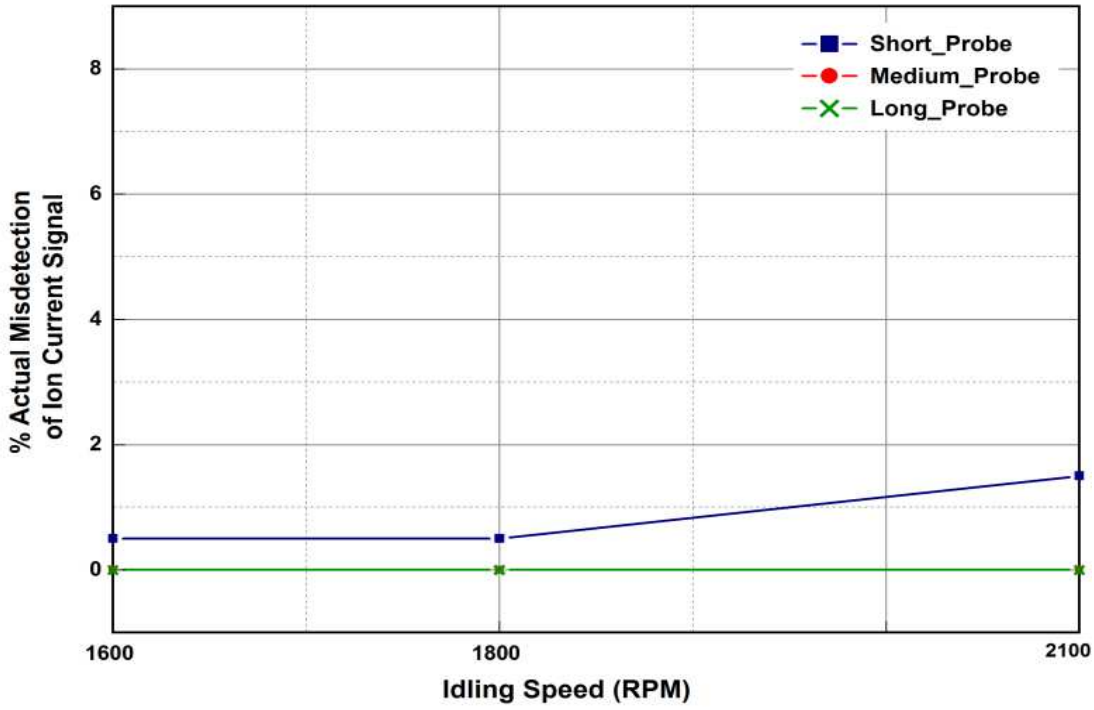

Figure 7.4-4. Percentage of actual misdetection of the ion current signal for different probe length and idling speeds at 350V (large probe diameter)

7.5 *Effect of Probe Length, Probe Diameter and Applied Voltage on the Maximum Amplitude of Ion Current Signal*

Due to heterogeneity of diesel combustion, the ion current signal from diesel combustion lacks reproducibility. As a result there exists variation in the amplitude of the ion current signal measured from the combustion event. Box plots for the ion current peak amplitude with short, medium and long probe are constructed from data recorded for different voltages and idling speeds. Box plots have been used in order to summarize the variation in amplitude and at the same time study the effect of the probe diameter, probe length and the applied voltage on the peak amplitude of the ion current signal. A typical box plot consists of the smallest observation (sample minimum), lower quartile, median, upper quartile, and largest observation (sample maximum). Thus the box plots used in the analysis give clear indication about the spread and the median of the variation in the peak amplitude of the ion current signal measured for each cycle for each test point.

Figure 7.5-1-(a) and (b) shows box plot for the small probe diameter at 1600 rpm. Figure 7.5-1-(a) shows peak amplitudes with applied voltage of 100V, where low amplitude is recorded for the peak of the ion current signal with a small cycle to cycle variation. It is observed that the peak amplitude did not increase with longer probe length but the variation in the signal slightly increases. Figure 7.5-1-(b) shows peak amplitudes with applied voltage of 350V, the peak amplitude increased compared with 100V. A significant increase in the cycle to cycle variation is observed at 350V. Also, the peak amplitude increases for longer probe length; this indicates that the sensitivity of the longer is more at higher voltage.

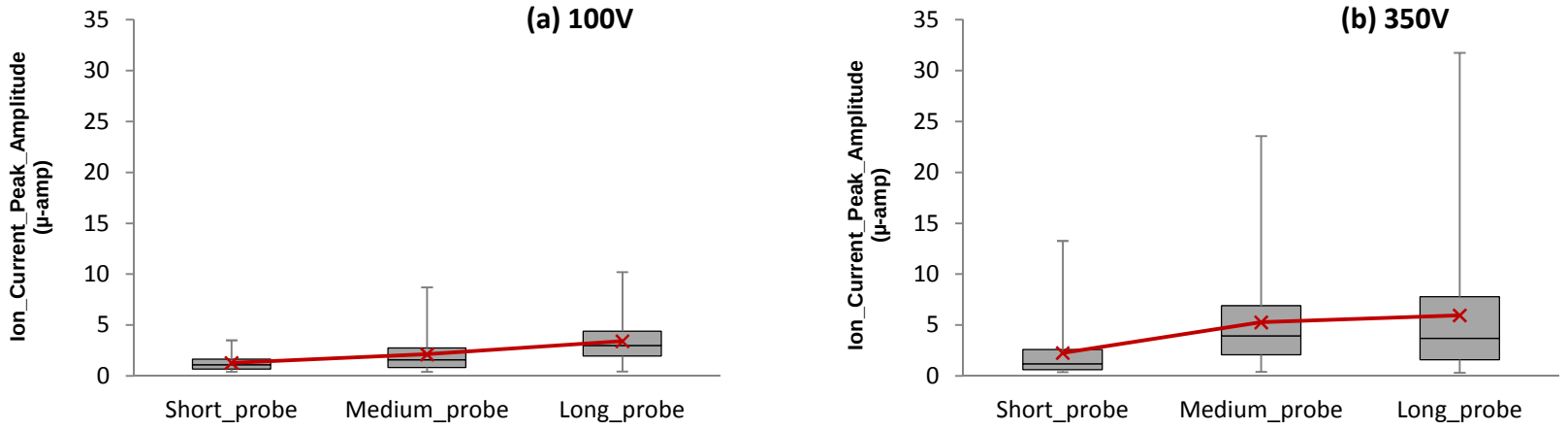

Figure 7.5-1.(a) and (b): Box plot for ion current amplitude peaks at 1600 rpm at 100V and 350V for the probes with smaller diameter

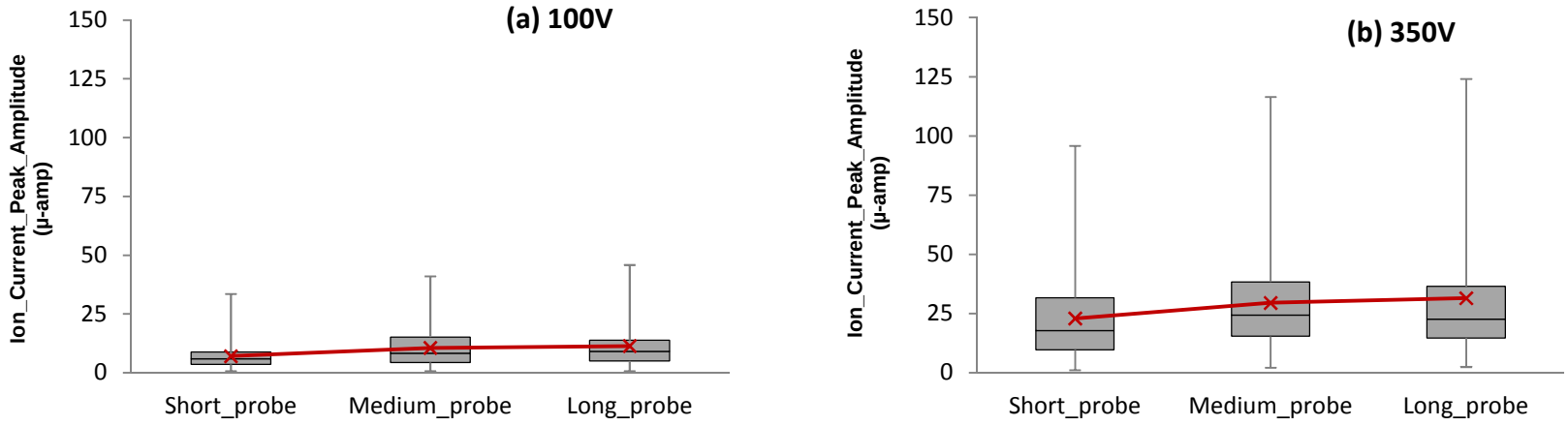

Figure 7.5-2. (a) and (b): Box plot for ion current amplitude peaks at 1600 rpm at 100V and 350V for the probes with larger diameter

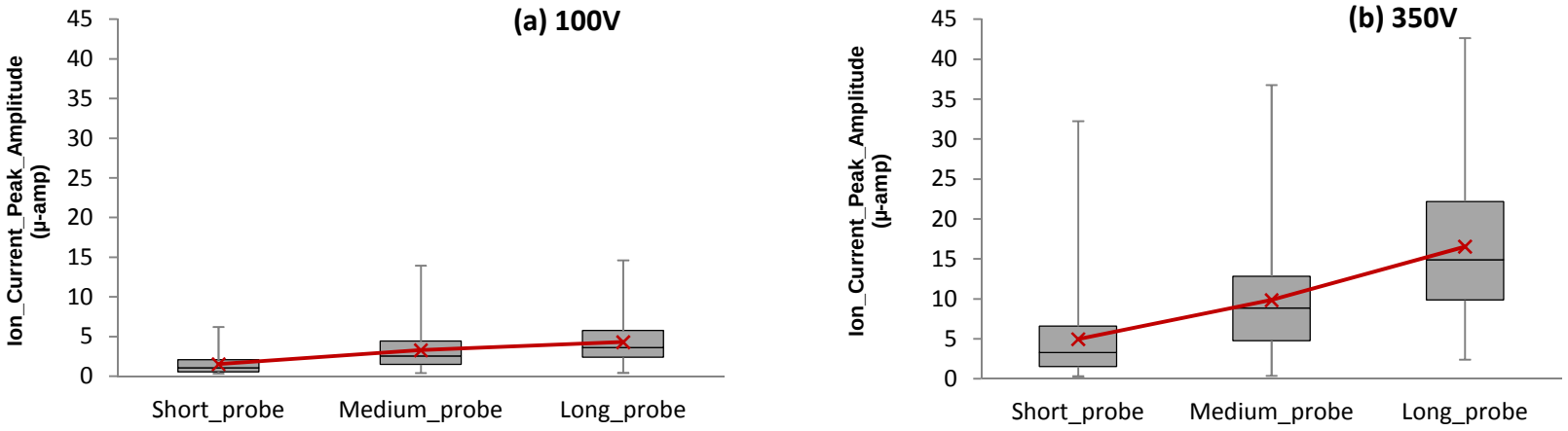

Figure 7.5-3. (a) and (b): Box plot for ion current amplitude peaks at 1800 rpm at 100V and 350V for the probes with smaller diameter

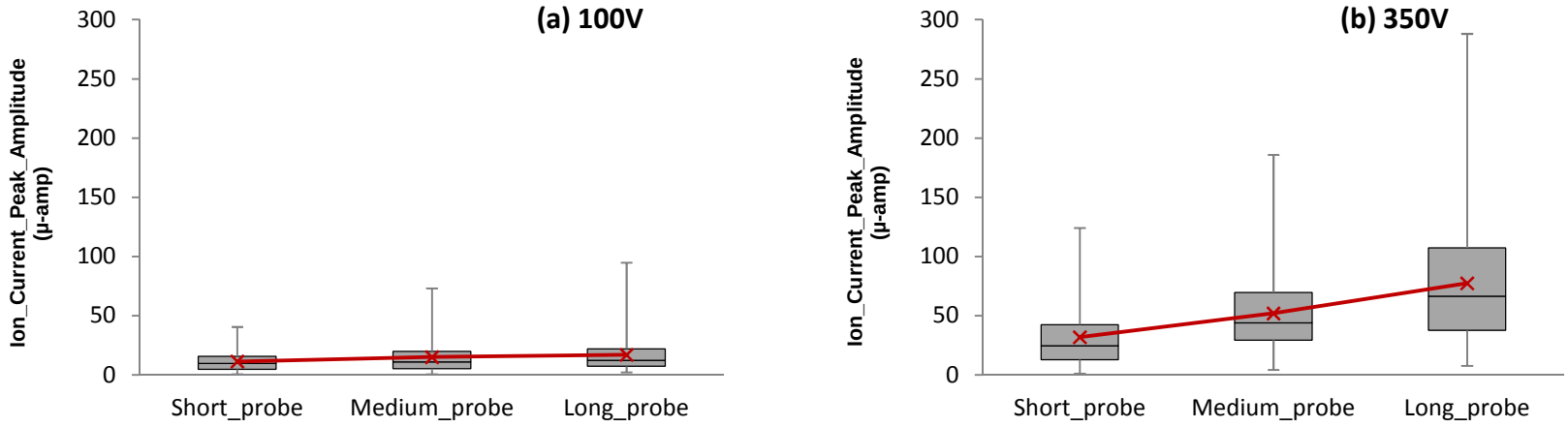

Figure 7.5-4. (a) and (b): Box plot for ion current amplitude peaks at 1800 rpm at 100V and 350V for the probes with larger diameter

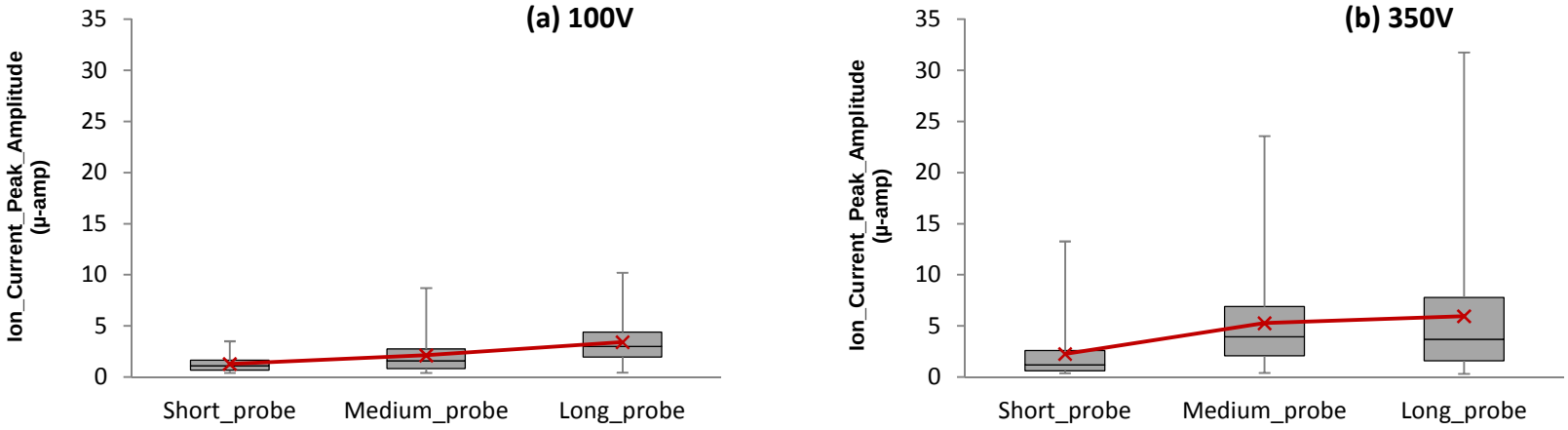

Figure 7.5-5. (a) and (b): Box plot for ion current amplitude peaks at 2100 rpm at 100V and 350V for the probes with smaller diameter

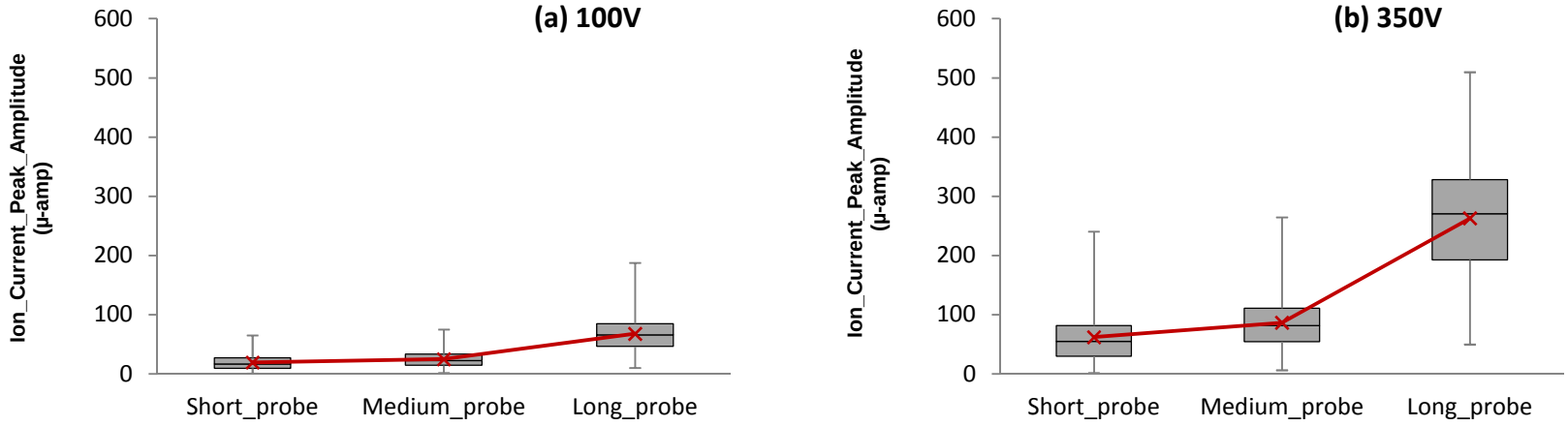

Figure 7.5-6. (a) and (b): Box plot for ion current amplitude peaks at 2100 rpm at 100V and 350V for the probes with larger diameter

By increasing the probe diameter, box plots for different probe lengths at 100V and 350V for the 1600 rpm are shown in Figure 7.5-2-(a) and (b). Although similar trends are observed for the effect of increasing the probe length and applied voltage on the peak amplitude and variation for the probe of large diameter, the amplitude of the peak ion current and its variation are observed approximately 6 times higher.

Figure 7.5-3-(a) and (b) show box plots for the small probe diameter and Figure 7.5-4-(a) and (b) show box plots for the large probe diameter at 1800 rpm. Similar trends are observed for the amplitude of the ion current peak and its variation at 1800 rpm. The peak amplitude and its variation increased approximately 3 times with the increase in applied voltage from 100 to 350V for the small probe and large probe diameter. In addition, the ion current peak and its variation increased roughly 5 times with increase in the probe diameter at respective applied voltage.

Figure 7.5-5-(a) and (b) show box plots for the small probe diameter and Figure 7.5-6-(a) and (b) show box plots for the large probe diameter at 2100 rpm. The trends observed for the amplitude of the ion current peak and its variation is in agreement with the lower speeds. Also, the peak amplitude and its variation increased approximately 3 times with the increase in applied voltage from 100 to 350V for the small probe as well as the large probe diameter. However, the ion current peak and its variation increased roughly 50 times with increase in the probe diameter at respective applied voltage.

7.6 *Chapter Summary*

The results from the detailed experimental investigation on the effect of ion current sensor design to improve ion current signal detection during no load operation is thoroughly described in this chapter. Cycle-to-cycle data is analyzed to study the effect of change in design parameters and probe location on ion current detection. Similar to the results from the previous chapter, the details from the processed cycle-to-cycle data analysis demonstrate a significant effect of the ion current probe design as well as its location in the combustion chamber on the ion current signal detection. Increasing the probe length, increasing the probe diameter and increasing the applied DC voltage helps to improve the ion current signal detection at different engine speeds for no load operation. However, effect of changing the probe length and changing the probe diameter shows more significant improvement as compared to increase in the applied voltage. Furthermore, it is also observed that increasing the probe length, probe diameter and applied voltage also improves the accuracy in determining the SIC during the no load operation. The effect of increasing the probe length and probe diameter at different applied DC voltage on the ion current signal peak amplitude is summarized using the box plots. The box plots also exhibit the cycle-to-cycle variation in the peak amplitude of the ion current signal.

CHAPTER 8

SUMMARY AND CONCLUSIONS

This experimental investigation on the ion current detection during cold starting and no-load operation indicated that the surface area of the probe exposed as well as its location in the combustion chamber significantly affect the ion current signal detection. Detailed discussion on the ion current signal characteristics at different engine operating conditions and the effect of changes in sensor design on the ion current signal detection are discussed in the following sections. Conclusions from the experimental investigations are listed at the end of this chapter.

8.1 *Thesis Summary*

Ionization in the gasoline and diesel engines occurs in different environments, due to the distinct differences between the quality of the combustible mixtures in the two engines. In case of gasoline engines, the mixture is almost homogenous and close to stoichiometric. It produces high ion current amplitudes because of high in-cylinder temperature reached during combustion. However, in diesel engines, the mixture is heterogeneous and the equivalence ratio varies from zero to infinity. But, the overall equivalence ratio, even at full load, is still lean resulting in lower combustion gas temperatures compared to gasoline engines. This explains the reason behind the lower ion current amplitudes reached in diesel engines. Moreover, the lighter the load, the leaner is the overall equivalence ratio and the lower is the combustion temperature. The worst condition for ionization is at no-load and cold starting. This explains the reason behind the absence of the ion current signal under the low temperature engine operating

conditions. Another reason for the absence or misdetection of the ion current signal is poor combustion and complete misfiring.

In order to solve the misdetection of the ion current signal at cold starting, no-load and idling operating conditions, the effect of increasing the applied voltage, probe length and probe diameter are investigated.

8.2 *Conclusions*

1) The absence of the ion current signal during cold starting and no-load operation, including idling, can be the result of the following:

a) Inability of the sensor and associated electric circuit to produce a detectable signal indicative of the combustion produced ionization. This is considered to be an Actual misdetection.

b) Failure of the combustion process to reach a temperature high enough to produce enough ionized species. This can be considered as engine misfiring caused by many problems related engine operation and referred to as Misdetection.

2) The detection of the ion current signal can be improved by one or a combination of the following:

a) Applying a higher DC voltage in the ion current electric circuit.

b) Increase the area of the sensing part of the probe, in diameters and/or length.

c) Changing the location of the sensing part of the probe in the combustion chamber. This can be achieved by adjusting the intrusion or position in the combustion chamber

3) The accuracy in determining the SIC is enhanced by using larger sensing area. The enhancement by increasing the applied voltage is not as remarkable as the increase in the surface area.

APPENDIX A

NOMENCLATURE

Actual Misdetection: Number of false misfire indications because of failure to detect ion current signal in fired cycles.

bTDC: Before top dead center

CAD: Crank angle degree

DC: Direct current

ECU: Electronic control unit

HCCI: Homogenous charge compression ignition

Ion Current Misdetection: Total number of apparent misfire indications based on ion current signal.

LPPC: Location of peak premixed combustion

RHR: Rate of heat release

RPM: Revolutions per minute

SI: Spark ignited

SIC: Start of ion current

SOI: Start of injection

REFERENCES

[1] Panousakis, D., Gazis, A., Patterson, J., and Chen, R., "*Analysis of SI Combustion Diagnostics Methods Using Ion-Current Sensing Techniques*," SAE International, 2006, SAE Technical Paper 2006-01-1345.

[2] Cavina, N., Moro, D., Poggio, L., Zecchetti, D., Nanni, R., and Gelmetti, A., "*Individual Cylinder Combustion Control Based on Real-Time Processing of Ion Current Signals*," SAE International, 2007, SAE Technical Paper 2007-01-1510.

[3] Klövmark, H., Rask, P., and Forssell, U., "*Estimating the Air/Fuel Ratio from Gaussian Parameterizations of the Ionization Currents in Internal Combustion SI Engines*," SAE International, 2000, SAE Technical Paper 2000-01-1245 .

[4] Cavina, N., Poggio, L., and Sartoni, G., "*Misfire and Partial Burn Detection based on Ion Current Measurement*," SAE Int. J. Engines, 4(2), pp. 2451-2460, 2011, 2011-24-0142 .

[5] Han, Z., Henein, N., Nitu, B., and Bryzik, W., "*Diesel Engine Cold Start Combustion Instability and Control Strategy*," SAE International, 2001, SAE Technical Paper 2001-01-1237.

[6] Osuka, I., Nishimura, M., Tanaka, Y., and Miyaki, M., "*Benefits of New Fuel Injection System Technology on Cold Startability of Diesel Engines - Improvement of Cold Startability and White Smoke Reduction by Means of Multi Injection with Common Rail Fuel System (ECD-U2)*," SAE International, 1994, SAE Technical Paper 940586 .

[7] Henein, N. A., "*Starting of Diesel Engines: Uncontrolled Fuel Injection Problems*," SAE International, 1986, SAE Technical Paper 860253.

[8] Hara, H., Itoh, Y., Henein, N. A., and Bryzik, W., "*Effect of Cetane Number with and without Additive on Cold Startability and White Smoke Emissions in a Diesel Engine*," SAE International, 1999, SAE Technical Paper 1999-01-1476.

[9] Henein, N. A., and Lee, C.-S., "*Autoignition and Combustion of Fuels In Diesel Engines Under Low Ambient Temperatures*," SAE International, 1986, SAE Technical Paper 861230 .

[10] Henein, N. A., Zahdeh, A. R., Yassine, M. K., and Bryzik, W., "*Diesel Engine Cold Starting: Combustion Instability*," SAE International, 1992, SAE Technical Paper 920005.

[11] Heywood, J., 1988, *Fundamentals of Internal Combustion Engines*, McGraw-Hills and Hall, London.

[12] Kubach, H., Velji, A., Spicher, U., and Fischer, W., "*Ion Current Measurement in Diesel Engines*," SAE International, 2004, SAE Technical Paper 2004-01-2922.

[13] Henein, N. A., Bryzik, W., Abdel-Rehim, A., and Gupta, A., "*Characteristics of Ion Current Signals in Compression Ignition and Spark Ignition Engines*," SAE Int. J. Engines, 3(1), pp. 260-281, 2010, 2010-01-0567.

[14] Andersson, I., "*A Comparison of Combustion Temperature Models for Ionization Current Modeling in an SI Engine*," SAE International, 2004, SAE Technical Paper 2004-01-1465.

[15] Abdel-Rehim, A. A., Henein, N. A., and VanDyne, E., "*Impact of A/F Ratio on Ion Current Features Using Spark Plug with Negative Polarity*," SAE Int. J. Passeng. Cars - Electron. Electr. Syst., 1(1), pp. 432-445, 2008, 2008-01-1005.

[16] Reinmann, R., Saitzkoff, A., and Mauss, F., "*Local Air-Fuel Ratio Measurements Using the Spark Plug as an Ionization Sensor*," SAE International, 1997, SAE Technical Paper 970856.

[17] Glavmo, M., Spadafora, P., and Bosch, R., "*Closed Loop Start of Combustion Control Utilizing Ionization Sensing in a Diesel Engine*," SAE International, 1999, SAE Technical Paper 1999-01-0549 .

[18] Henein, N. A., Badawy, T., Rai, N., and Bryzik, W., "*Ion Current, Combustion and Emission Characteristics in an Automotive Common Rail Diesel Engine*," Journal of Engineering for Gas Turbines and Power, 134(4), pp. 042801-042807, 2012 .

[19] Rai, N. D., "*Measurement and Analysis of Ion Current Signal in an Automotive Common Rail Diesel Engine*," Master of Science, Wayne State University, Detroit, Michigan, USA, 2010.

[20] Badawy, T., Rai, N., Singh, J., Bryzik, W., and Henein, N., "*Effect of design and operating parameters on the ion current in a single-cylinder diesel engine*," International Journal of Engine Research2011, 1468087411412033.

[21] Badawy, T., "*Investigation of the ion current signal in Gen-set turbocharged diesel engine*," Master of Science, Wayne State University, Detroit, Michigan, 2010.

[22] Badawy, T., Khaled, N., and Henein, N., "*Fuzzy Logic Control of Diesel Combustion Phasing using Ion Current Signal*," *ASME Internal Combustion Engine* Italy2012, ICES2012-81211.

[23] Badawy, T., "*Ionization in Diesel Combustion for On-board Diagnostics and Engine Control*," Doctor of Philosophy Dissertation, Wayne State University, Detroit, Michigan, 2012.

[24] Gargo, S., Badawy, T., Estefanous, F., and Henein, N., "*Simulation of Ionization in Diesel Engines Premixed Combustion*," *International Conference on Advanced Research and Applications in Mechanical Engineering* Notre-Dame University- Louaize, Lebanon 2011.

[25] Estefanous, F., "*Ionization in diesel combustion: Mechanism, new instrumentation and engine applications*," Doctor of Philosophy Dissertation, Wayne State University, Detroit, Michigan, 2011.

[26] Estefanous, F., and Henein, N., "*Multi Sensing Fuel Injector for Electronically Controlled Diesel Engines*," SAE International, 2011, SAE Technical Paper 2011-01-0936.

[27] Abdel-Rehim, A. A., Henein, N. A., and VanDyne, E., "*Ion Current in a Spark Ignition Engine using Negative Polarity on Center Electrode*," SAE International, 2007, SAE Technical Paper 2007-01-0646.

[28] Yoshiyama, S., Tomita, E., Mori, M., and Sato, Y., "*Ion Current in Homogeneous Charge Compression Ignition Engine*," Society of Automotive Engineers of Japan, 2007, SAE Technical Paper 2007-01-4052.

ABSTRACT

ION CURRENT SIGNAL DETECTION DURING COLD STARTING AND IDLING OPERATION IN A DIESEL ENGINE

by

SANKET A GUJARATHI

December 2013

Advisor: Dr. Naeim A Henein

Major: Mechanical Engineering

Degree: Master of Science

Cold starting of diesel engines is characterized by inherent problems such as long cranking periods and combustion instability leading to an increase in fuel consumption and the emission of high concentrations of hydrocarbons which appear as white smoke. Accordingly, a signal indicative of combustion during cold starting and idling operation is important for combustion and emission control. The ion current signal has been considered for the feedback control of both gasoline and diesel engines. However, the ion current signal produced from the combustion of the heterogeneous charge in diesel engines is weaker compared to that produced from the combustion of the homogeneous charge in gasoline engines because of the lower combustion temperatures reached in diesel engines. Consequently, this presents a problem in the detection of the ion current signal in diesel engines, particularly during starting and idling operations. This research investigates and addresses the ion current detection problems pertaining to cold starting and idling at various speeds. Also, different approaches have been endeavored to improve the signal detection under these conditions so as to aid its application for misfire detection.

AUTOBIOGRAPHICAL STATEMENT

I was born in Sinnar, India on June 1st, 1988. My avid interest in exploring and learning about the world of automobiles drove me to select engineering as my career path. I completed my Bachelor's degree in mechanical engineering from Pravara Rural Engineering College, University of Pune, India in June 2009. Internal combustion engine being the heart of the automobiles, I elected combustion as my specialization while I joined Wayne State University, Detroit, Michigan in January 2010 to pursue of the Masters degree in mechanical engineering. After being through one year of coursework of my master's degree program, Prof. Dr. Naeim Henein gave me the opportunity to work in Center for Automotive Research as a Graduate Research Assistant (GRA) under his guidance. I was both excited and thrilled for my first experience with research. My research work mainly comprised of studying ionization in the heterogeneous combustion. I extensively worked on mutli-cylinder diesel engine to study ion current signal detection during cold starting and idling. I have always believed in being curious and so my stride for the pursuit of knowledge continues as I took up the Diesel After-treatment System Calibration Engineer position with Ford Motor Company in October 2012.